NTNU – Trondheim
Norwegian University of
Science and Technology

Fatigue of Smart Composite Metal Joints

Even Vardenær Lunder

Mechanical Engineering
Submission date: June 2013
Supervisor: Andreas Echtermeyer, IPM

Norwegian University of Science and Technology
Department of Engineering Design and Materials

THE NORWEGIAN UNIVERSITY
OF SCIENCE AND TECHNOLOGY
DEPARTMENT OF ENGINEERING DESIGN
AND MATERIALS

MASTER THESIS SPRING 2013
FOR
STUD.TECHN. EVEN VARDENÆR LUNDER

Fatigue of smart composite metal joints
Utmatting av smarte kompositt metall forbindelser

Adhesive joints are ideal for connecting dissimilar materials in optimized structures. However, their use is currently limited by uncertainties about the long-term performance of these joints. Smart materials that could monitor their state of health would be ideal for monitoring long-term performance and eventually also for improving the joints.

This project shall explore the fatigue behavior of composite metal joints. Optical fibers shall be used to model growth of debonding vs. number of cycles as a method of integrated health monitoring. The experimental strain measurements shall be compared against finite element modeling.

The thesis should include the signed problem text, and be written as a research report with summary both in English and Norwegian, conclusion, literature references, table of contents, etc. During preparation of the text, the candidate should make efforts to create a well arranged and well written report. To ease the evaluation of the thesis, it is important to cross-reference text, tables and figures. For evaluation of the work a thorough discussion of results is appreciated. Safety evaluations for experimental work shall be added to the Appendix.

Three weeks after start of the thesis work, an A3 sheet illustrating the work is to be handed in. A template for this presentation is available on the IPM's web site under the menu "Masteroppgave" (http://www.ntnu.no/ipm/masteroppgave). This sheet should be updated one week before the Master's thesis is submitted.

The thesis shall be submitted electronically via DAIM, NTNU's system for Digital Archiving and Submission of Master's thesis.

Torgeir Welo
Head of Division

Andreas Echtermeyer
Professor/Supervisor

NTNU
Norges teknisk-
naturvitenskapelige universitet
Institutt for produktutvikling
og materialer

Preface

This thesis is written in the spring of 2013. During my one year of study abroad at University of California San Diego I had a course called Mechanics of Composite Materials and Laminates. In this course I did a project on Non Destructive Testing of composite materials and gained some interest in the subject of Structural Health Monitoring. This was part of the reason why I chose to write a project on Smart Materials in Adhesive Joints in the fall 2012. The work in this thesis is based on the knowledge I gained during this project.

I would like to thank PhD Candidate Jon Harald Lambert Grave for great help and collaboration, PhD Candidate Giovanni Perillo for help with the the finite element analysis. I would also thank Halvard Støwer for setting up parts of the data acquisition and Bjarne Stolpnessæter for milling of the composite patches.

At last I would like to thank my supervisor Professor Andreas Echtermeyer for help and guidance during the work with the thesis.

Abstract

Adhesive joints are ideal for connecting dissimilar materials in optimized structures. Low weight and potential savings in manufacturing costs are major advantages related to such joints, but their use is currently limited by uncertainties about the long-term performance of the joints. A smart material with the ability to monitor its state of health would be ideal for monitoring of the long-term performance and also for making improvements to the joints. This thesis has explored the fatigue behavior of composite metal joints and how optical fibers can be included in the joints as a method of integrated health monitoring.

Cracked IPE100 steel beams were repaired with composite patches. The fatigue life of the patch repaired beams was tested in a four point bend test. Optical fibers were embedded in the adhesive layer of the composite patch and on top of the patch. An optical backscatter reflectometer was used to measure the strains in the composite metal joint during testing. These measurements were compared against finite element analysis and strain gauges. The results were found to coincide well with the finite element analysis and the strain gauges. The optical fibers were proven to detect damage propagation and growth versus number of cycles. It was observed that different failure modes propagating in the composite metal joint could be detected and distinguished by the optical fibers.

Sammendrag

Limsammenføyninger er ideelle for å sammenføye ulike materialer i optimiserte strukturer. Lav vekt og potensielle besparelser i produksjonskostnader er store fordeler med slike sammenføyninger, men deres bruk er nå begrenset av usikkerhet rundt deres langtids yteevne. Et smart materiale med muligheten til å overvåke sin egen helse ville være ideelt for å overvåke langtids yteevnen og også for å forbedre sammenføyningene. Denne masteroppgaven har utforsket utmattingsegenskapene til kompositt-metall sammenføyninger og hvordan optiske fibre kan implementeres i sammenføyningen som en metode for integrert helseovervåking. IPE100 stålbjelker med sprekk har blitt reparert med komposittlapping. Utmattingsegenskapene til de reparerte bjelkene har blitt testet i en firepunkts bøyeprøve. Optiske fibre har blitt innlagt i limlaget til sammenføyningen og på toppen av komposittlappen. En optisk tilbakespredningsreflektor har blitt brukt til å måle tøyningene i kompositt-metall sammenføyningen i løpet av testingen. Disse målingene har blitt sammenlignet med elementanalyse(FEA) og strekklapper. Resultatene stemte godt overens med både elementanalyse og strekklapper. Det har blitt bevist at de optiske fibrene kan detektere skadeutvikling og veksten av denne mot antall sykler. Det ble observert at forskjellige feilmodus i kompositt-metall sammenføyningen kunne bli oppdaget og skilt fra hverandre ved bruk av de optiske fibrene.

Contents

List of Figures

List of Tables

1 Introduction

1.1 Structural health monitoring

Structural health monitoring (SHM) can be described as the process of implementing a damage identification strategy for aerospace, civil and mechanical engineering infrastructure[1]. The interest for SHM has been rapidly increasing the past years and it is motivated by the potential of higher life-safety and economic benefits. For a structure or a mechanical system that is about to suffer failure, damage in terms of changes to the material and/or geometric properties of the system will take place prior to failure[1]. Regular periodic inspection by NDT is expensive and can take a structure out of service for a long time. If a structure could have the health monitored periodically between cycles or continuously during operation, the periodic inspections could be avoided. The design life of a structure could be increased or designed with smaller safety factors if a SHM system was proven to be a reliable method of defect detection prior to the development of failure[2]. A SHM system have to be reliable and should not add any large amount of extra mass to the system. Using optical fibers in a SHM system would be ideal because of the length of the sensing range in the fiber fiber, low weight and a single connection point.

A composite metal joint is an adhesive joint. Since the main objective of this thesis is to explore how the optical fibers can be used for integrated health these joints, only the basic theory for adhesive joints is presented. Parts of this thesis are adopted from the preliminary project, Smart Materials in Adhesive Joints,[3].

2 Theory

2.1 Adhesive joints

An adhesive can join two parts of similar or dissimilar materials together without the use of any mechanical fastening. An adhesive layer on the connecting surfaces of the parts is binding them together forming an adhesive joint. The parts that are to be bonded together are referred to as adherends. Many configurations of adhesive joints have a geometry with an overlap, such joints are often called simple lap joints. The single lap joint is maybe the most common of these and it has been used to a great extent in the industry as a standard test specimen.

2.1.1 Single lap joint

When axial load is applied to a single lap joint, this passes from adherend to adherend through the adhesive layer, also named the bondline. The load generates shear in the
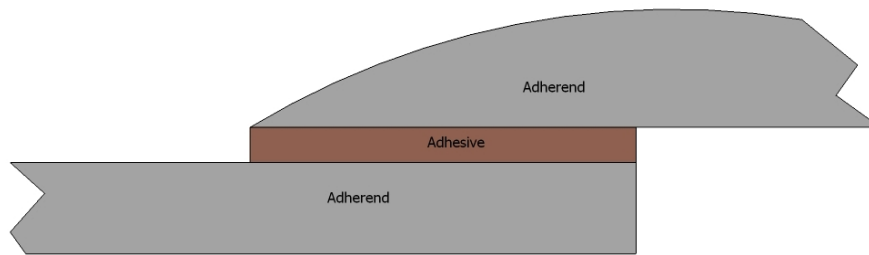
Figure 1: Adhesive joint

bondline. With the adherends not being rigid they will have longer elongation at their ends, thus the shear stress will have a non-uniform distribution over the bondline[5]. The basic geometry and the non-uniform adhesive shearing for the single lap joint is shown in Figure 2.

Figure 2: Single lap joint with non-uniform adhesive shearing. From [5]

2.1.2   Joint strength

For the single lap joint as well as for all adhesive joints there are some important factors that influence the joint strength. Geometry of the joint and material properties of the adhesive and adherends have the largest contribution to the joint strength.

Increasing the strength of the adhesive does not necessarily result in a increased joint strength, an adhesive with low strength has higher flexibility and ductility than an adhesive of higher strength. A flexible and ductile adhesive is able to distribute the stress more uniformly in the bondline and this can result in a higher joint strength than if a stiffer, but less ductile and flexible adhesive is used. Joints with stiff adhesives are having higher stress concentrations at the overlap ends and the stress distribution is less uniform than with a flexible adhesive, see Figure 3. Brittle adhesives are not able to redistribute the load to other parts of the overlap in the similar way as a ductile adhesive. They concentrate the load at the overlap ends, resulting in a lower average shear stress[4]. See Figure 4.

For the adherend the load transfer takes place at the overlap ends, where it is desired to have as low deformation as possible in order to reduce the effect of differential strain in the adhesive. Thus, a high modulus for the adherend is essential for the joint strength. High strength of the adherend material can reduce the risk of adherend yielding causing
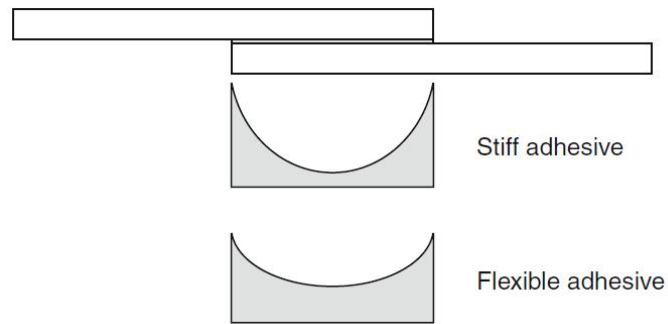
Figure 3: Different stress distribution in the overlap with a stiff or flexible adhesive. From [4].

a premature joint failure. If the stress at the overlap ends reaches the steel yield point, this results in large plastic strains and the joint fails if the maximum adhesive strain is exceeded. For the adherend of a composite laminate a problem is the low strength through the thickness of the laminate. This makes it sensitive for high peel stresses that arises at the overlap ends causing interlaminar failure. By altering the thickness of adherends of different material their longitudinal stiffness can be equalized, thus reducing the non-uniform stress distribution.[4]

3 Optical backscatter reflectometer

Strain measurements with optical fibers are in this thesis done with an Optical Backscatter Reflectometer (OBR) from Luna. Luna's OBR 4600 in combination with their sensing software allows the use of a standard telecom-grade fiber as a high spatial-resolution strain sensor[6].

The OBR system measures the Rayleigh backscatter as a function of length in the optical fiber[6]. This is done with light from the tunable laser source in the OBR system and an optical frequency domain reflectometry (OFDR) technique[7]. External strain leads to changes in the local Rayleigh scatter period and will shift the locally reflected spectrum. Such spectral shifts is calibrated and assembled to form a distributed strain measurement[8]. The Rayleigh spectral shift is relative to a reference scan.

The system achieves high spatial resolution down to 2 mm, a measurement range up to 70 meters and a strain resolution of 1μ. It is also able to measure temperature changes of 0.1 °C. The strain is calculated in the OBR Desktop software. When performing a scan with the OBR, a file with the measurement of the whole length of the optical fiber is created. It can be saved and be used for analysis at any time. A desired gauge length and sensor spacing is chosen in the software, and the strain is calculated based on these preferences. If a gauge length of 0.5 cm and sensor spacing of 0.1 cm is chosen, the
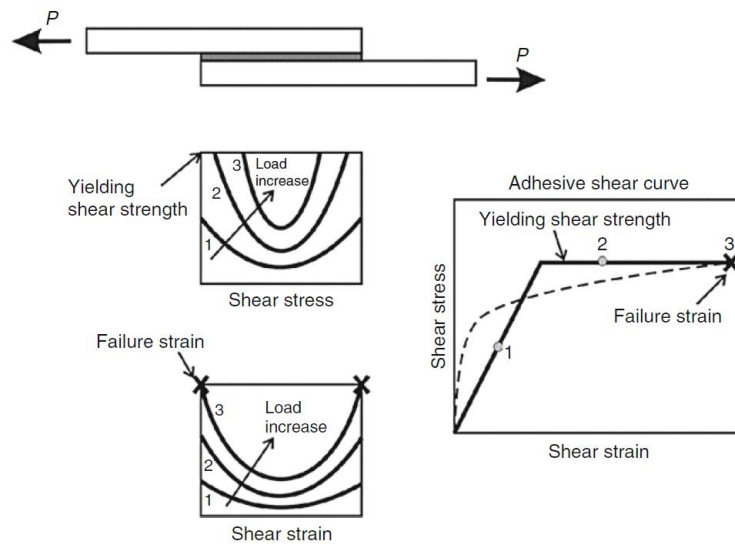
Figure 4: Adhesive ductility affecting the stress distribution in the overlap. From[4].

software calculates the strain over sensors of 5 mm length with a sensor for every 1 mm.
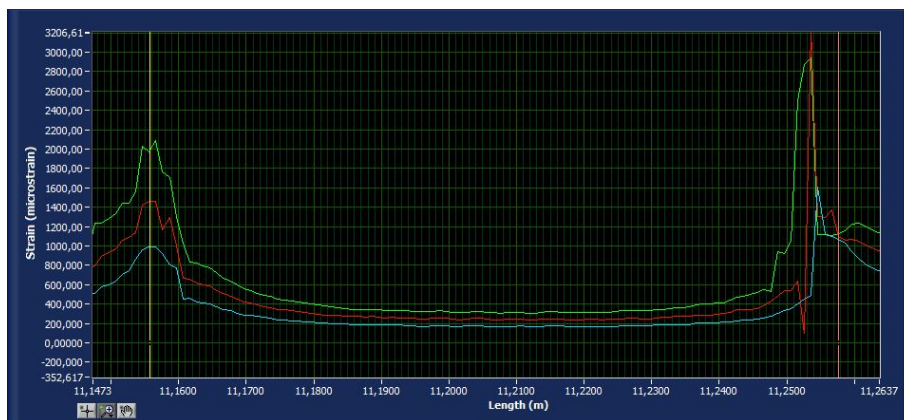
Figure 5: View of strain measurements with the Luna OBR 4600.

4 Experimental work

The main experimental work done in this thesis was testing of cracked standard steel IPE100 beams repaired with carbon fiber reinforced polymer(CFRP) composite patches. The beams were of the same type produced and tested in the Co-Patch project participated by NTNU. The fatigue life of such beams was tested in a four point bend test and the strains in the patch were measured during the test. Details of the beams and the test method are presented later in Sections 4.2 and 5.

There is no method for measuring the shear stress along the overlap in the adhesive layer directly. But from what explained in section 2 and Figure 3 and 4 the shear stress should have a non-uniform distribution with peaks at the ends. This creates a curve that can be referred to as the "bathtub curve". Axial strain is measured by the optical fibers and any change in the shear stress in the adhesive layer will also cause changes in the axial strain. If correct sensing of the strain in the adhesive layer is obtained, the results should have a curve similar to the "bathtub curve".

The theory for adhesive joints explained in Section 2 can be directly related to these beams repaired with CFRP patches. With the beam having a crack in the center of the top flange, the patch can be described as an adhesive joint with two overlap lengths. Considering the patch and the beam as two adhesive joints in series, the strain measured by the optical fibers in the adhesive layer should have two curves looking like the "bathtub" curve. Both curves having peaks at the patch end and at the crack tip of the beam. See Figure 6
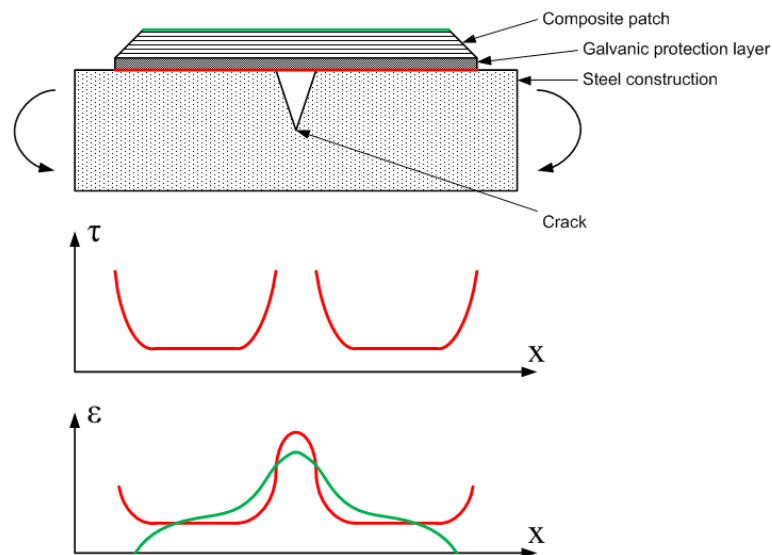
Figure 6: Red curves illustrating shear stress and strain along the adhesive layer of the patch. Adapted from [9].

4.1 Geometry

The patched beam was 1000 mm long with crack sawn through the top flange at the center of the beam. The crack was terminated by a hole through the web. Cross-sectional dimensions were standard IPE100, see Figure 7. The cracked beam was repaired with a 400 mm long CFRP patch with a 50 mm long tapering on each end. The beam was instrumented with seven strain gauges and one optical fiber on top of the patch and one optical fiber embedded in the adhesive layer of the patch, see Figure 8 and 9.
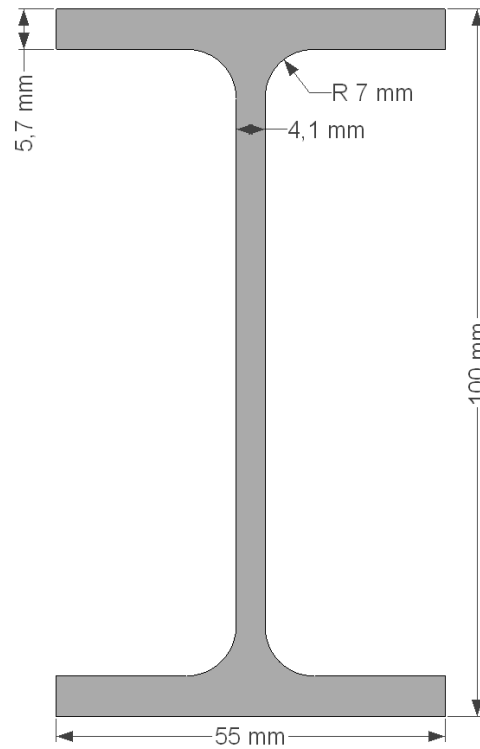
Figure 7: Cross-sectional dimensions, IPE100.
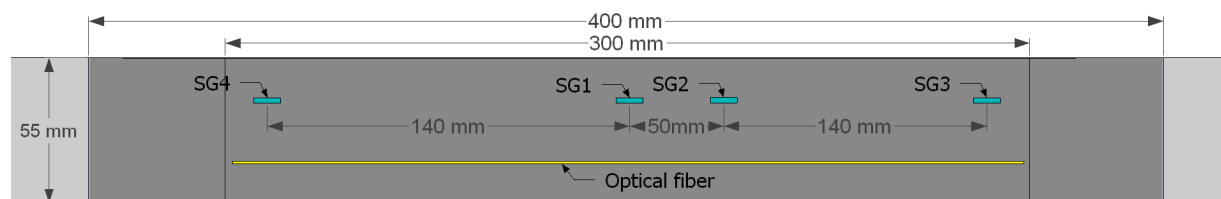
Figure 8: Instrumentation on top of the patch.
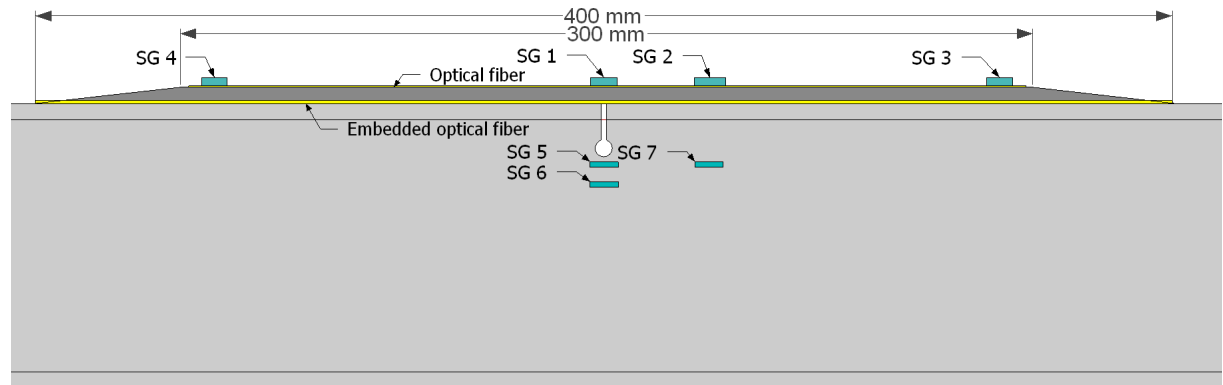
Figure 9: Instrumentation of the beam.

4.2   Specimen production

Beams with four different patch configurations were tested in this thesis:

- IPE 100 PP C/E 400 GB SA UHMC
- IPE 100 PP C/E 400 GB SA PP UHMC
- IPE 100 PP C/E 400 GB DB UHMC
- IPE 100 PP C/E 400 GB DB HMC

Abbrevations:

- 400 = The length of the patch is 400 mm.
- PP C/E = Patch of carbon epoxy laminate produced using prepreg material and hot curing.
- UHMC = Prepreg material of Ultra High Modulus Carbon.
- HMC = Prepreg material of High Modulus Carbon.
- GB = Grit blasted surface of the steel beam.
- SA = Adhesive film.
- PP = Glass fiber reinforced polymer(GFRP) from prepreg material as galvanic protection between the steel and patch.
- DB = Hand lay-up GFRP as galvanic protection between beam and patch.

Four beams of IPE 100 PP C/E 400 GB DB HMC and two beams of IPE 100 PP C/E 400 GB DB UHMC were produced. These beams were produced with three lengths of the optical fiber embedded in the adhesive layer. This was done in order to investigate

if there was any difference in the damage propagation through the width of the beam and if such difference could be detected by the optical fibers.

The remaining beams were already produced by PhD Candidate J.H.L. Grave, but they were not yet measured and instrumented. These had a single length of the optical fiber embedded in the adhesive layer.

4.2.1 Materials

Composite materials

As mentioned above the CFRP laminates used in the test specimens were produced from prepreg material. A prepreg material consists of reinforced fibers that are pre-impregnated by a machine with a pre-catalysed resin system. However, it is not yet cured so it is soft and flexible. The material is cured by heating to a certain temperature over a given period of time. There were two types of unidirectional CFRP prepreg materials used in this thesis. It was an Ultra High Modulus Carbon(UHMC) material and a High Modulus Carbon(HMC) material from Gurit. The curing time had to be 80 °C for 10 hours or 85 °C for 12 hours [10].

The GFRP adhesive layer act as a galvanic protection to prevent corrosion between the steel and the CFRP patch. The DB810 is a ±45 glass fiber fabric produced by AMT Devold. The material called PP is the GFRP pre-preg SE84LV/RE295 from Gurit. SA is an SA80 adhesive film from Gurit that is to be used with the SE84LV prepregs.

Laminate properties for the HMC, UHMC and PP was tensile tested in the preliminary project [3]. The properties found for the CFRP are presented in Table 1.

Material	E_{1T} [GPa]	ν_{12}
UHMC	231.9	0.31
HMC	199.4	0.36

Table 1: CFRP material properties.

The rolls of prepreg materials were cut in pieces of desired size according to the size of the laminate aimed to produce. The roll of prepreg is bagged in plastic and kept deepfrozen in a freezer during storing. The prepreg has been given a certain amount of time that it can be kept at room temperature by the manufacturer. If this time is exceeded they will no longer guarantee for the quality of the product.

Steel

The steel for the beams was of quality S355JR+AR after the DIN1025 standard and was provided by E.A Smith Stål. It was characterized by tensile tests in the preliminary project[3], and a report for this characterization was written as a part of this thesis and can be found in Appendix B. The steel properties are presented in Table 2.

E-modulus	Poisson ratio, ν	Yield stress	Ultimate tensile stress
203.1 GPa	0.3	450.3 MPa	525.2 MPa

Table 2: Steel properties

4.2.2 Preparation of the optical fibers

The optical fibers that are embedded in the test specimens have to be prepared to the desired length. The method is as follows:

First, the optical fiber with yellow plastic coating is cut to a length of 20-30cm. Such length is needed as this fiber is later spliced with the optical fiber measuring the outside of the composite laminate. The fiber is also protected with a thin coating layer between the optical fiber and plastic coating. 30-40mm of both of these layers are removed at one end with a wire stripper. The disclosed fiber is cleaned with the cloth and spray until a squeaky sound is heard. After cleaning the FITEL S325 is used to cut a straight cut with the correct length at the end of the fiber as shown in Figure 10.
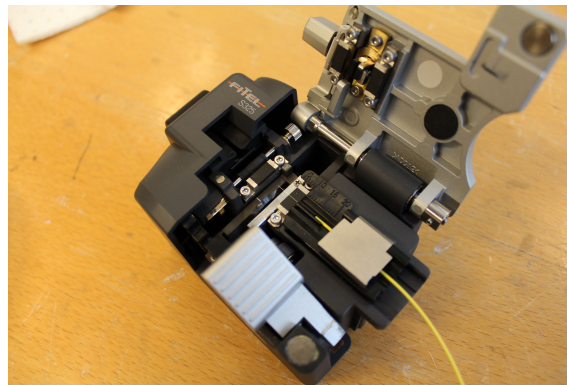
Figure 10: FITEL S325 is used to cut the fiber

The optical fiber that is being embedded in the adhesive layer should be cut to a length that is 100-150 mm longer than the length of the adhesive layer. This is a fiber with a different type of coating, 30-40mm of the coating at one end is melted away by the flame of a lighter. The optical fiber itself will not suffer any damage from this. The soot layer

is cleaned away with the cloth and spray until a squeaky sound is heard, the end is cut in the FITEL S325.

The FITEL S178 is used to splice the ends of the fibers together. The two fibers have different diameters at the coated parts of the fiber so two different inserts are used to keep the fibers in position. The fibers are installed in the machine as Figure 11 is showing. Closing the lid and pushing the green play button, the machine will check if the fibers have a satisfactory straight cut and then splice them together.
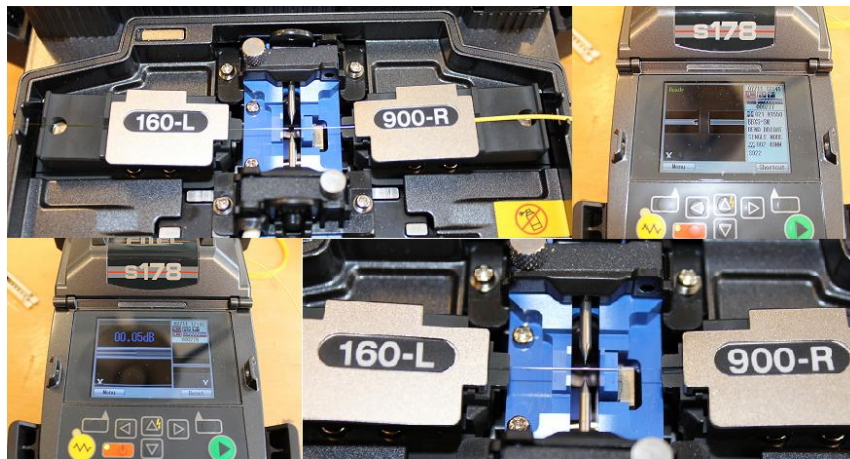
Figure 11: FITEL S178 is used to splice the fiber.

The region surrounding the spliced part of the fiber is then protected by a splice tube. The splice tube of plastic with a metal pin inside is put around the fiber at the spliced region. This is put in the upper chamber on the FITEL S178 where it is heated so that the plastic tube glues onto the fiber. See Figure 12
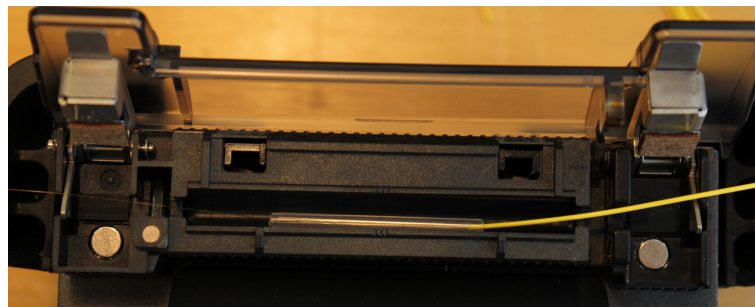
Figure 12: Splice tube is melted on by heat.

A small pouch made of glass fiber lamina is put around the fiber in the transition of the splice tube and the optical fiber. This is done to protect the embedded optical fiber at the part where it enters the joint between the composite and the steel. This is illustrated

in Figure 13
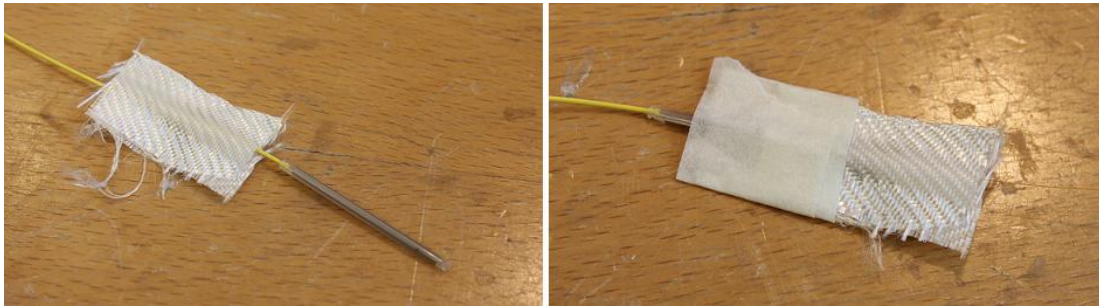
Figure 13: Protective pouch.

The end of the yellow fiber is coiled up and protected between two pads in a small plastic bag, see Figure 14. The bag is closed by tape and two small cuts are made at the end of it to let air out. The bag shall prevent the optical fiber from damage later in the production process. This optical fiber is now ready for further use.
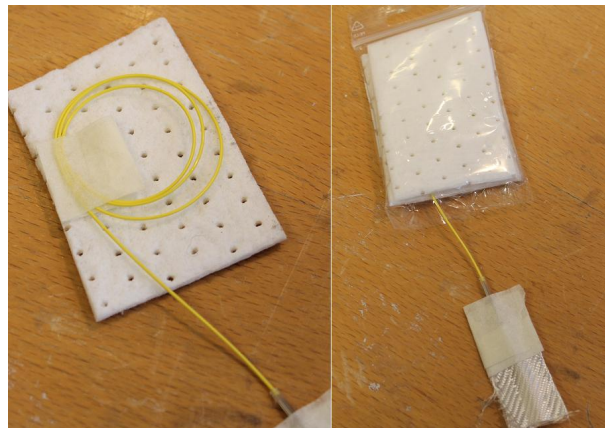
Figure 14: End of fiber coiled up and protected in plastic bag.

4.2.3 IPE100 beam

The IPE 100 beams were cut to a length of 1000 mm. A 6 mm diameter hole was drilled through the web of the beam and broached. The center of the hole was positioned at the middle of the beam's length and 20 mm from the top of the flange. A cut was made through the flange and down the web stopping at the hole drilled. The top of the flange was grit blasted at Asbjørn Krogstad AS and the surface roughness was measured, see Table 3. Next step was to coat the grit blasted area with epoxy and it was left to cure with a peel ply on until the following day, see Figure 15.
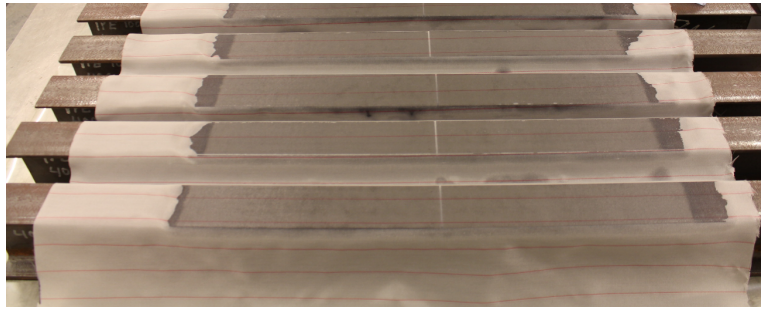
Figure 15: Beams grit blasted and coated with epoxy.

4.2.4   Lay-up of CFRP patch

For the subsequent steps in the production process it was required that vacuum could be applied to the specimens after bagging. In order to achieve this two steel supports with Teflon film was mounted parallel to the flange of the beam. Sealant tape for hot curing was used to seal the gaps between the supports and the beam, in addition, a small piece of vacuum bag was used on each side of the beam below the flange to seal the induced crack, see Figure 16.
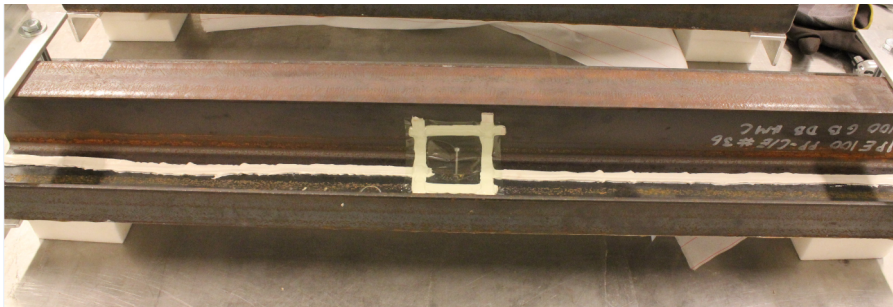
Figure 16: Supported and sealed beam, seen from the bottom.

The grit blasted surface earlier coated with epoxy was wiped off with acetone and a fiber cloth prior to hand lay-up of the ±45 DB810. The epoxy used was Epikote MGS RIMR 135 resin and MGS RIMH 137 curing agent with a mix ratio of 100 weight percent resin and 30±2 weight percent curing agent. A soft paintbrush was used to apply the epoxy, a thin layer was applied prior to placement of the DB810 lamina. The DB810 lamina was then soaked with epoxy before a small paint roller was used to eliminate air bubbles in the lay-up, see Figure 17. Peel ply, release film and breather was put on top of the lamina. This was then sealed with a vacuum bag, connected to the vacuum pump and cured at room temperature for 24 hours.

Unidirectional pre-preg material was thawed and ready for lay-up. The laminate was put together from 17 plies of pre-preg, 9 groups of different lengths from 400 mm to
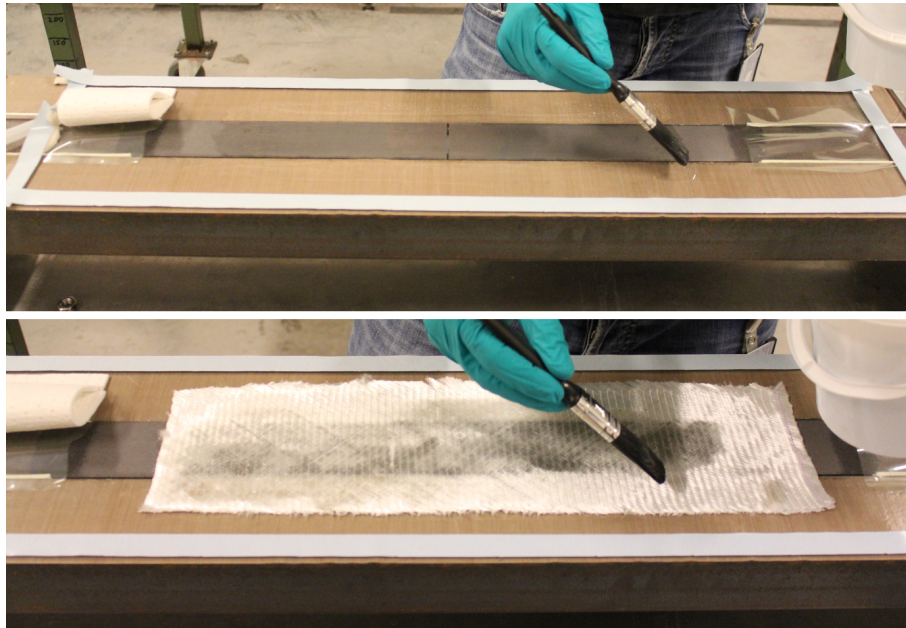
Figure 17: Hand lay-up of DB810.

300 mm, with the first 8 groups having two plies within each group and the last group finishing the laminate with one single ply of the shortest length. The stacking sequence is illustrated in Figure 18
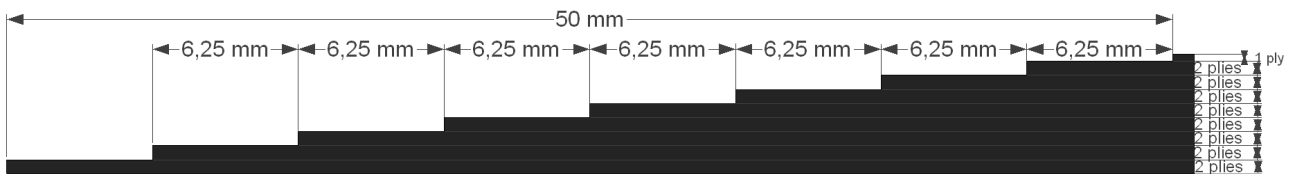
Figure 18: Stacking sequence for the laminate in order to produce a tapering at each end.

Prior to stacking the prepreg laminate, the optical fibers for the adhesive layer were aligned in the longitudinal direction on top of the DB810 layer. For beams with one single optical fiber in the adhesive layer, this was aligned in the center of the beam 27.5 mm from the sides of the flange. Three lengths of the optical fiber was embedded by preparing a fiber that was approximately 1400 mm of length after the splicing tube and protective pouch. This optical fiber was then aligned at the center of the beam over the 400 mm long patch length, 27.5 mm from each side. It was then looped back and aligned 5 mm from the edge of the beam, looped back again and aligned 5 mm from the opposite edge, see Figure 19.

The plies were stacked on top of the optical fibers as described above. Peel ply, release
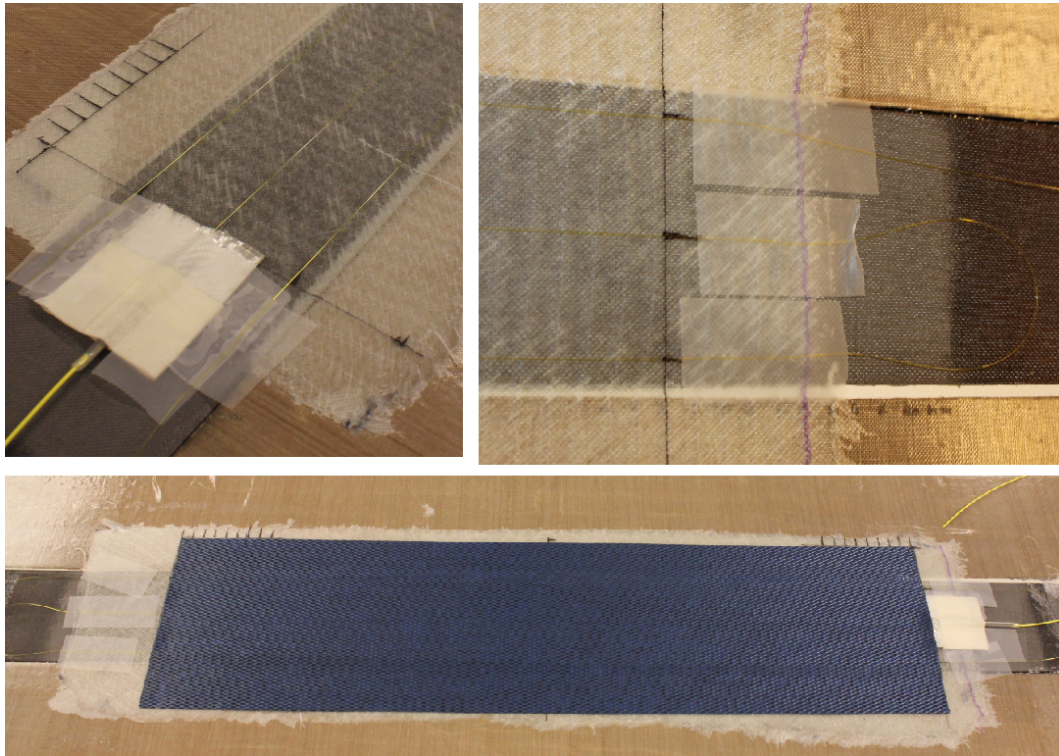
Figure 19: Top: Alignment of three optical fibers. Bottom: First ply of prepreg applied.

film and breather was put on top of the laminate, sealed with vacuum bag and connected to the vacuum pump. The end of the yellow optical fiber was taken out through the sealant tape. Curing was done in an oven at 85°C for 10 hours. Figure 20 shows the patch repaired beam after curing.

After curing the steel supports were dismounted and the excessive width of the composite patch was milled down to the same width as of the IPE100 beam at IPM NTNU.

4.2.5   Instrumentation

Every beam had it's dimensions measured:

- The width and thickness was measured at six spots along the length of the composite patch, this was done on both sides.

- The diameter of the hole and the crack mouth opening on both sides.

- The total length of the beam.

- The length from one end of the beam to both ends of the composite patch, both tapering ends of the patch and to the crack center.
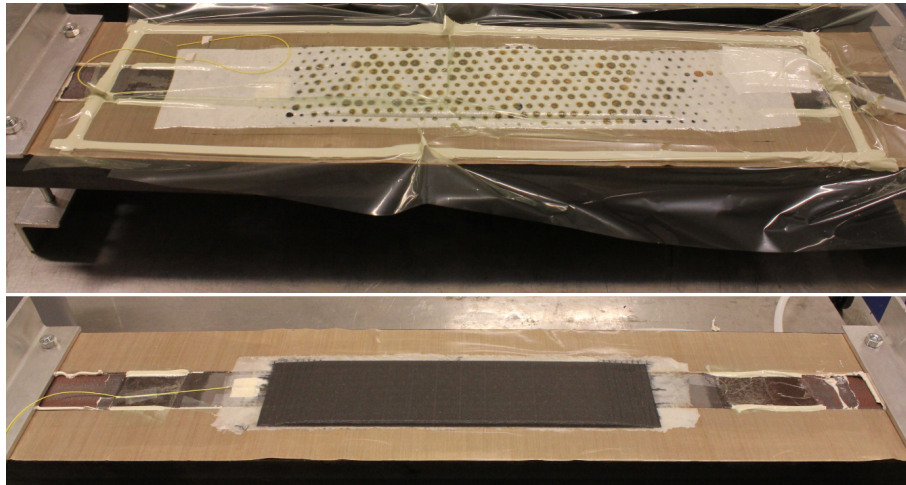
Figure 20: Beam with patch after curing.

Next step was to prepare the beam for instrumentation with three strain gauges in the web, four strain gauges and one optical fiber on top of the composite patch. To ensure adhesion, the areas of the web and patch were slightly sanded with a sanding paper and cleaned with acetone. The optical fiber was spliced to the end of the yellow fiber from the one embedded in the adhesive layer. It was glued along the top of the composite patch, 20 mm from the side, and spliced with a "pig tail" connection that could connect to the Luna OBR 4600. The strain gauges were glued at their positions, illustrated by Figure 8 and 9 in Section 4.1. In order to directly compare the axial strains measured by the OBR and the strain gauges on top of the patch, the strain gauges were placed 20 mm from the opposite side of the optical fiber. Figure 21 and 22 illustrates the instrumentation with strain gauges and optical fiber.
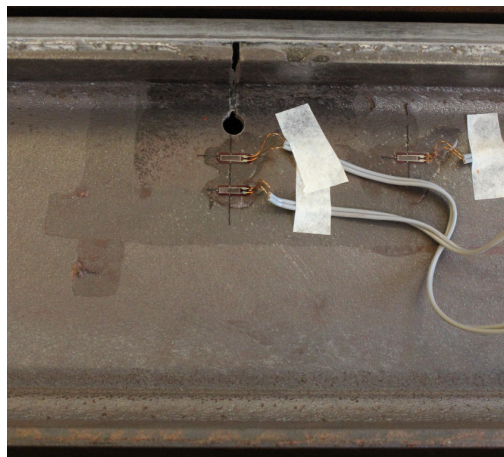
Figure 21: SG 5, SG 6 and SG 7 in the web.
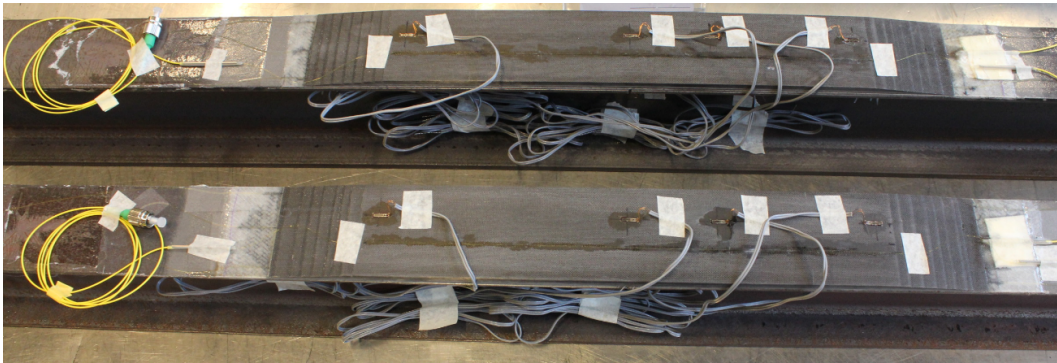
Figure 22: Beams instrumented with optical fiber and strain gauges.

The strain gauges were 5 mm long and their gauge resistance was 120.3±0.5 Ω. Prior to testing each beam had a clip gauge mounted at the crack tip to be able to measure the crack mouth opening displacement (CMOD). White correction fluid was painted on the edges of the beam and the patch along the patch length. The purpose was to make any crack propagation more visible during the testing.

4.2.6   Quality variations

When hand lay-up is used in the production process of the composite laminate factors like temperature, humidity, correct alignment of the fiber and the amount of epoxy added to the lay-up contribute to the end quality of the patch. It can be a challenge to produce adhesive joints under equal conditions and of the same quality every time. The time between grit blasting and epoxy coating of the steel surface is also critical in order to prevent corrosive initiation on the steel surface.

The picture in Figure 23 was taken during the production process. It shows the DB810 galvanic protection layer applied and cured to beam number 36 and 37. Beam 36 is in the top of the picture and beam 37 is in the bottom part of the picture. It can be observed that there is a larger amount of epoxy permeated in the galvanic protection adhering it to the steel for beam 37 than 36. The layer of beam 36 is not as transparent and looks less saturated with epoxy than the case of beam 37. A laminate has to be saturated with epoxy to ensure proper adhesion to the steel. A laminate not saturated will experience voids in the material, with air pockets making the material brittle and reducing the adhesion to the steel. This illustrates how the quality of a hand lay-up can differ.

Figure 23: Beam 36 in top part of picture, beam 37 in the bottom part.

The beams of IPE100 PP C/E 400 GB SA UHMC and IPE100 PP C/E 400 GB SA PP UHMC were produced prior to this thesis using the co-cure technique[3, 11]. Hand-lay up is avoided using this technique. These patches are produced using pre-preg materials only, and the whole patch is stacked on top of the steel in one production session and cured to the steel in the oven. The probability of achieving a high quality patch is higher using this technique and pre-preg materials only.

Beam	Mean [μm]	Standard deviation [μm]
IPE100 PP C/E 400 #32 GB DB UHMC	91.30	26.61
IPE100 PP C/E 400 #33 GB DB UHMC	140.93	18.60
IPE100 PP C/E 400 #34 GB DB HMC	95.68	24.64
IPE100 PP C/E 400 #35 GB DB HMC	143.20	26.92
IPE100 PP C/E 400 #36 GB DB HMC	87.63	24.22
IPE100 PP C/E 400 #37 GB DB HMC	85.95	20.70

Table 3: Measured surface roughness of beams.

5 Testing

5.1 Four point bend test

The beams were tested in a four point bend test at IPM NTNU. The test machine used had a load capacity of 250 kN and was controlled by an Instron controller.
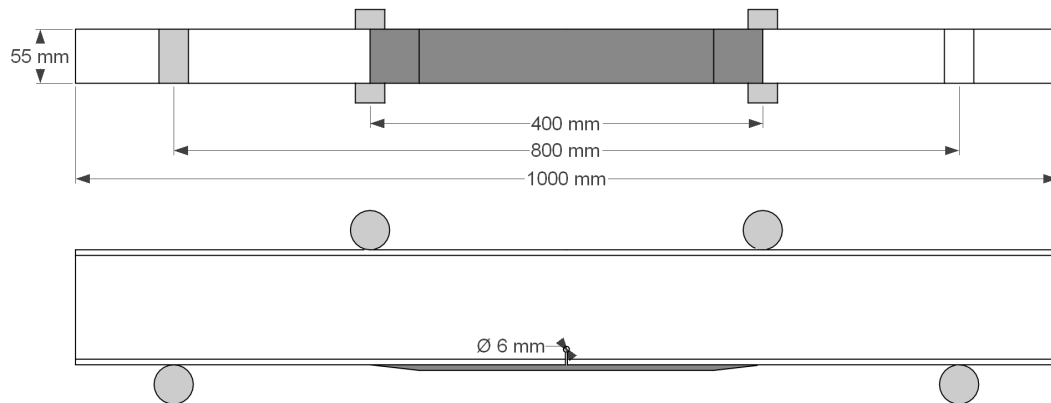
Figure 24: Illustration of the setup of the four bend test.

The beam was mounted in the four point bend test with the crack and patch facing downwards. The load span had a width of 400 mm, equal to the patch length, and the position of the points of load were 300 mm from each end of the beam. The support span had a width of 800 mm, with each support being 100 mm from its adjacent beam end. This is illustrated in Figure 24. The actual setup is shown in Figure 27. The four point bend test has been described and used in other articles[13, 14]. There are a constant moment between the two load spans in a four point bend test. With small displacements at the center of the beam, the test will only produce mode II-loading, see Figure 25.
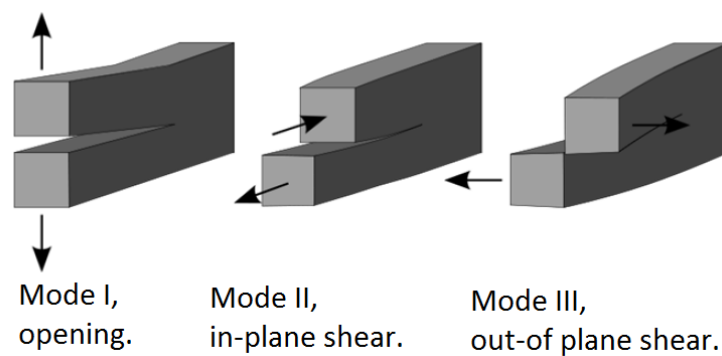
Figure 25: Fracture modes. Figure adapted from [15].
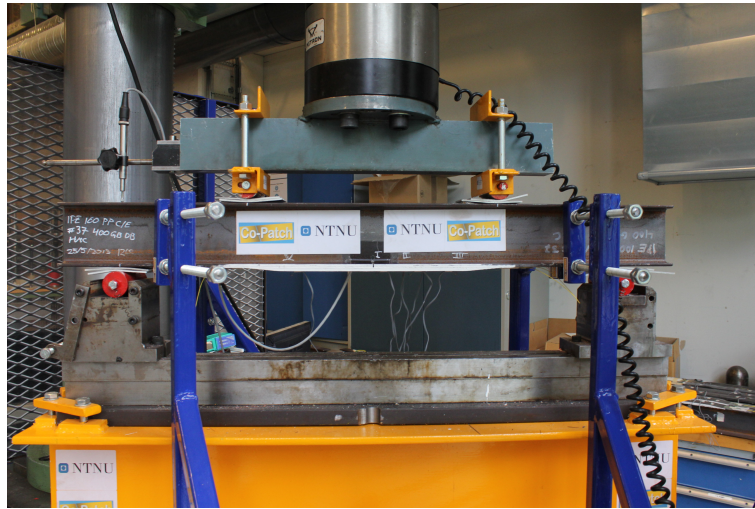
Figure 26: Actual setup of the four point bend test at IPM NTNU.

5.2 Test procedure

The seven strain gauges, the CMOD and a LVDT placed in a vertical position above the support span were connected to a computer. Signals from the Instron machine giving load, displacement and number of cycles from the test machine were also connected to this computer. The digital acquisition software CatmanEasy was used to record the data from these instruments at a sample rate of 50Hz.

The optical fiber was connected to the Luna OBR 4600 and two reference scans were made while the beam was unloaded. A reference scan to find the center position of the patch along the optical fiber on top of the patch was made. It was done by pressing an ID-card against the optical fiber at the position corresponding to the center of the crack, adjacent to SG 1.

Fatigue test procedure for the beam:

- The beam was loaded in displacement control at a rate of 0.3 mm/min from 0 to 100 kN. The strain in the optical fiber was measured by doing a scan with the OBR for every 10 kN increase in load, including a scan at 55 kN.

- When reaching the load of 100 kN, load control was introduced.

- 55 kN was set as a set point for the load and cyclic load with an amplitude of 45 kN and 2 Hz was applied. Meaning the load cycled between 10 kN and 100 kN.

- The test was set to run for any given number of cycles and the load was put to hold at the set point of 55kN when that number of cycles was reached.

- A measurement with the optical fiber was done every time the beam was put to hold at 55 kN.

Each different patch configuration was made in batches of four beams. One of the four specimens from each batch was run in a static test before tested in fatigue. This followed almost the same procedure as described above. It was loaded in displacement control at the same rate of 0.3 mm/min until the max load the beam could hold was reached. This was usually about 160-165 kN. The beam was now yielding and the load started to drop. It was put in displacement control at the same rate but in the opposite direction until the load had decreased to 55 kN. It then followed the same procedure as the fatigue test with cyclic load.

An external computer running a LabView script was used to tell the Luna OBR 4600 when to perform a scan of the optical fiber. In this script it was also defined where to save the data files and what prefix the data files should be given. In a test series, these files would be given an individual number after the file prefix, beginning with 1 for the first file, 2 for the second file and so on. A spreadsheet was made for each beam tested in order to keep track of these files and to the corresponding number of cycles and/or what load they were measured at.

The data recorded in the CatmanEasy software was visualized on the computer screen. By monitoring this visualization, changes in the measured data could be interpreted and it could to some extent be predicted if the test was approaching failure.

Figure 27: Actual setup of the four point bend test at IPM NTNU.

5.2.1   Failure modes

Figure 28 illustrates different failure modes that adhesive joints are exposed to.
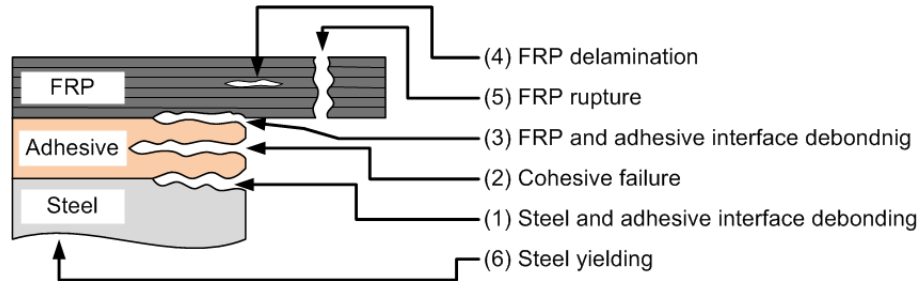
Figure 28: Failure modes for adhesive joints. Drawn by J.H.L. Grave.

Different failure modes observed during the fatigue testing of the patch repaired beams were debonding between the steel and adhesive interface, cohesive failure in the adhesive layer and delaminations in the CFRP patch.

6 Finite element analysis

6.1 Geometry and boundary conditions

One quart of the beam geometry was modelled using Abaqus 6.12-1. Three individual parts were modelled, the beam, the DB810 layer and the CFRP laminate. Each part was modelled in 3D Modeling Space using deformable solid shape and extrusion. The solid for the DB810 layer had a thickness of 0.6 mm. The carbon fiber laminate had a thickness of 5.1 mm and the tapering was identical to the geometry showed in Figure 18 in Section 4.2.3. The longitudinal direction of the beam was along the Z-axis, with Z=0 mm being the center of the beam and Z=-500 mm being the end. The height direction was in Y-direction.

A circular hole of 6 mm diameter was cut through the web of the beam in X-direction, with the center of the hole being 17 mm below the top flange at Z=0. The crack was made by a 1 mm cut extrude from the center of the hole to the top flange in the negative Z-direction.

Partitions were made at the tapered end of the patch, the ends of the radius between the flange and the web of the beam and around the hole terminating the crack.

The parts were connected together using tie constraint between each surface. In addition, hard contact interaction was used for the area close to the crack tip between the DB810 and beam. This prevented the parts from moving into each other when deformed. See Figure 31. Symmetry with XSYMM and ZSYMM was added as boundary condition, see Figure 29.
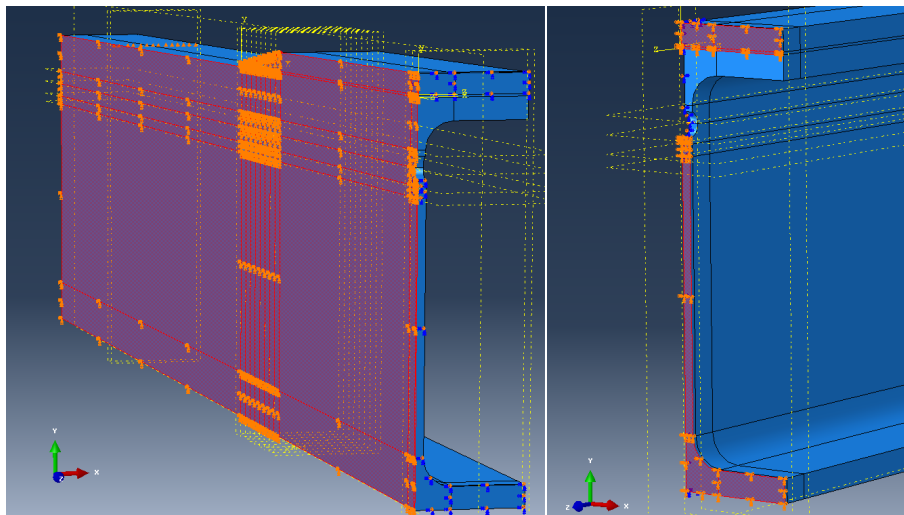
Figure 29: Symmetry condition applied to X and Z direction.

A set of nodes was made at the position of the support span on the beam flange at Z=-400 mm, these were constrained in the Y-direction with U2=0. The load was applied in the Y-direction to a set of nodes on the beam flange opposite of the support span at Z=-200 mm. See Figure 30.
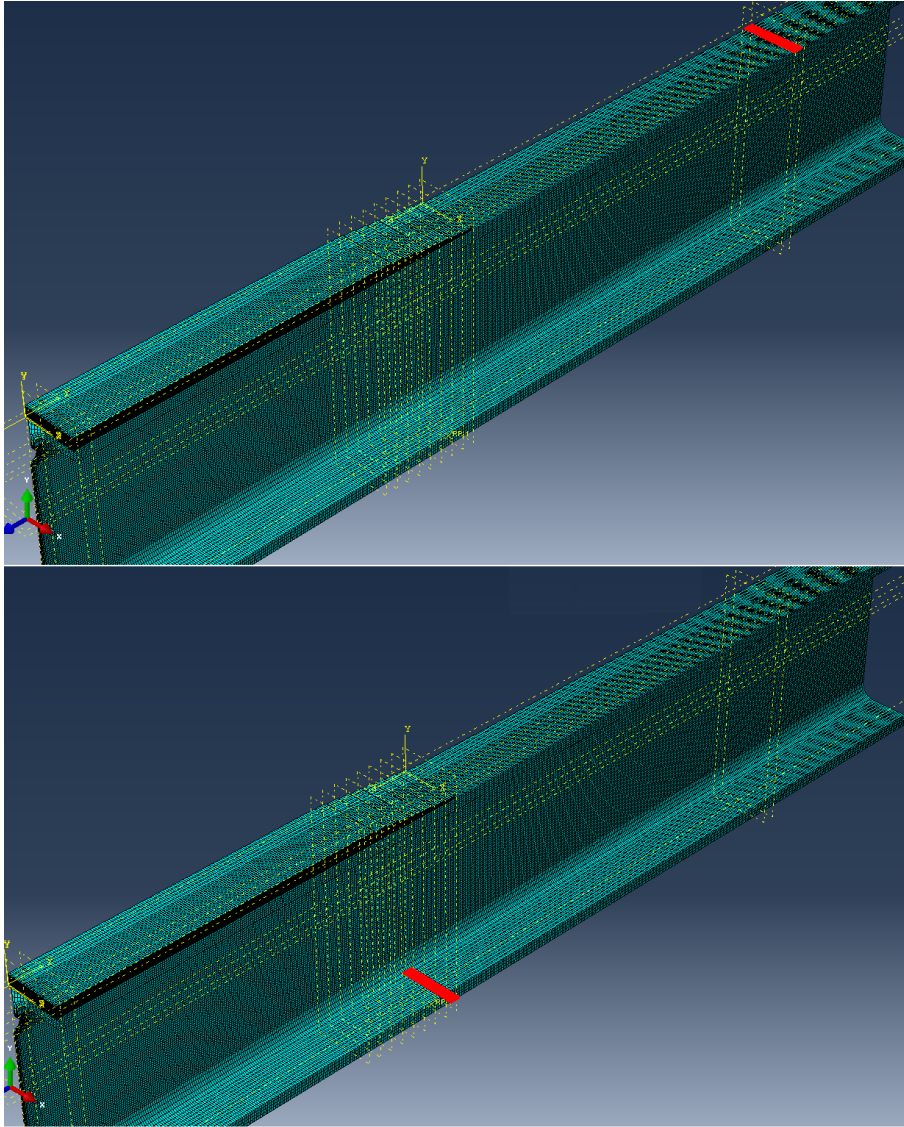
Figure 30: Nodes for support span in top and nodes for load span in the bottom.
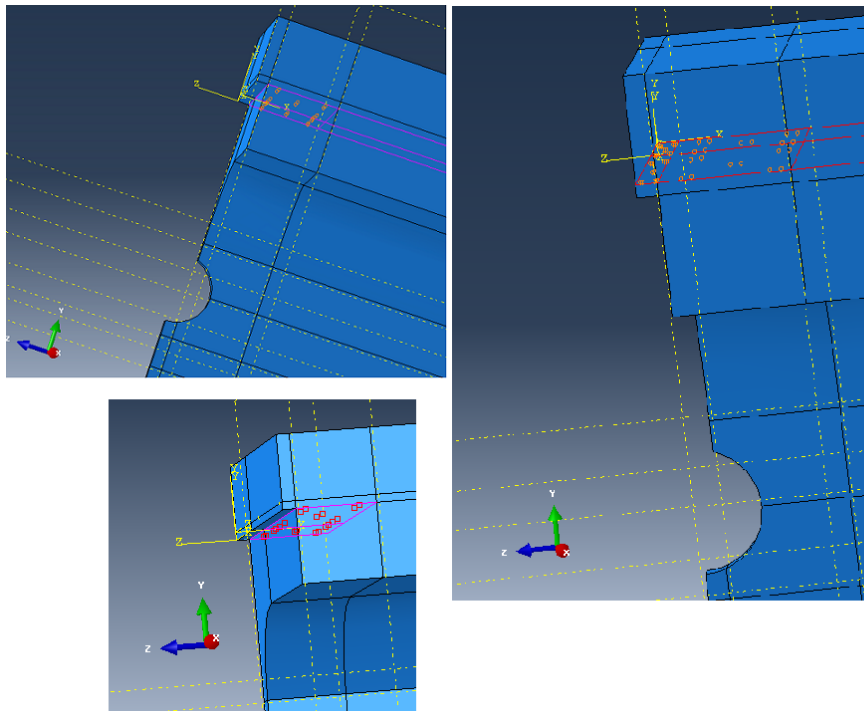
Figure 31: Top: Tie constraint between DB810 and beam. Right: Tie constraint between carbon fiber patch and DB810. Bottom left: Hard contact interaction between DB810 and beam.

6.2 Elements and mesh

The model was meshed using linear hexahedral elements of type C3D8R, the total number of elements was 361 414. The mesh was verified and no warnings or errors were found. More details for each instance are presented in Table 4.

Part instance	Number of elements	Average aspect ratio	Worst aspect ratio
Beam	275 589	1.89	6.05
Carbon fiber laminate	75 825	3.88	6.03
DB810	10 050	3.89	6.03

Table 4: Results from verifying of the mesh.

6.3 Materials

A composite layup with two plies was assigned to the DB810 solid part, one ply in +45 direction and one ply in the -45 direction. The material data for DB810 was assigned to

this composite layup. Solid, homogeneous sections with the material properties for for each material were assigned to the HMC, UHMC and steel solid. The material data for the composites are presented in Table 5 and the material used for the steel are the same as presented in Table 2 in Section 4.2.1.

Material	E1	E2	E3	ν_{12}	ν_{13}	$\nu23$	G12	G13	G23
HMC	199400 MPa	6500 MPa	6500 MPa	0.35	0.35	0.5	4500 MPa	4500 MPa	1500 MPa
UHMC	231900 MPa	6500 MPa	6500 MPa	0.31	0.31	0.5	4500 MPa	4500 MPa	2000 MPa
DB810	39000 MPa	8600 MPa	8600 MPa	0.28	0.28	0.5	3800 MPa	3800 MPa	1267 MPa

Table 5: Material data used for the composite materials. Taken from [12].

6.4 Analysis

Load was applied to the load node set. This was done with the use of a reference point with an equation constraint to these nodes. For 55 kN load, 12 500 N was applied. For 100 kN, 25 000 N was applied. For the steps in the analysis the initial increment size was 0.01, with a minimum 1E-08 and a maximum of 1.

When the job completed, two paths were created to extract the strain along the top of the patch and in the adhesive layer. A path was made in the nodes on top of the patch, ≈20 mm from the outer beam edge, see Figure 32. The other path was created along the bottom nodes at X=0 in the CFRP part of the patch, see Figure 33. The axial strain in E11 direction was plotted together with the true distance in undeformed shape along the paths. These results were used in the comparison with the optical fibers from the experimental test.
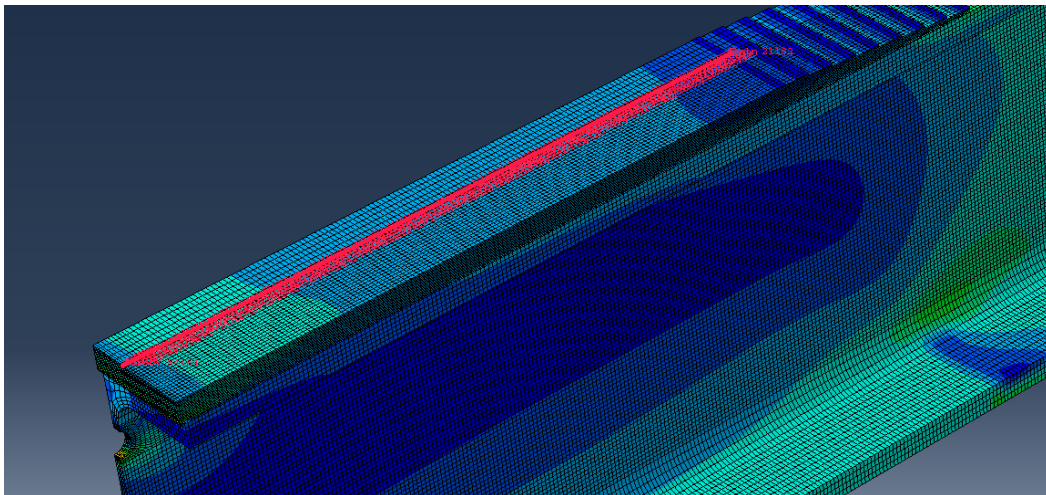
Figure 32: Path along nodes on top of the patch.
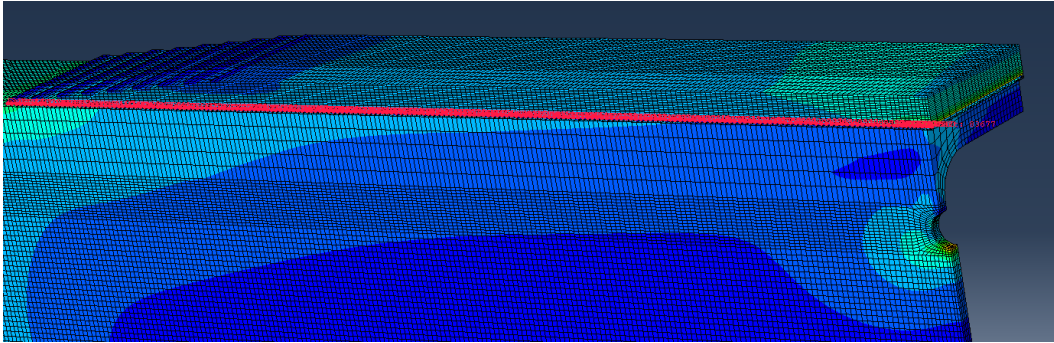
Figure 33: Path along the adhesive layer of the patch.

7 Results

The results from the testing of 11 different patch repaired beams are presented. Table 6 shows the number of cycles at failure for each beam.

Beam	Cycles at failure	Static tested? (Y/N)
IPE100 PP C/E 400 #17 GB SA UHMC	262 479	Y
IPE100 PP C/E 400 #21 GB SA PP UHMC	321 000*	Y
IPE100 PP C/E 400 #22 GB SA PP UHMC	298 120	N
IPE100 PP C/E 400 #27 GB DB UHMC	1 235	N
IPE100 PP C/E 400 #28 GB DB UHMC	2 560	N
IPE100 PP C/E 400 #32 GB DB UHMC	6 640	N
IPE100 PP C/E 400 #33 GB DB UHMC	13 650	N
IPE100 PP C/E 400 #34 GB DB HMC	7 966	Y
IPE100 PP C/E 400 #35 GB DB HMC	10 691	N
IPE100 PP C/E 400 #36 GB DB HMC	14 741	N
IPE100 PP C/E 400 #37 GB DB HMC	67 620	N

Table 6: Number of cycles at failure. (*Manually stopped before complete failure.)
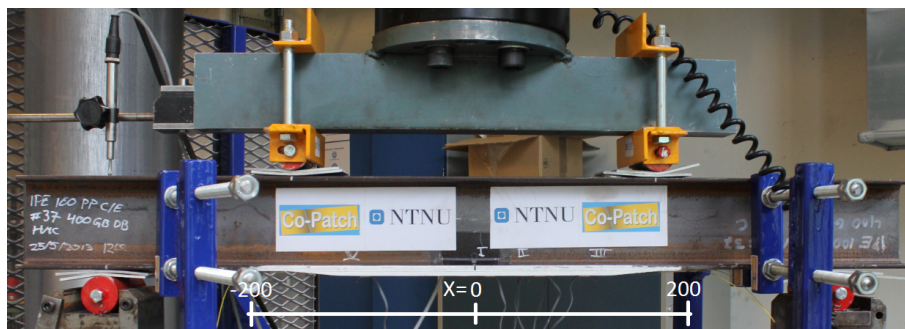
Figure 34: Definition of the x-axis used to present the results.

The graphs presenting the results have strain on the y-axis and length along the composite patch in [mm] on the x-axis. The x-axis along the composite patch is defined as in the picture in Figure 34. With X=0 mm being the center of the patch and the crack mouth opening. With this angle of view X=200 mm at the right end of the patch and X= -200 mm at the left end of the patch. The patch top is facing downwards. "Front edge fiber" is the optical fiber embedded 5 mm from the edge closest to the camera. "Back edge fiber" is the optical fiber embedded 5 mm from the edge furthest away from the camera. When referring to images, "front" is used for a view of the beam from the side viewed in Figure 34 and "back" is used for images taken from the opposite side of the beam.

It is important to keep in mind when reading the results that the strain values are in

microstrain. It means that a small difference in the results might look bigger than what it really is.

As described in Section 3 it can be chosen a gauge length and sensor spacing that the OBR software shall use to calculate the strain. The results presented are calculated with a gauge length of 0.5 cm and a sensor spacing of 0.1 cm.

Matlab scripts were written in order to extract the relevant data and to compare and plot different results in graphs.

7.1 Comparison of FE analysis and experimental results

The strains measured by the embedded optical fibers were compared with the strains from the finite element analysis(FEA) along the corresponding path. The strain from the center fiber was used for those beams having three embedded fibers. The strains on top of the patch measured by the optical fiber were compared with the FEA and the strains measured by the corresponding strain gauges. Data come from the measurements done at 55kN and 100kN during load with displacement control prior to the cyclic load. This was plotted together in graphs and presented in the following figures.
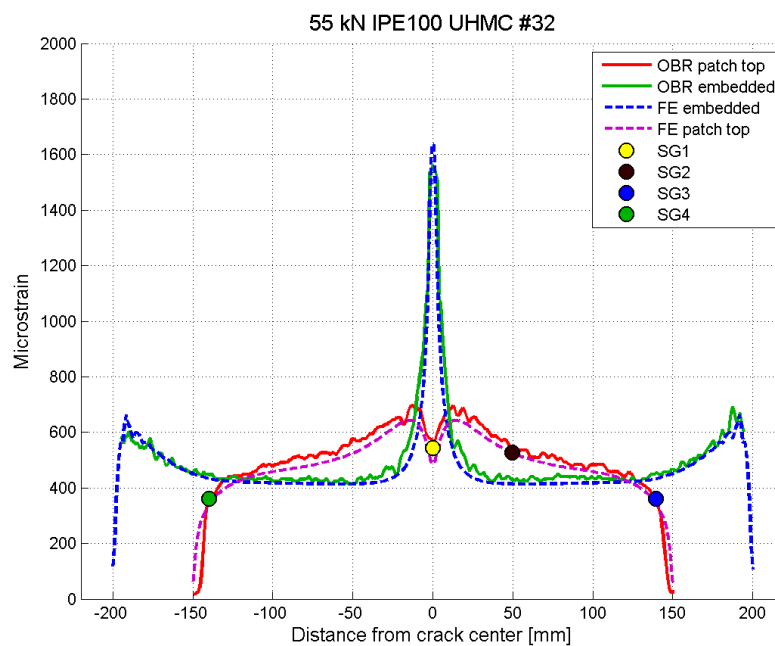
Figure 35: Comparison of OBR, FEA and strain gauges at 55 kN load. Beam 32.
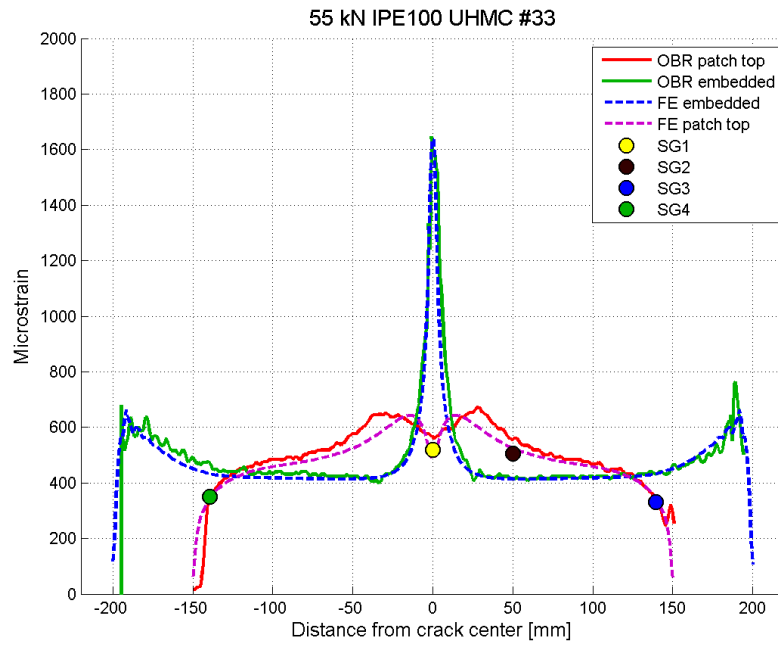
Figure 36: Comparison of OBR, FEA and strain gauges at 55 kN load. Beam 33.
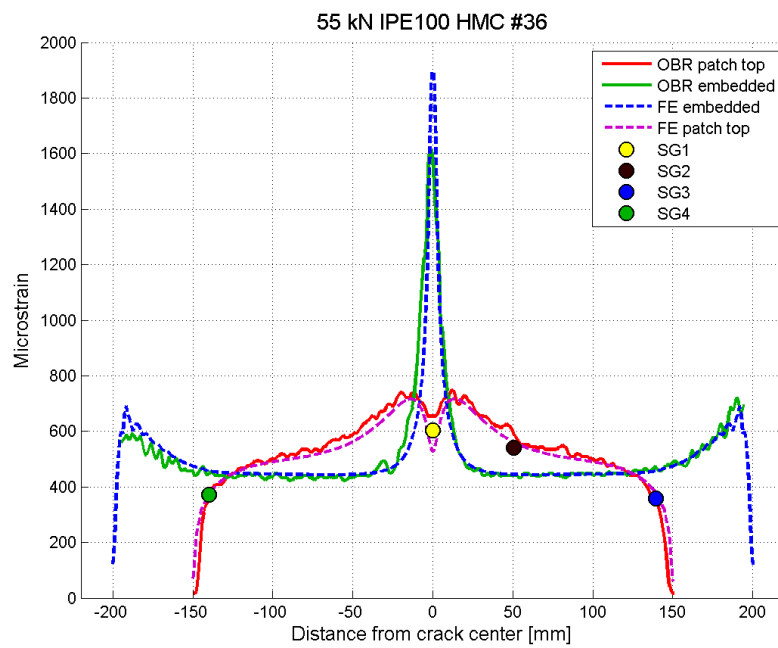
Figure 37: Comparison of OBR, FEA and strain gauges at 55 kN load. Beam 36.

Results presented in Figure 35, Figure 36 and Figure 37 are good examples of how well the results from the OBR, FEA and strain gauges coincide at a load of 55 kN for beams with both UHMC and HMC material.
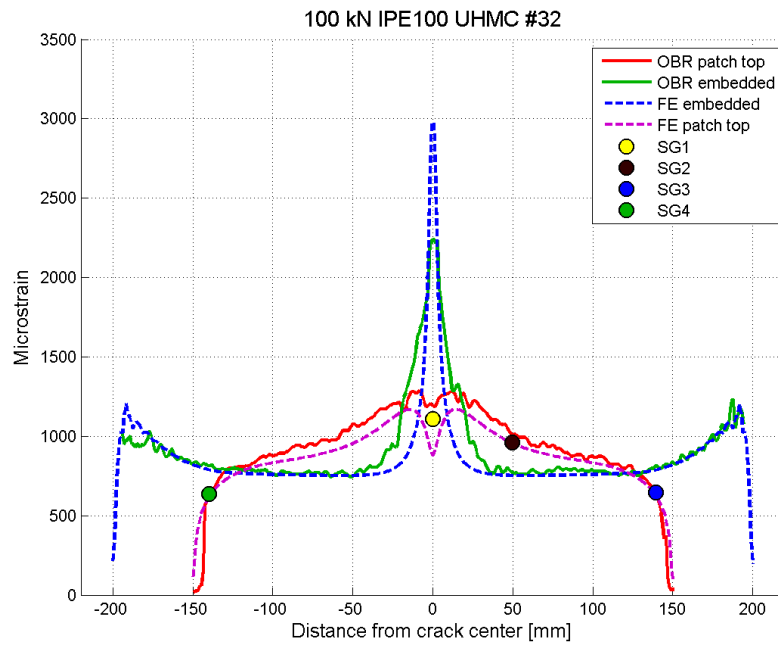
Figure 38: Comparison of OBR, FEA and strain gauges at 100 kN load. Beam 32.
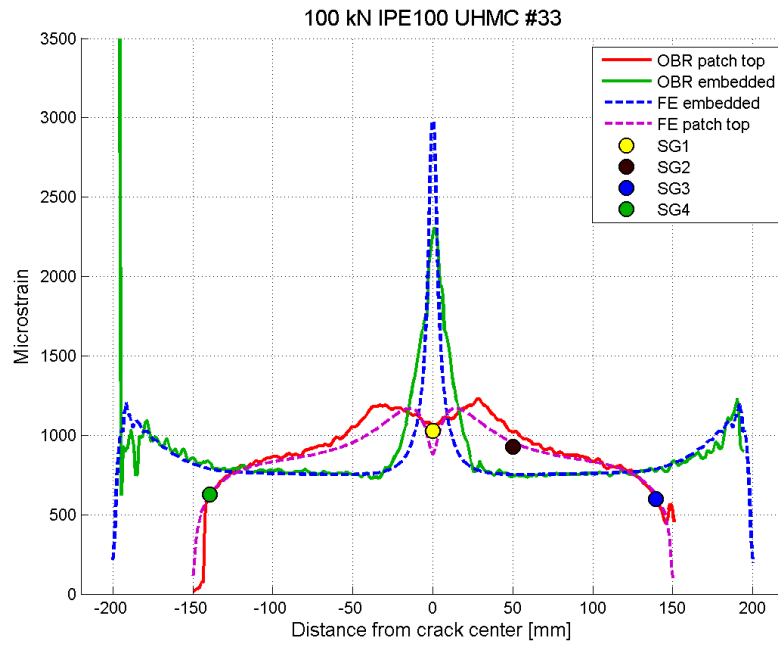
Figure 39: Comparison of OBR, FEA and strain gauges at 100 kN load. Beam 33.

Results at the load of 100 kN differ slightly more but are still very good. As seen in Figure 38 and 39 at the center of the patch, the strain peak in embedded fiber and the strain valley at the patch top differs a bit more between the FEA and the experimental results at 100kN than 55 kN.
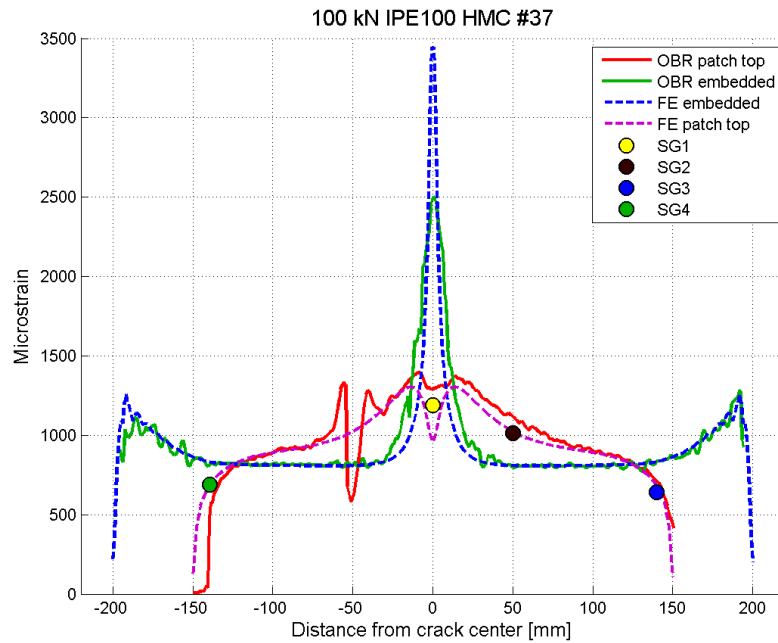
Figure 40: Comparison of OBR, FEA and strain gauges at 100kN load. Beam 37.

For beam number 37 presented in Figure 40 an irregularity occurs in the strain measured by the optical fiber on the patch top at a distance -50mm from the crack center. This is due to insufficient adhesion between the optical fiber and the composite patch at this particular point, accordingly the strain measured there is not correct. At this irregularity the area under the curve seems to equal the area over the curve, indicating that the average of these curves probably would align correctly with the rest of the strain curve.

More results are presented in Appendix A.

7.2 Comparison of strain gauges and optical fibers during fatigue life

Presented next are the results of the strain measured on top of the patch with the optical fiber and the strain gauges. The purpose is to see if the optical fibers measures the same as the strain gauges and how the optical fiber behaves during fatigue testing.
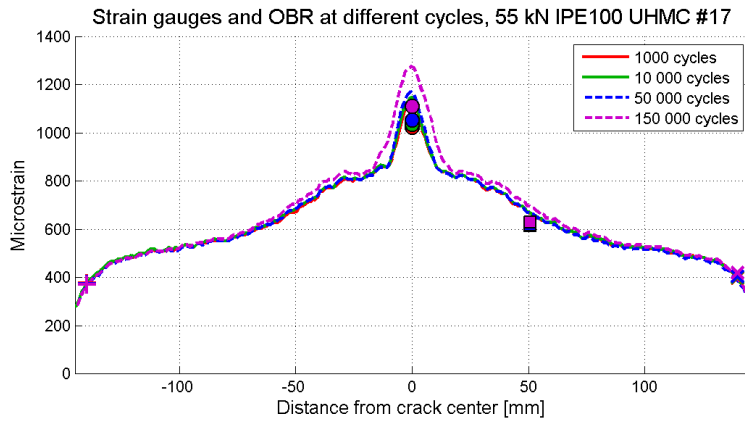
Figure 41: Comparison of OBR and strain gauges at different cycles, beam 17.
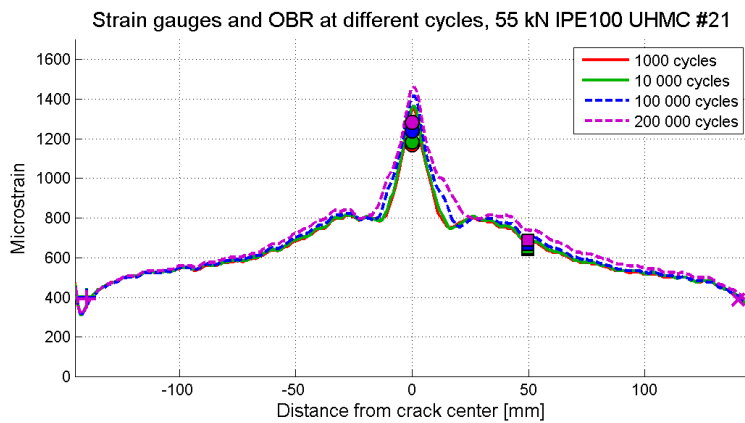
Figure 42: Comparison of OBR and strain gauges at different cycles, beam 21.
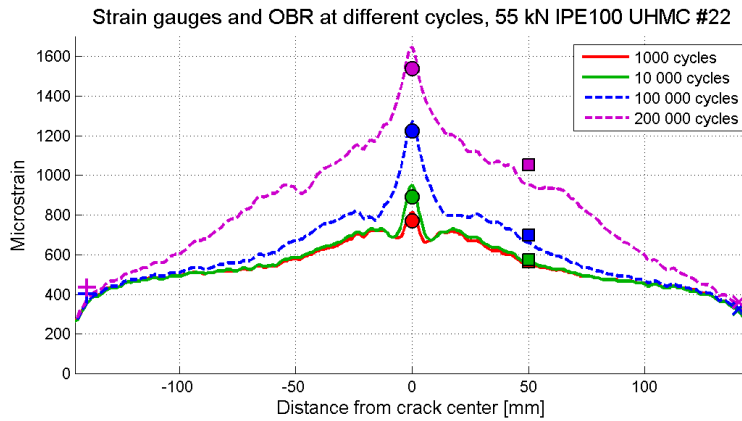
Figure 43: Comparison of OBR and strain gauges at different cycles, beam 22.

The results presented in all of these figures show that the optical fibers coincide very well with the strain gauges. For beam 17 and 21 in Figure 41 and Figure 42 the strains measured by the optical fiber at the positions of SG1 and SG2 at 0 mm and 50 mm are slightly higher than the strain gauges. But at the same time the increase in strain between each cycle measured is close to the same for the fiber and the strain gauges.

For beam number 22, Figure 49, the difference in the strain measured between each cycle is much greater than what seen for beam 17 and 21. Despite this, the accuracy between the optical fibers and the strain gauges is very good. And these results show no indication of the high number of cycles affecting the optical fibers ability to measure the correct strain. The reason for the big changes in the strain curve on top of the patch for beam 22 is due to damage propagating in the adhesive layer, and will be further explained in Section 7.3.

7.3   Optical fibers and damage propagation

Here results from the strain measurements done with the optical fibers during fatigue testing of the beams are presented. Some specimens have more interesting results than other and will be given a more detailed presentation. The results found from the analysis of the data measured by the optical fibers will be compared with damage propagation detected by visual inspection during testing.

IPE100 PP C/E 400 #21 GB SA PP UHMC
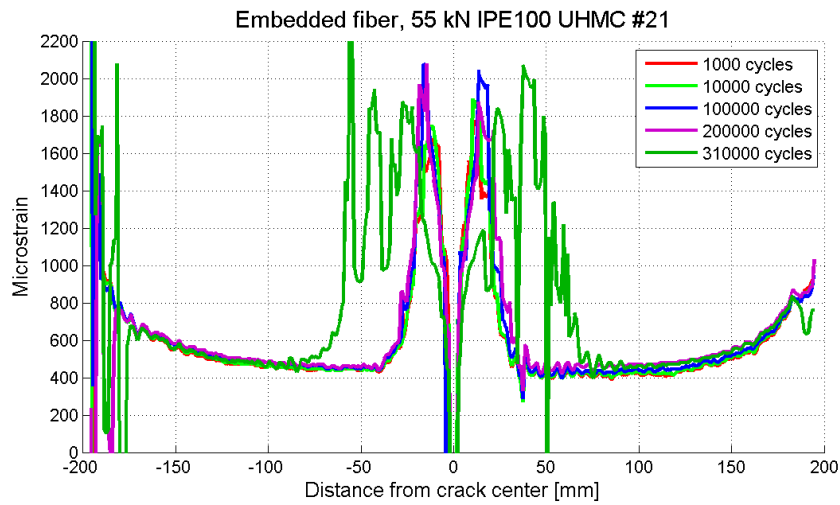
Figure 44: Embedded optical fiber at different cycles, beam 21.
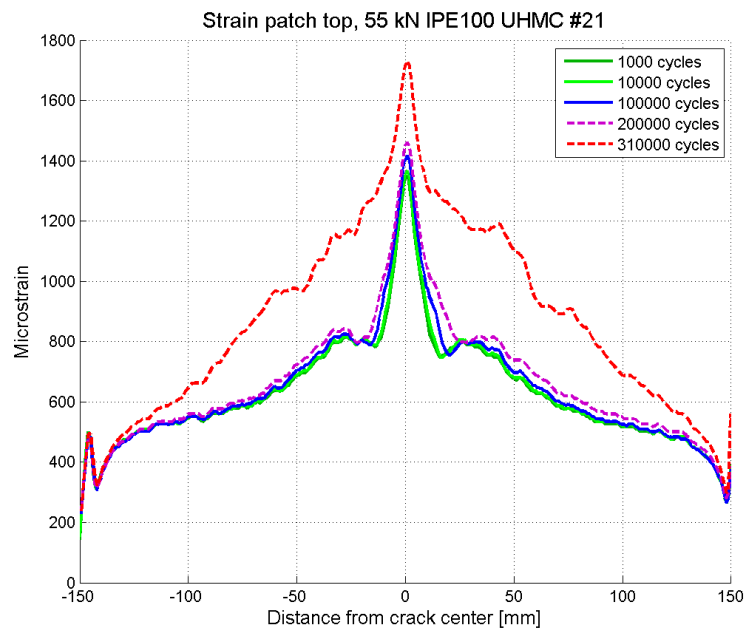
Figure 45: Optical fiber patch top at different cycles, beam 21.

This beam was not tested until failure, it was stopped after 321 000 cycles and dismounted. At this point the measurements from the embedded fiber experienced a lot

of noise, good measurements were only given by the fiber along the patch top. From Figure 44 and 45 it can be seen that the condition of the joint remains about the same with small to no damage propagation for up to 200 000 cycles. At 310 000 cycles the front of the strain curve in the embedded fiber shifts away from center on both sides. It indicates a debonding or a cohesive damage propagating in the adhesive layer between the CFRP patch and the steel. This is moving from the center of the beam towards both ends. At 291 998 cycles this damage from the center is detected by visual inspection, seen in Figure 46 and Figure 47. The lengths of the observed cracks from the center towards the ends are presented in Table 7. These values are given in mm from the center along the x-axis.

The changes indicated by the embedded fiber can also be found in the strain curve on top of the patch. In Figure 45 the strain increases a lot between 200 000 and 310 000 cycles on top of the patch. The slope of the curve also seems to be changing a bit, having a steeper curve towards the ends. This can be related to the damage propagating from center of the adhesive layer. As the damage propagates from center in the adhesive layer, the stress distributed in the patch above this damaged area increases and so does the strain on top of the patch.

Number of cycles	Back [mm]	Front [mm]
291 998	-20 and 55	-40 and 16
321 000	-42 and 67	-69 and 25

Table 7: Measured debond length from center in x-direction, beam 21.

Figure 46: Damage propagation from center towards both ends. Front of beam 21.

Figure 47: Damage propagation from center towards both ends. Back of beam 21.

IPE100 PP C/E 400 #22 GB SA PP UHMC
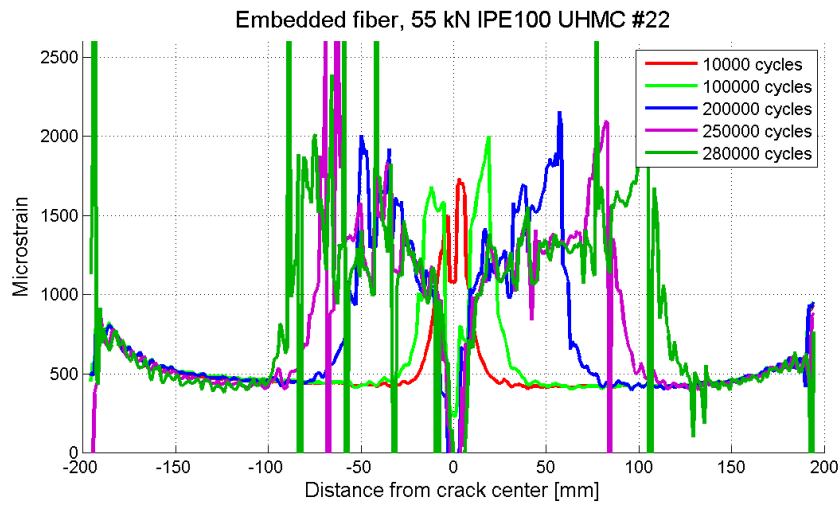
Figure 48: Embedded optical fiber at different cycles, beam 22.
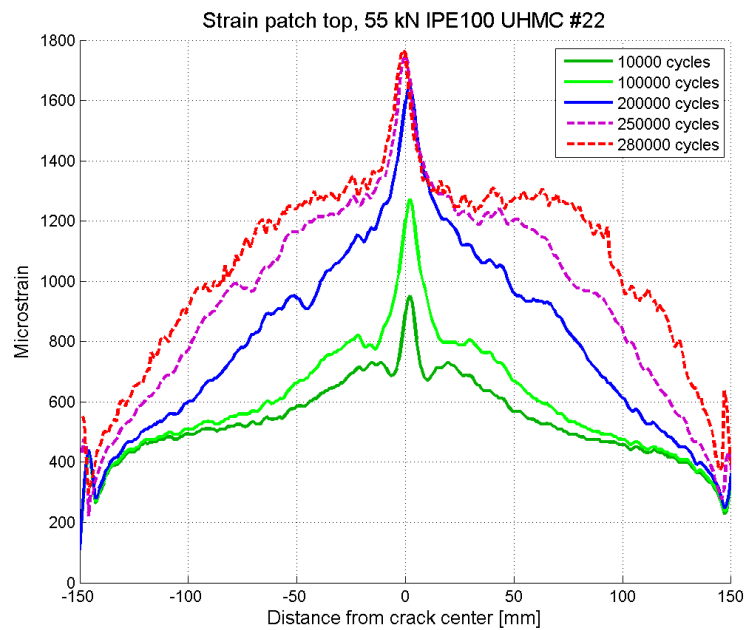
Figure 49: Optical fiber patch top at different cycles, beam 22.

As seen in Figure 48 and 49 the damage propagation here is very similar to that explained of beam 21 above. They have the same composite patch configuration but the damage

propagation from center occurs earlier and at a faster rate for this specimen than what seen for beam 21. The strain on top of the patch increases as the damage in the adhesive layer is reaching closer to the patch ends. At 280 000 cycles the length of the damage in the adhesive layer is longer to the right side than the left. This can compared with the strain in top of the patch, where the length of the plateau in the strain curve from center is longer to the right side. When the test reaches a high number of cycles, the noise in the results from the embedded fiber increases but it is still possible to detect the length of the propagated damage.

An interesting result for both beam 21 and 22 was that the crack tip in the web of the beam started to grow up the web. This was detected by visual inspection at 90 000 cycles for beam 21. Figure 50 shows a picture of how long this crack had propagated up the web at 270 000 cycles. This indicates that the repair with the composite patch does not give enough load reduction to prevent the crack in the beam from propagating in the web.

Prior to failure, a delamination in the top groups of UHMC plies occurred closest to the front from the right side of the beam. This delamination can be seen in the Figure 51. Some values for the measured crack length by visual inspection are presented in Table 8.
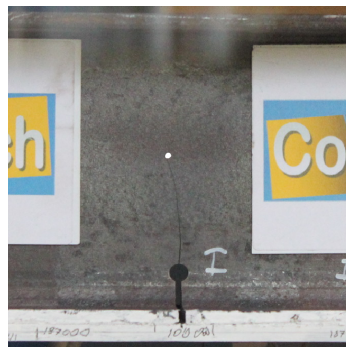
Figure 50: Crack propagation in the web, beam 22.
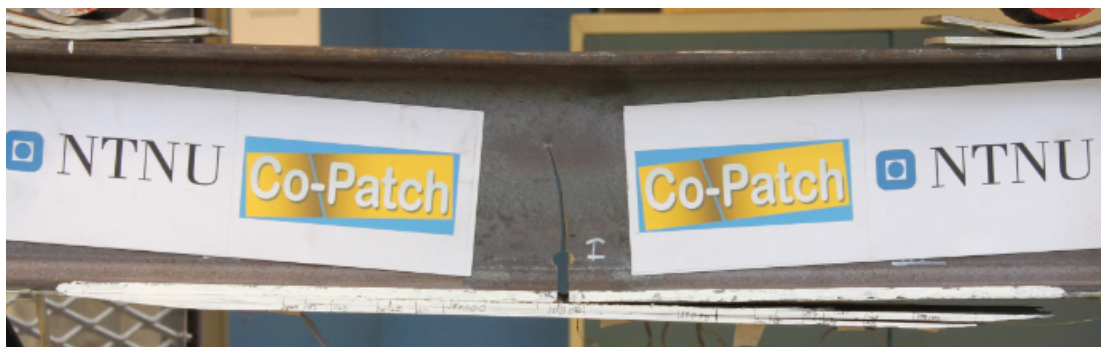
Figure 51: After failure, beam 22.

Number of cycles	Back [mm]	Front [mm]
187 000	-18 and 40	-47 and 64
245 000	-57 and 53	-74 and 88
285 000	-75 and 95	-102 and 111
298 100	-75 and 140	-111 and 144

Table 8: Measured crack length from center in x-direction, beam 22.

IPE100 PP C/E 400 #27 GB DB UHMC

Figure 52: Embedded optical fiber at different cycles, beam 27.
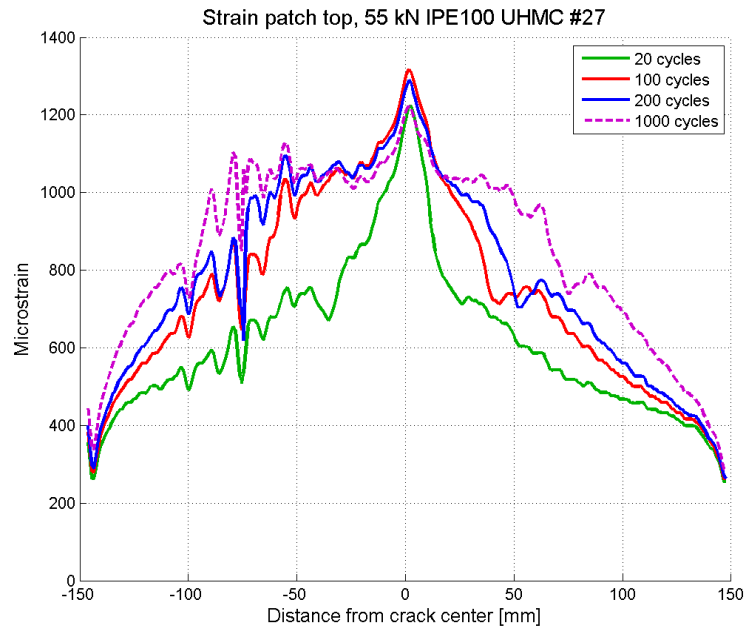
Figure 53: Optical fiber patch top at different cycles, beam 27.

The beam failed at only 1235 cycles. From Figure 52 and 53 it is seen that the damage propagates from the center towards the ends. The measurements show that the damage grows faster to the left side and the patch does fails on the left side.

IPE100 PP C/E 400 #28 GB DB UHMC

Figure 54: Embedded optical fiber at different cycles, beam 28.

Figure 55: Optical fiber patch top at different cycles, beam 28.

The measurements with the embedded fiber are not very accurate at the end of the left side in the patch, but the moving front of the strain curve due to damage propagation

in the adhesive layer can still be detected. A too short length of the remaining optical fiber going out of the patch can contribute to these inaccurate measurements due to reflections at the end of the fiber. The damage propagates faster to the right side and the beam fails due to cohesive damage.

IPE PP C/E 400 #32 GB DB UHMC

Figure 56: Embedded optical fiber at different cycles, beam 32.
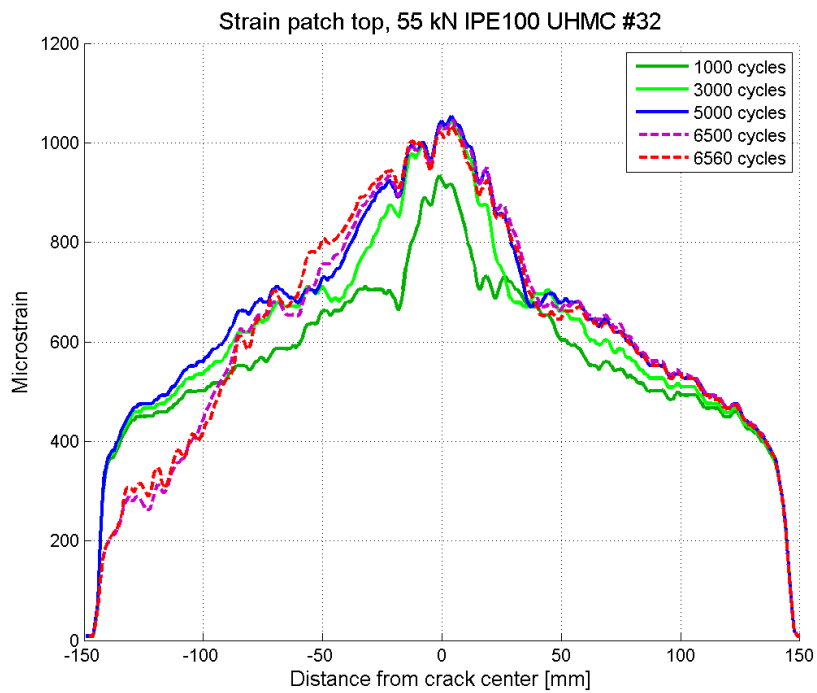
Figure 57: Optical fiber patch top at different cycles, beam 32.

From Figure 56 it can be seen that damage propagated from both center and from left side of the patch. The front of the strain curve shifts from center and towards the patch ends. This indicates a debonding or a cohesive damage propagating in the adhesive layer. The length of the damage can be seen as the length the front of the strain curve has moved. The curve moves faster towards the left side and the length of the damaged area towards the right side stays constant after 5000 cycles.

From the left side there is a small decrease in the strain at 3000 cycles. This has decreased further at 5000 cycles and at 6500 cycles the curve has moved much closer to the center. The strain in the left side of the patch decreases when the end of the patch is released from the steel. The end releases if a debonding or cohesive damage is propagating in the adhesive layer. For both scenarios the patch end or areas of the patch end is no longer connected to the beam. The loose end does not contribute to load transfer or to the joints strength and the shear stress releases, as the shear stress releases so does the axial strain.

As the damage from the center and the damage from the end approach each other, the remaining length of the bondline that the loads are transmitted through decreases. Failure will occur when the length of the bondline is so short that it no longer can withstand the loads being transmitted through it. This can be read from the strain measurements as when the front of the curve from the center damage meets the front of the curve from the left end. Cycle 6560 was the last good measurement of the embedded optical fiber and it can be seen that these two fronts have almost reached the same spot, and that the bondline preventing the joint from failure is extremely short. The patch failed shortly after, at 6640 cycles. The failure mode seemed to be a mix of cohesive failure and debonding. A picture of the specimen after failure is shown in Figure 58.

The strain in the top of the patch seen in Figure 57 increases and the curve close to center shifts a bit towards the ends up to 5000 cycles. The reason for these shifts of the strain curve is the damage that propagates from center in the adhesive layer. As the length of the optical fiber measuring strain here is about 280 mm of the patch length, the damage propagating from the left can not yet be detected. At 6500 cycles a decrease and shift in the strain curve towards the right is seen on top of the patch. The length of the damage from the left side has now reached the measuring range on the patch top. The left end does not transfer the same load and the strain on top of the patch decreases on the corresponding side. From Figure 56 it can be confirmed that the length of the damaged area has reached the range of the optical fiber on the patch top at 6500 cycles. The damage growth from the left end has reached the length on the x-axis of approximately -125 mm.

Figure 58: Beam 32 after failure. Debond and cohesive failure on the left side.

IPE100PP C/E 400 #33 GB DB UHMC
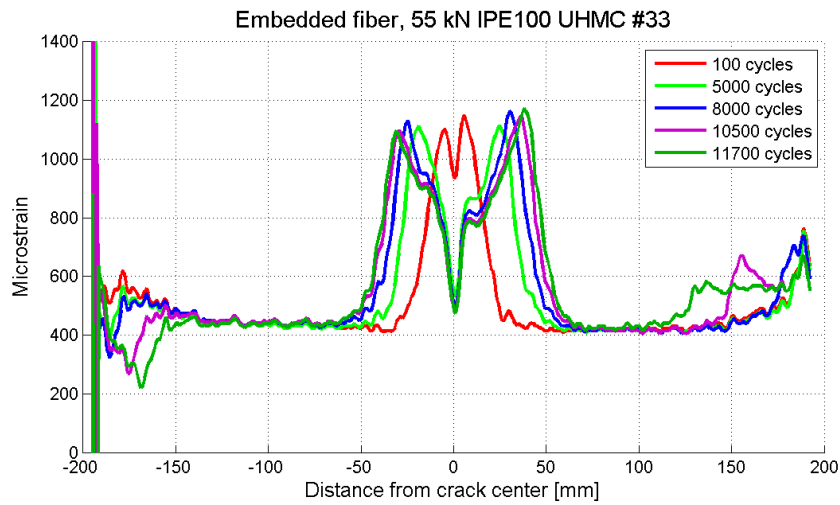
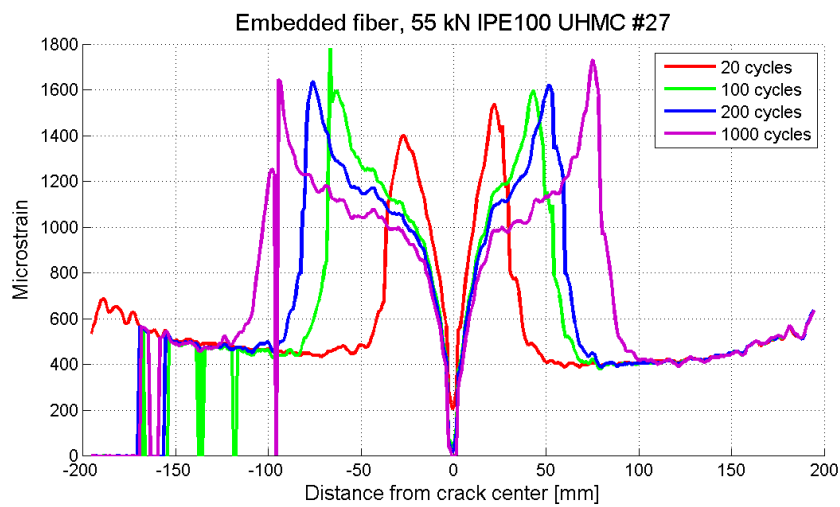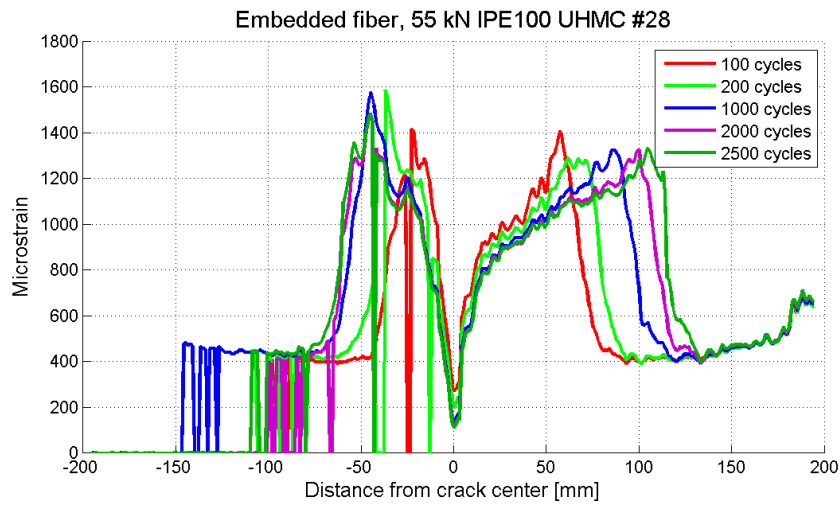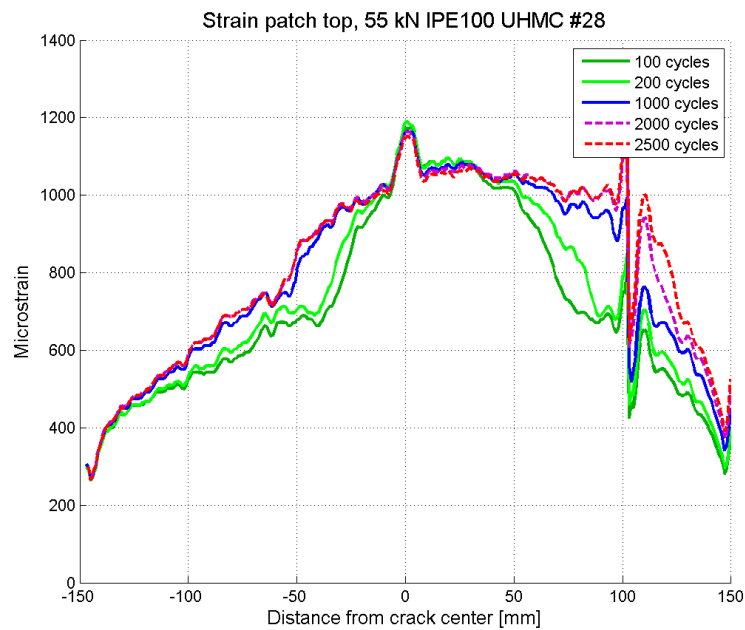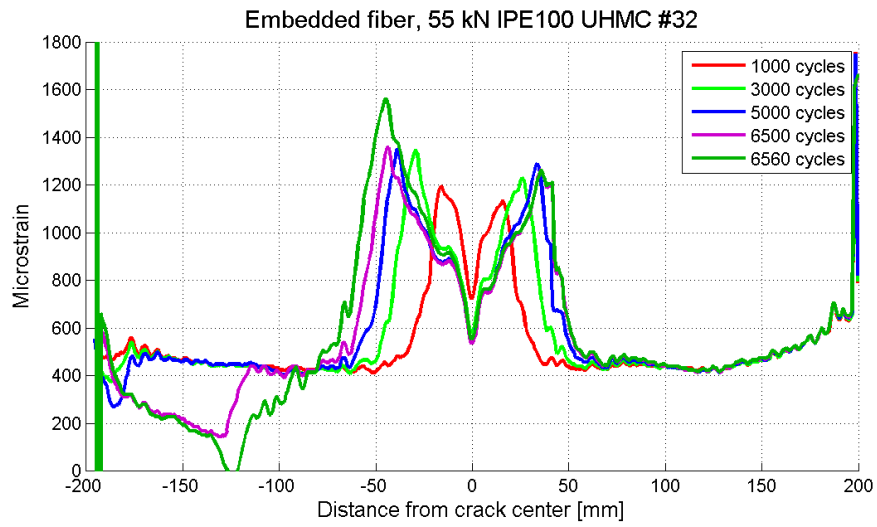Figure 59: Embedded optical fiber at different cycles, beam 33.
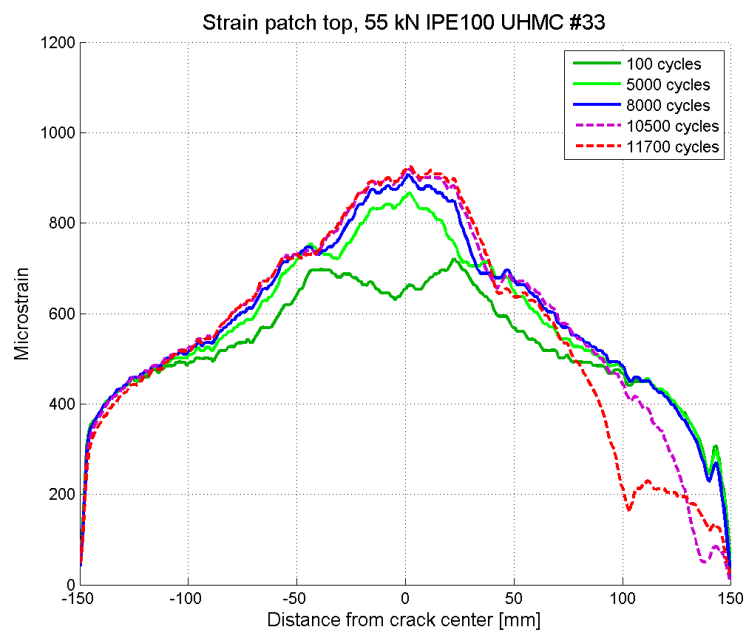
Figure 60: Optical fiber patch top at different cycles, beam 33.

In Figure 59 a similar damage propagation from the left side as for beam 32 is seen. Damage is also propagating from center of the patch towards each end but this damage

is not propagating very much between 5000 and 11700 cycles. A new phenomenon occurs at the right end of the patch, seen at 10500 and 11700 cycles. The strain curve from the right end is moving closer to the center, but the strain is not decreasing as it is from the left side. This is due to delamination in the UHMC laminate between the first and second group of plies starting at the right end of the patch. The strain increases because higher stress is transferred through the adhesive layer as the load transfer contribution from the delaminated part of patch decreases. The delamination was detected by visual inspection at 10500 cycles and could be seen from the back of the beam, see Figure 61 and 62.

The delamination also results in changes in the strain on top of the patch. At 10500 and 11700 cycles the delamination can be seen as a shift in the strain curves on the right side in Figure 60. The load transferred through the laminated part of the patch decreases, and this results in a decrease in the strain on top of the patch.

The lengths of the delamination at different cycles are presented in Table 9. These are measured on the back side of the beam at the initiation of the delamination towards center of the patch. Delamination eventually reached center of the beam as seen in Figure 63. Failure occurred along the right side of the patch as a combination of the delamination and cohesive damage in the adhesive layer from the center at 13650 cycles, see Figure 64.
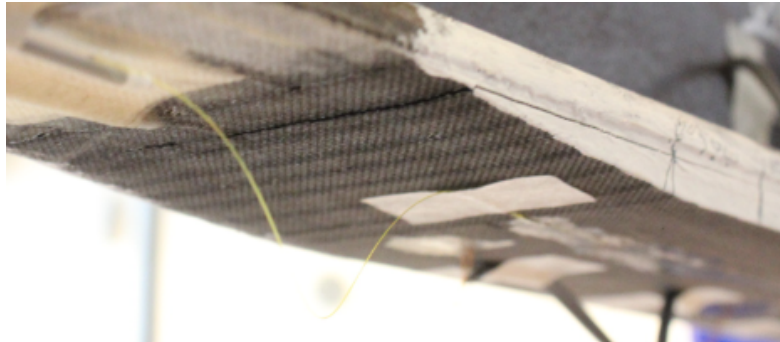
Figure 61: Delamination from right side of the patch. Beam 33, seen from the back.
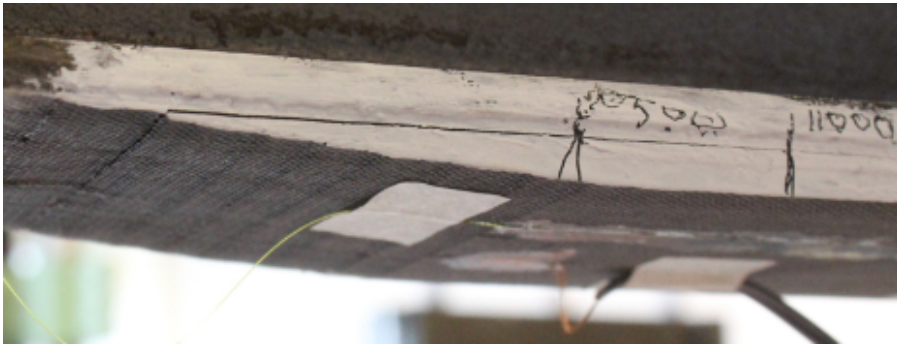
Figure 62: Delamination from right side of the patch. Beam 33, seen from the back.

Figure 63: Delamination reaching center of the patch. Beam 33, seen from the back.

Number of cycles	Length of delamination [mm]
10 500	50
11 000	74
11 700	110

Table 9: Measured length of delamination. Back of beam 33.

Figure 64: Failure of beam 33, seen from the back.

IPE100 PP C/E 400 #34 GB DB HMC

Figure 65: Embedded optical fiber at different cycles, beam 34.

Figure 66: Optical fiber patch top at different cycles, beam 34.

The embedded fiber was damaged during preparation of the specimen, it broke after the first length of optical fiber in the adhesive layer. This caused reflections in the

measurements and it did not give any results able to be analyzed after 4000 cycles. It was seen by visual inspection that damage propagated from center and from the right end of the patch. From Figure 65 it can be observed a decrease in the strain curve of the embedded fiber from the right side at 4000 cycles. This indicates a damage propagating in the adhesive layer from the right end of the patch. Cohesive failure in the right side occurred at 7966 cycles.
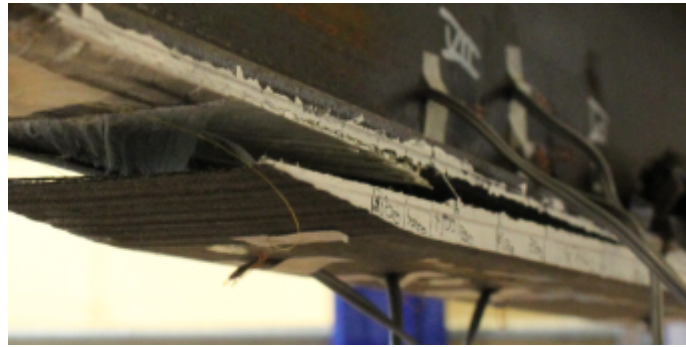
Figure 67: Failure of beam 34, seen from the back.

IPE100 PP C/E 400 #35 GB DB HMC
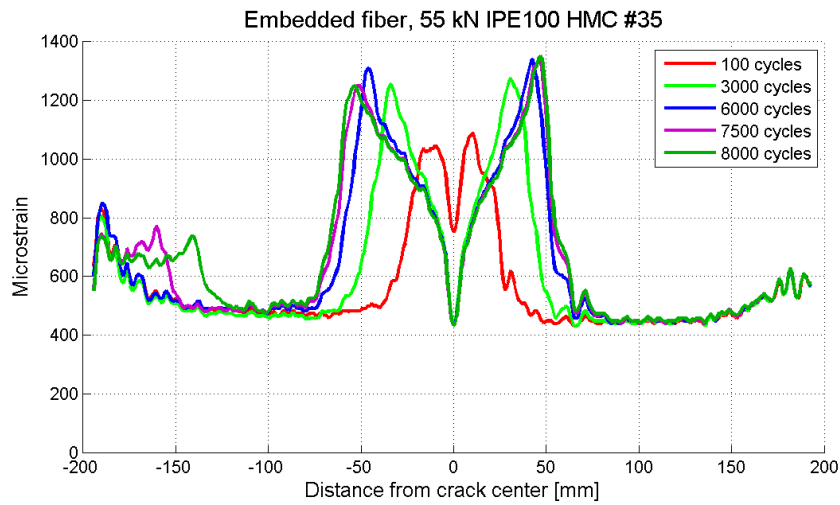
Figure 68: Embedded optical fiber at different cycles, beam 35.
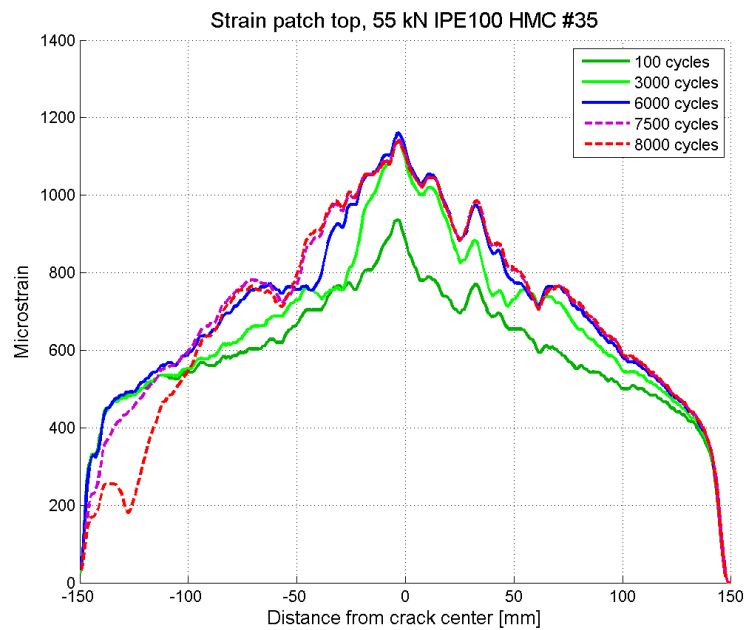
Figure 69: Optical fiber patch top at different cycles, beam 35.

As seen in Figure 68 this patch also experienced delamination in the HMC laminate, this time from the left side of the patch. The strain curve is comparable to that of the right

side of the embedded fibers in beam 33 presented above. The strain curve on top of the patch is again affected by the delamination, see Figure 69. The stress is released in the part of the patch that has delaminated, resulting in reduced strain that are detected by the optical fiber on the patch top. For this reason an observable shift in the strain curve is seen at 8000 cycles. 38.7 mm of the width of the patch was delaminating at this point, see Figure 70. The length of the delamination was measured to be 74 mm from the left end at 8000 cycles.
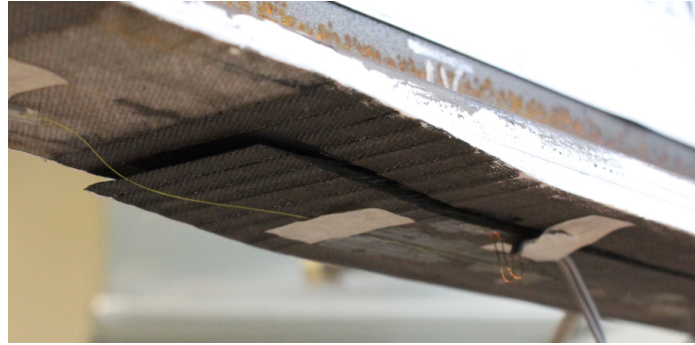
Figure 70: Delamination from left side of the patch. Beam 35, seen from the front.

In Figure 72 and 71 the measurements done by the optical fiber at 8700 cycles are included. At this point the length of the delamination has reached the center of the beam and grown some distance across center and into the right side of the patch, see Figure 73. The optical fiber on top of the patch is glued along the delaminated part of the laminate. It is clearly seen in Figure 72 that the strain has decreased significantly from the left and across center at 8700 cycles. Forces are only being transferred to this part of the laminate at the right end which not yet have suffered from delamination. This is the reason for the higher strain curve at the right side of the patch at 8700 cycles.

The very high strain increase in the embedded fiber at 8700 cycles is because the strength of the HMC laminate is severely reduced by the delamination. The same forces now have to be distributed to the parts of the laminate that are still intact. This increases the shear stress distributed in the bondline of the remaining laminate on the left side. It is seen as the uniform increase of axial strain from approximately 500 to 600 microstrain in the left side of the adhesive layer, see Figure 72
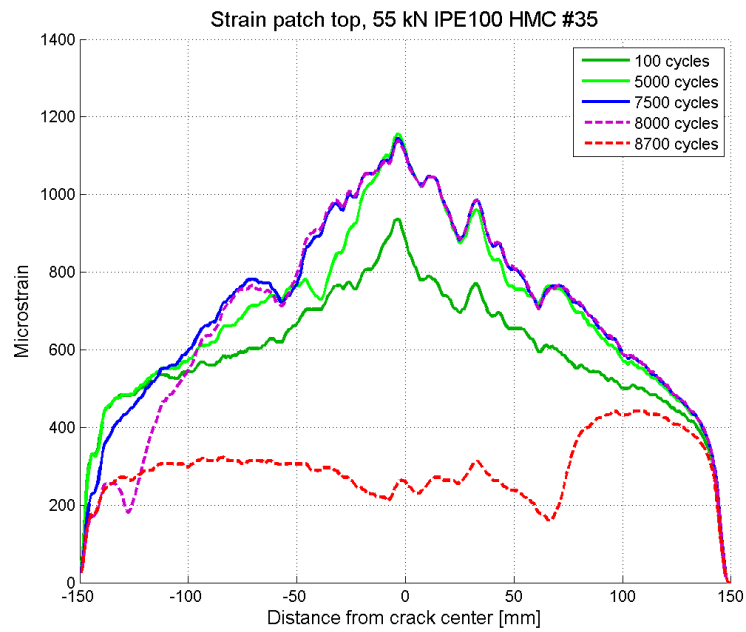
Figure 71: Optical fiber patch top at different cycles, beam 35.
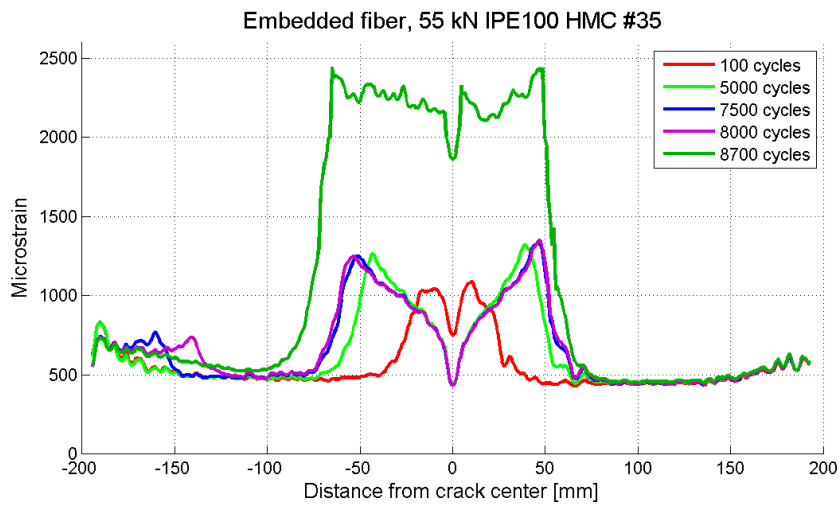
Figure 72: Embedded optical fiber at different cycles, beam 35.

Figure 73: Delamination from the left side. Beam 35, seen from the back.

IPE 100 PP C/E 400 #36 GB DB HMC
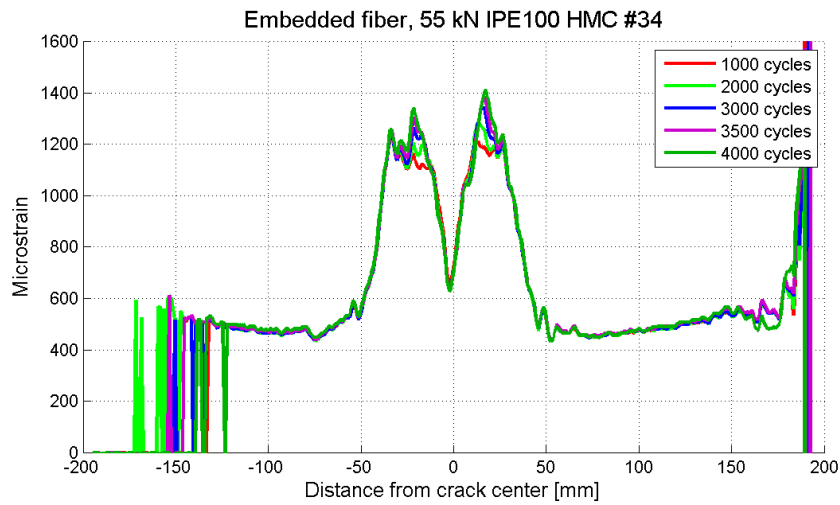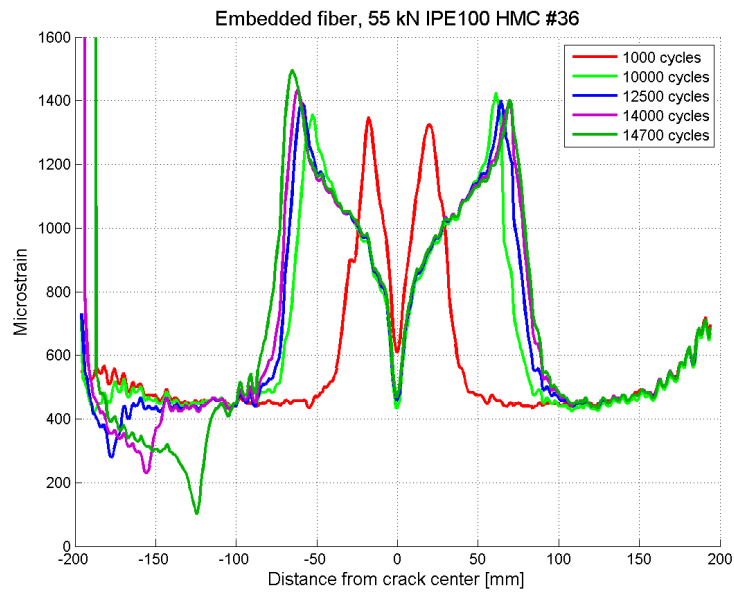

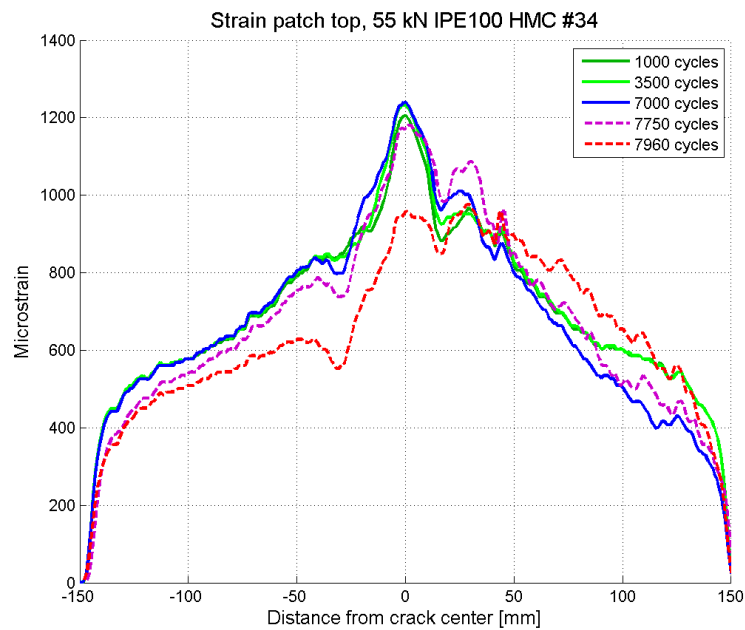Figure 74: Embedded optical fiber at different cycles, beam 36.
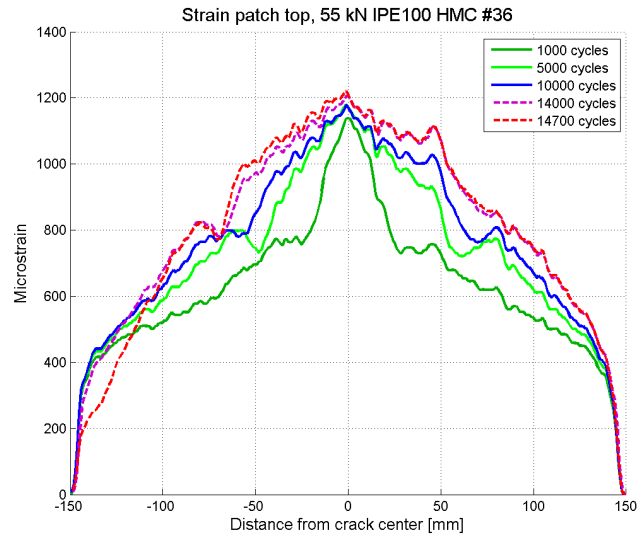
Figure 75: Optical fiber patch top at different cycles, beam 33.

For beam 36 with the HMC material the damage propagation is of the same character as described for beam 32. In Figure 74 it is seen that the the damage propagation from center and towards the ends is close to equal for both sides. At 10 000 cycles the damage propagating from center was also detected by visual inspection of the beam. This was seen as cracks in the white paint along the steel and composite patch. This is shown in Figure 76. The lengths of these cracks were measured by visual inspection at different cycles and are reported in Table 10.
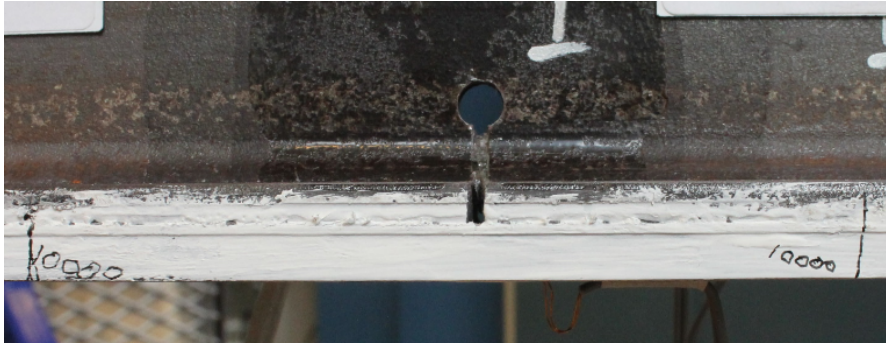
Figure 76: Damage propagation from center at 10 000 cycles. Beam 36.

There is no damage propagation from the right end, but it can be detect from the measurements that damage is propagating in the adhesive layer from the left side. At 14700 cycles the damage propagating from the left end reaches the range of the optical fiber on top of the patch. In Figure 75 it is seen that the damaged area in the patch from the left end results in a shift in the the strain curve on top of the patch. The damage from the left end was detected by visual inspection at 14 000 cycles and the length of the crack was measured to be 45 mm, see Figure 77. The beam failed at 14 741 cycles in the left side of the patch and the failure mode was cohesive failure, see Figure 78.

Figure 77: Damage propagation from left at 14 700 cycles. Beam 36.

Number of cycles	Back [mm]	Front [mm]
10 000	-49 and 49	-51 and 44
12 500	-49 and 49	-59 and 58

Table 10: Measured crack length from center in x-direction, beam 36.

Figure 78: After failure, beam 36.

IPE100 PP C/E 400 #37 GB DB HMC
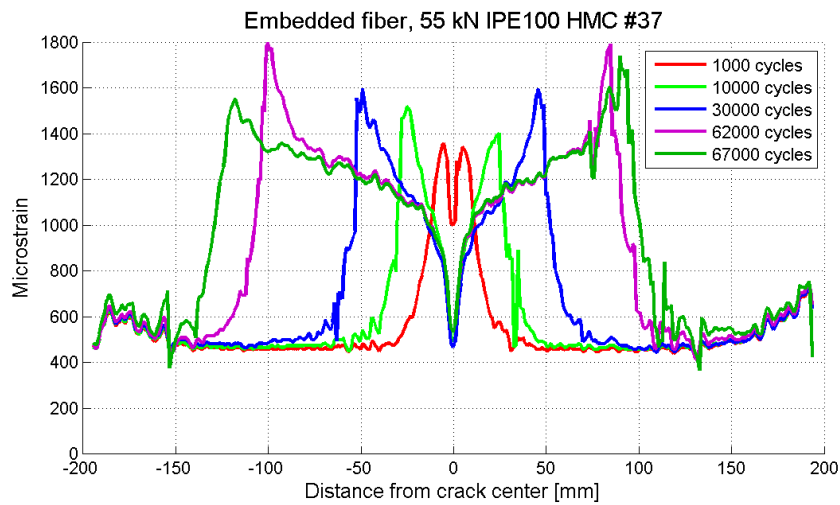
Figure 79: Embedded optical fiber at different cycles, beam 37.
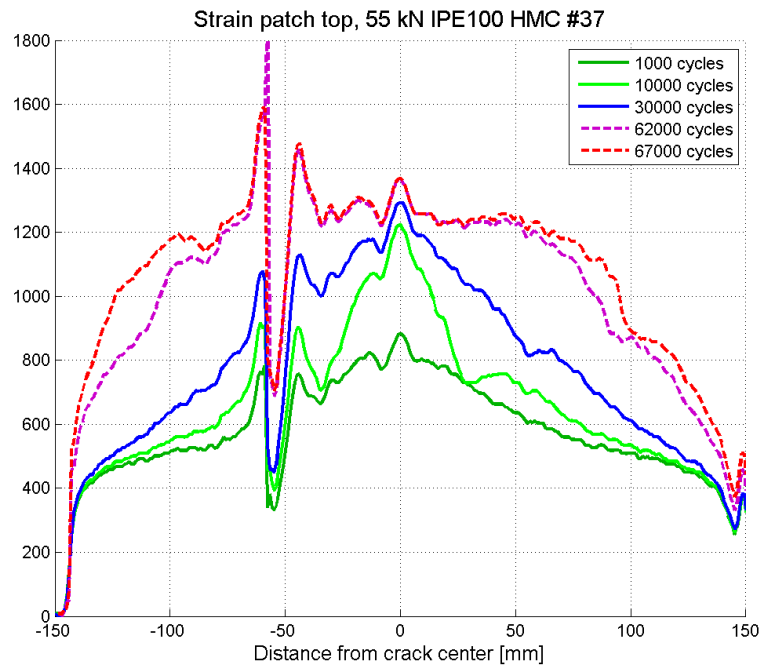
Figure 80: Optical fiber patch top at different cycles, beam 37.

From Figure 79 it can be seen that damage is propagating in the adhesive layer from center and towards both ends of the patch. At 62 000 and 67 000 cycles the damage has propagated a bit longer to the left side than the right side in the patch. This is also documented by visual inspection and the crack lengths from center were measured and are presented in Table 11. Failure occurs at 67 620 cycles in the right side of the patch. Why failure is in the right side and not in the left side is explained below in Section 7.4.

The beam also experienced the same crack propagation in the web as beam 21 and 22, see Figure 81.
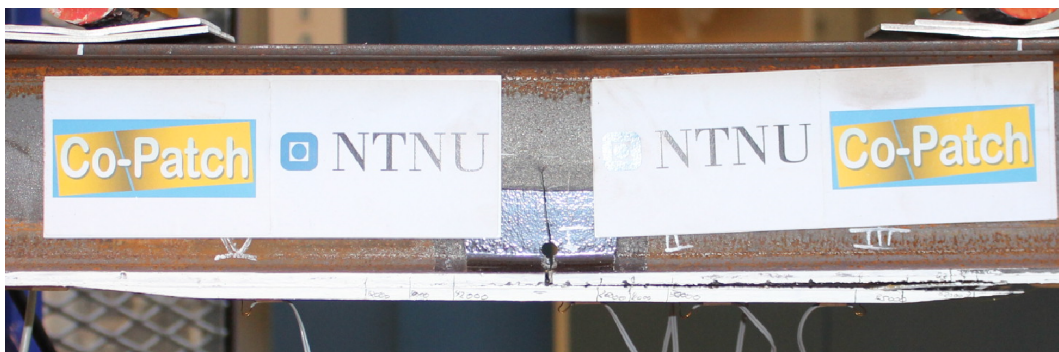
Figure 81: After failure, beam 37.

7.4 Three embedded optical fibers

Three lengths of the optical fiber were embedded in the adhesive layer for beam 32 through 37 as described in Section 4.2.3. This was done in order to investigate if there was any difference in the damage propagation through the width of the beam and if such difference could be detected by the optical fiber.

IPE100 PP C/E 400 #33 GB DB UHMC
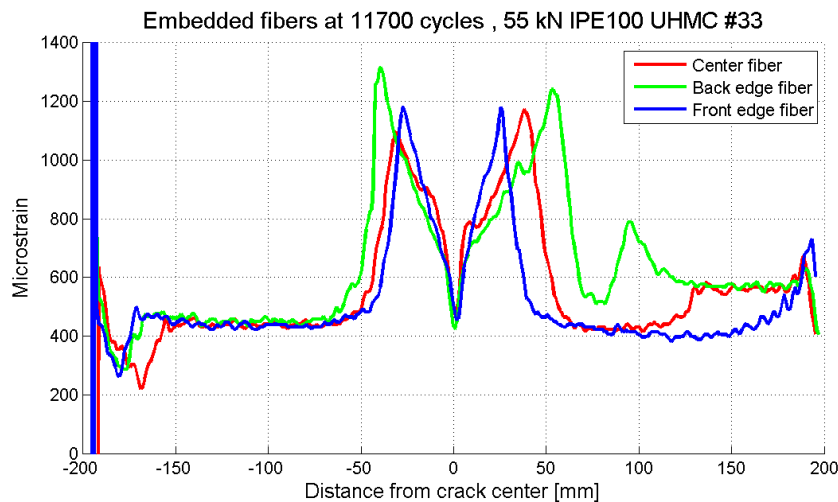
Figure 82: Three embedded optical fibers at 11 700 cycles, beam 33.

At 11700 cycles it is seen that the strain in the back edge fiber indicates a delamination from the right side and a failure propagating from center towards the right side. The front edge fiber does not indicate this delamination. Damage propagation from the left side is seen in all three fibers, but most significant in the center fiber. Figure 83 supports what detected by the optical fibers. The picture is taken from the back, and shows a delamination in the right back side of the patch. The delamination does not occur through the entire width of the patch and this is why it is not detected by the front edge fiber. The damage from the left side could not been observed by visual inspection from either sides of the beam. This supports that the left end damage is propagating from center of the patch.
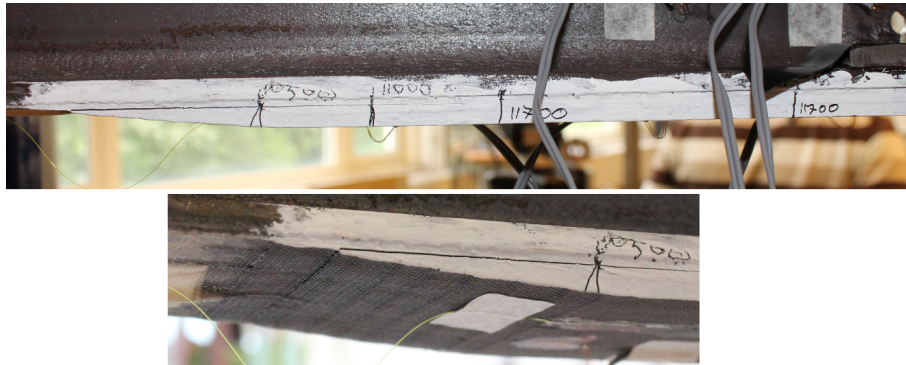
Figure 83: Damage propagation in the right side. Beam 33, seen from the back.
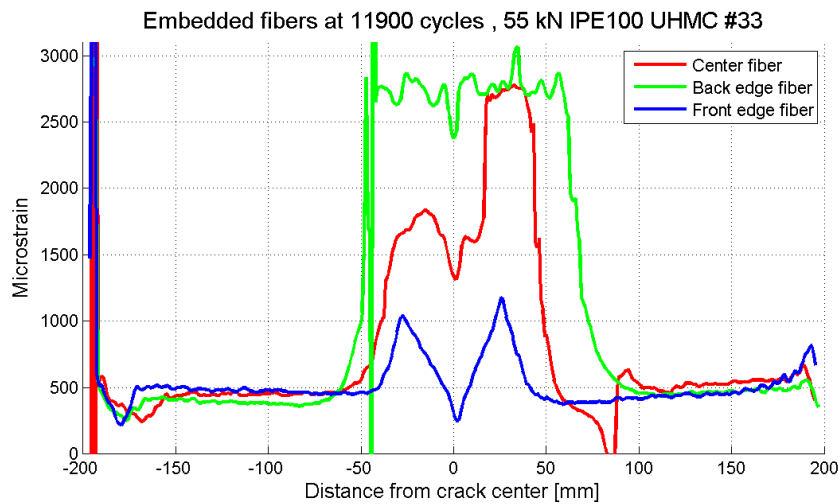
Figure 84: Three embedded optical fibers at 11 900 cycles, beam 33.

At 11 900 cycles the length of the delamination has reached the center of the patch and the strains from the embedded optical fibers are shown in Figure 85. The strain along the front of edge of the patch remains more or less the same, but the strain in the adhesive layer where no damage has propagated has increased from ≈400 to ≈500 microstrain, see Figure 84.

. At the back edge the delamination in the patch
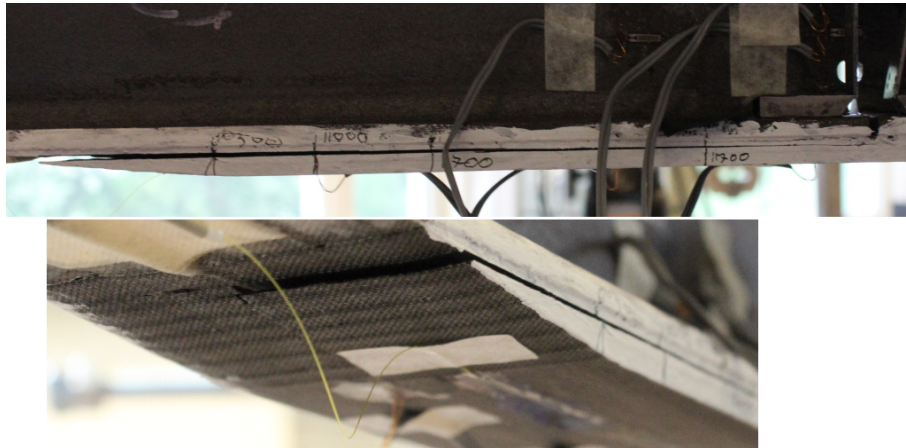
Figure 85: Delamination from right side, beam 33. Seen from the back.

IPE100 PP C/E 400 #37 GB DB HMC
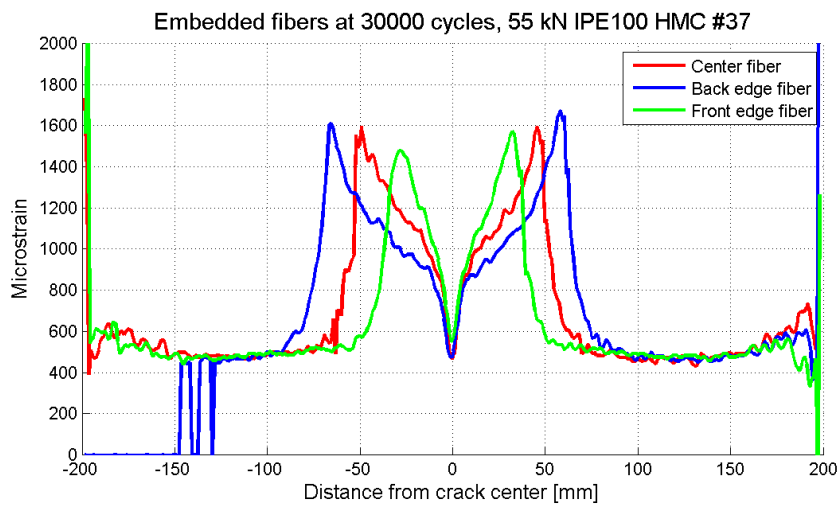
Figure 86: Three embedded optical fibers at 30 000 cycles, beam 37.
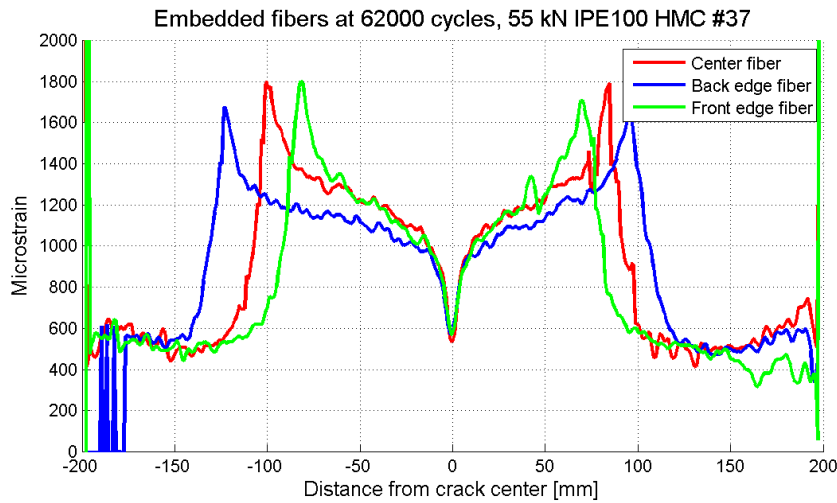
Figure 87: Three embedded optical fibers at 62 000 cycles, beam 37.

The reason for beam 37 having failure in the right side of the patch and not in the left side can be found from Figure 86 and 87. It is seen that a damage is propagating from the front edge of the right side, indicated by the decrease and movement of the front edge strain curve. This damage is not detected by the center and back edge fibers. The damage is documented as a crack measuring 21 mm from the right end towards center at 62 000 cycles, and is only detected at the front side of the beam, see Figure 88.

The curves show that the length of the damage propagating from center is longer in the back of the patch than in the front of the patch. This is supported by visual inspection and the measured lengths are presented in Table 11. This combination of damage propagating both from center and the right end leads to failure in the right side of the patch.

Some more results can be found in Appendix A.
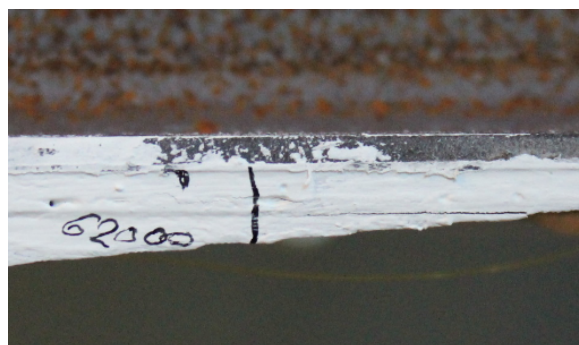
Figure 88: Damage propagating from the right end, beam 37. Seen from the front.

Number of cycles	Back [mm]	Front [mm]
26 000	-48 and 46	22
50 000	-95 and 75	-58 and 52
62 000	-117 and 91	-76 and 52

Table 11: Measured crack length from center in x-direction, beam 37.

8 Finite element analyses with fictitious damages

Two new FE analyses were made after seeing different type of damage propagation giving different strain curves in the optical fibers. The goal was to see if a similar alteration of the strain curves could be seen with a FE analysis. This analysis was compared with the measurements from the optical fibers of IPE100 PP C/E 400 GB DB HMC 36, a specimen that was found to have damage propagation from center and one end.

8.1 FE-analysis with fictitious damage from center

The exact same model and mesh was used as described previous in Section 6. A new partition was made in the XY plane at Z=-50 mm. A debonding between the galvanic protection and the steel from center towards the end was modeled. This was done by using tie constraint between the surfaces of the steel and the DB810 between Z=-50 mm and Z=-200 mm. Hard contact interaction was applied between the two surfaces from Z=0 mm to Z=-50 mm. This would simulate a debonded length of 50 mm from center towards each side in the patch.
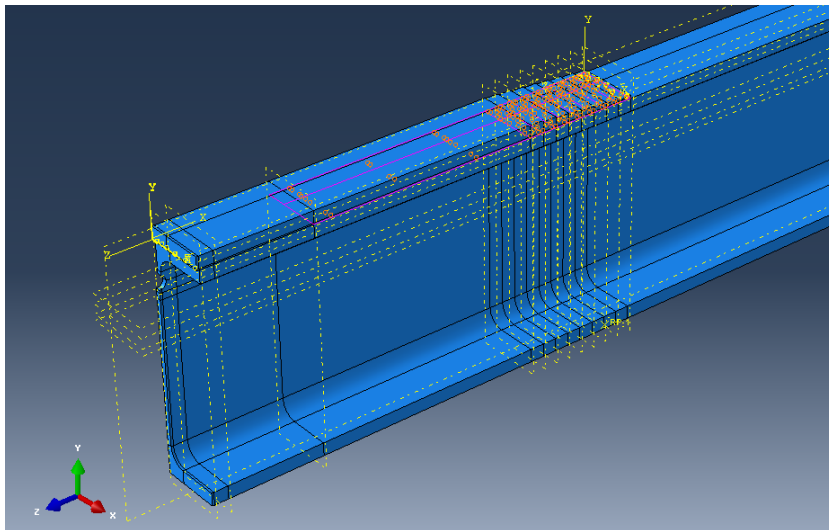
Figure 89: New tie constraint between steel and DB810.
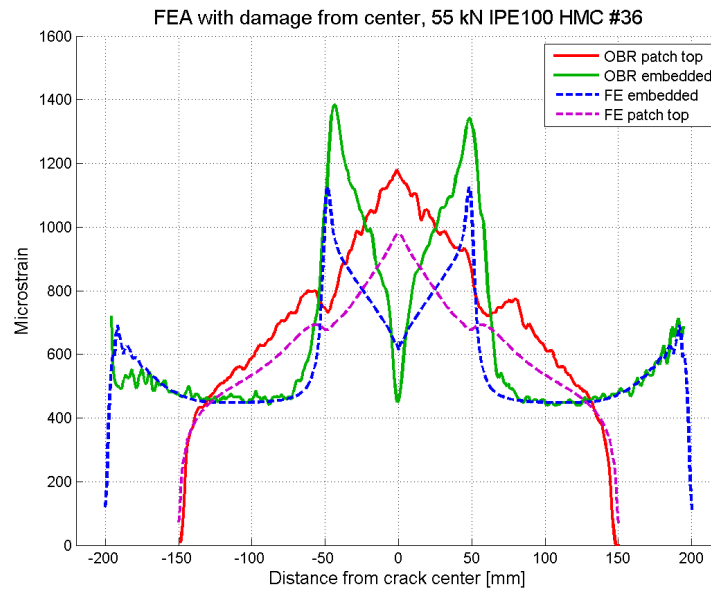
Figure 90: FEA with fictitious damage and IPE100 36 at 5000 cycles.

Figure 90 shows the comparison of the FE analysis and the strain measured by the optical fibers in beam 36 at 5000 cycles. Here the difference between the embedded fibers at the left patch end can be ignored because this damage was not simulated in the FE analysis. The shape of the curves coincide very well between the FE analysis and the measurements with the optical fibers. However, the values of the strain differ quite a bit between the FE-model and the optical fibers. This can be explained by the lack of degradation of the material in the FE-analysis. The test specimen has experienced 5000 cycles and some degradation due to shear stresses has probably occurred in the material. In the FE-analysis there is no friction involved when using hard contact interaction, this will also affect the strain.

8.2   FE-analysis with fictitious damage from center and patch end

A model with fictitious damage from both center and end was modeled. The debonded length from center was 50 mm, using the same procedure as described in the prevoius section. The debond from the end was modelled by removing the tie constraint between the DB810 part and the steel for some of the area at the patch end. This area was along the whole length of the tapering and from center and 7 mm towards the edge. Meaning from Z=-150 mm to Z=-200 mm and between X=0 and X=7 mm in the model. Figure 91 shows the area with tie constraint between the DB810 and the steel beam. Hard contact interaction was applied for the area of the patch not having tie constraint between the DB810 and the steel beam.
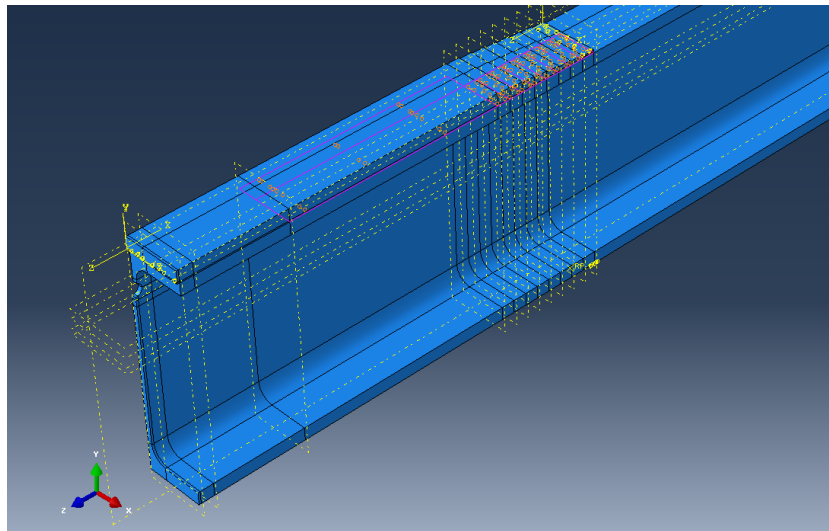
Figure 91: New tie constraint between steel and DB810.
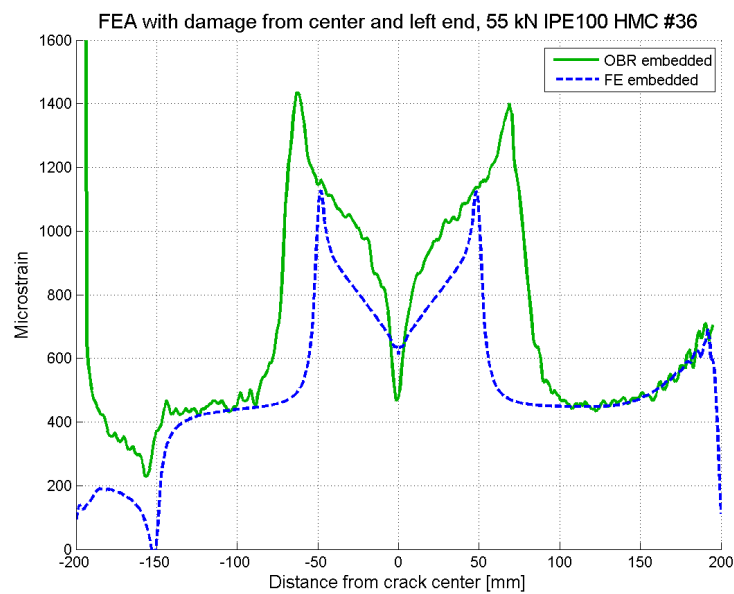
Figure 92: FEA with fictitious damage and IPE100 36 at 14 000 cycles.

In Figure 92 the FE-analysis with fictitious damages from center and end is compared with the embedded optical fiber in beam 36 at 14 000 cycles. The result of the FE-analysis is manipulated together with the result from the previous section in a way that the end damage is only seen in the left side of the patch. This result also shows a comparable shape of the curves when these types of damages are present. The case is

the same as described above with no degradation of the material or friction involved in the FE-analysis. This contributes t no shear degradation in the fe-analysis.

Different damage propagations in the composite metal joints resulted in strain curves of different shape, measured by the optical fibers. The motivation for these analyses was to investigate if similar shapes of the strain curves could be found with FE-analyses. From these results it was found that these damages generates strain curves from the FE-analyses of similar shape as those measured with the optical fibers. This supports the optical fibers ability of the detecting different damage propagations in the joints.

9 Discussion

9.1 Material selection and production method affecting the fatigue life of a composite metal joint

The results presented show that the fatigue life of a composite metal joint is dependent on the joints composition. The cracked beams repaired with UHMC and HMC using hand lay-up of the DB810 as galvanic protection all failed between 1 235 and 67 620 cycles. Seven out of eight of these beams failed prior to reaching 15 000 cycles. IPE 100 PP C/E 400 GB DB UHMC number 27 and 28 failed at 1 235 cycles and 2 560 cycles. Beam 32 and 33 of the same composition failed at 6 640 and 13 650 cycles. They were produced during the production process in this thesis and tested a couple of days after they were produced. As described in Section 4.2.6 producing composite metal joints of equal quality may be difficult when hand lay-up is part of the production process. Here a quality difference of the DB810 layer applied to beam 36 and 37 was found. This can be an explanation for why failure of beam 36 occurred at a number of cycles much lower than of beam 37. The beams of IPE100 PP C/E 400 GB SA UHMC and IPE100 PP C/E 400 GB SA PP UHMC composition experienced a lot higher number of cycles prior to failure. This also indicates that the best quality of the composite metal joint is achieved when using pre-preg material and co-curing technique, avoiding hand lay-up in the production process.

It was also seen for beam 21, 22 and 37 that after a high number of cycles the crack in the beam propagated towards the neutral axis of the beam before the patch was about to fail. This indicates that the repair with the composite patch does not give enough load reduction to prevent the damage in the beam to escalate. A reason for this can be that the stiffness of the CFRP material is too low or that the adhesive layer in the composite metal joint is to flexible, not preventing the crack mouth opening from moving. The joint strength can be increased by increasing the stiffness of the CFRP laminate or the adhesive layer. The stiffness of the CFRP patch can be altered by changing the thickness of the laminate. Before using a stiffer adhesive, it should be taken into account that a stiffer adhesive also will introduce higher stress concentrations at the patch ends, as described in Section 2.1.2. A large increase of the strain in SG 5 indicated that the crack was about to propagate in the web.

Problems with delamination of the patch between groups in the laminate were present. The tapering is there to reduce peel stresses at the ends of the patch, but the delamination occurs between groups in the tapering. To explore if the tapering is a weak spot in the patch, introducing delamination, a patch without tapering is suggested to be tested.

9.2   Optical fibers as a method of structural health monitoring

The strain measurements done by the optical fibers in the composite metal joints have showed remarkably good results. They have proven to be reliable in measuring strain even after a high number of cycles. Strain measured by the optical fibers are very well comparable with the strain measured by the strain gauges. The strain measured by the optical fibers differ very little from the strain measured by the corresponding strain gauge. In cases they differ, the relative increase for the strain gauge and the optical fiber between a given number of cycles seems to be the same. This indicates that the strain measured by the optical fiber is correct, but that there are some deviations in the strain on top of the patch from one side to the other. The thickness of the patch can vary for each side and the alignment of the strain gauges might not be 100% correct.

The results from the Finite Element Analysis coincide well with the experimental strain measurements done with the optical fibers. In FEA analysis the strain peak in the embedded fiber and the strain valley at the patch top differ more from the experimental results than for the rest of the optical fiber's length. An explanation for this can be a difference in how the strain is calculated by Abaqus 6.12-1 and by the OBR software. As described in Section 3 the strain is calculated over a given sensor gauge length by the OBR software. When using a 0.5 cm long gauge length the resulting strain calculated by the software is the average strain over this length. If a very high strain peak is concentrated over a length of say 2 mm the software may not display the correct strain for this short length. By reducing the gauge length, such peaks are more detectable but the strain curve will have more noise and it will be less beneficial for interpretation of the results.

The experimental work has proven that the optical fibers are able to detect damage propagation in the composite metal joints. This is supported by comparing the measurements done with the optical fibers with visual inspections of the damage propagation during the tests. The different failure modes can be detected from the resulting strain curves measured by the optical fibers. The most reliable way of detecting what type of damage that is propagating in the composite metal joint is by observing the embedded optical fiber. A good example is explained in the results of beam 33 in Section 7.3, Figure 59. Here a delamination is propagating from the right side and a debonding or cohesive damage in the adhesive layer is propagating from the left side. A difference was observed in the strain curve of the embedded optical fiber if there was a delamination in the patch or a damage in the adhesive layer. For a delamination from the end, the peak of the strain curve would move towards center as the delamination propagated towards center. This strain curve would not decrease as it would do if the damage was debonding or cohesive failure, it would rather see an increase along the length equal to the length of the delamination of the patch.

It was also possible to detect damage propagation by observing the optical fiber on top of the patch. It was not as easy to distinguish between a delamination or a damage in the adhesive layer from the strain on top of the patch as for the embedded fiber. For

both cases the forces transferred through the patch are reduced and the strain curve on top of the patch decreases and changes shape. By embedding three lengths of optical fibers in the adhesive layer it could be detected if the damage propagation was non-uniform through the width of the patch. With three embedded fibers the monitoring of the composite metal joint enhances and damage propagation that would not be detected with a single fiber can be detected.

The FE analysis with fictitious damages also have comparable shapes of the strain curves as the strain curves measured with the optical fibers for the same type of damage. Supporting that the optical fibers are able to detect different types of damage.

As damage in the composite metal joint propagates, the strain curves measured by the optical fibers change. The strain curve moves a length equal to the length of the damage in the adhesive layer, and the optical fibers are able to detect the growth of debonding versus the number of cycles. When the load transmitted through the adhesive layer exceeds the load that the adhesive layer can withstand, the adhesive layer fractures and the composite metal joint fail. The optical fibers have been found reliable as a method of health integrated monitoring and can be used to predict failure of the composite metal joints.

10 Conclusion

The fatigue behavior of smart composite metal joints has been explored. Eleven IPE100 steel beams with induced cracks repaired with carbon fiber-reinforced polymer patches have been tested in a four point bend test with a load cycling between 10kN and 100kN. Every beam was instrumented with an optical fiber in the adhesive layer of the CFRP patch and along the top of the patch. Six of the beams were instrumented with three lengths of the optical fiber in the adhesive layer. These optical fibers were connected to an Optical Backscatter Reflectometer and the strains in the composite metal joint were measured during testing. The goal of the thesis was to explore how the optical fibers can be used as a method of integrated health monitoring.

The beams were made with different configurations of the composite patches. Beams produced using hand lay-up with a ±45 glass fiber layer as the galvanic protection reached the lowest number of cycles at failure. It was found that it is difficult to produce laminates of equal quality when hand lay-up is part of the production process. The beams found to reach the highest number of cycles at failure were all produced exclusively with pre-preg materials using the co-curing technique. Some beams reaching a very high number of cycles experienced a crack propagation in the web from the crack tip of the induced crack. This indicates that the repair with the composite patch does not give enough load reduction to prevent the crack in the beam to propagate in the web. Altering the thickness of the CFRP laminate or the stiffness of the adhesive layer is proposed in order to increase the joint strength.

Finite element analysis of the beam was made and compared against the strain measured with the optical fibers. The optical fibers were also compared against corresponding strain gauges on top of the patch. Both results from finite element analysis and strain gauges coincide well with the optical fibers.

The optical fibers were proven to detect and distinguish between different failure modes developing in the composite metal joints. By embedding three lengths of the optical fiber in the adhesive layer it was observed a non-uniform damage propagation through the width of the joint. This damage distribution across the width could not be detected if only one fiber length of the fiber was embedded the adhesive layer. The length of the propagated damage in the joint can be found using the optical fibers and this can be used to predict failure of the joint. From the experimental results in this thesis the optical fibers are found to be reliable as a method of integrated health monitoring.

References

[1] Farrar, Charles R.; Worden, Keith. *An introduction to structural health monitoring.* Phil. Trans. R. Soc. A., vol. 365, pp. 303-315, 2007.

[2] Cawley, Peter., *Inspection of Composites - Current Status and Challenges*, ECNDT, Mo.2.6.1, 2006.

[3] Lunder, E.V.,*Smart Materials in Adhesive Joints*, 2012.

[4] Silva, Lucas F. M.da; Öchsner, Andreas; Adams, Robert D. *Handbook of Adhesion Technology.* 1st Edition., 2011: Springer.

[5] Silva, Lucas F. M.da. *Modeling of Adhesively Bonded Joints.* 2008:Springer

[6] *Distributed Temperature and Strain Measurements*, `http://lunainc.com/products/fiber-sensing-solutions/distributed-temperature-and-strain-measurements/`.

[7] Duncan, Roger G., et. al., *OFDR-Based Distributed Sensing and Fault Detection for Single- and Multi-Mode Avionics Fiber-Optics*,Joint Conference on Aging Aircraft, April 2007

[8] Kreger, Stephen T., et. al., *High Resolution Distributed Strain or Temperature Measurements in Single- and Multi-mode Fiber Using Swept-Wavelength Interferometry*, Optical Fiber Sensors Conference, 2006

[9] Grave, J.H.L.; Håheim, M.L.; Echtermeyer, A.T. *Evaluation of the strain field in a composite-metal adhesive joint with an optical backscatter reflectometer*, 2012.

[10] *SE 84LV Low Temperature Cure Epoxy Prepreg System*, `www.gurit.com/files/documents/se-84lvv13pdf.pdf`.

[11] Karatzas, V.A., et. al., *The manufacturing process of co-cured single and double lap joints and evaluation of the load-bearing capacities of co-cured joints*, Journals of Materials Processing Technology, vol. 138, pp. 89-96, 2003.

[12] Grave, J.H.L.; Echtermeyer, A.T. *Copatch NTNU-TR-WP4-3*, 2013.

[13] McGeorge, Dag, *Inelastic fracture of adhesively bonded overlap joints*, Engineering Fracture Mechanics, vol. 77, pp. 1-21, 2010.

[14] Det Norske Veritas, *Design, Fabrication, Operation and Qualification of Bonded Repair of Steel Structures*, DNV-RP-C301, April 2012

[15] Log, A.R.,*Fatigue Properties of Adhesive Joints in Patch Repairs*, 2012

A Results from FEA and experimental work
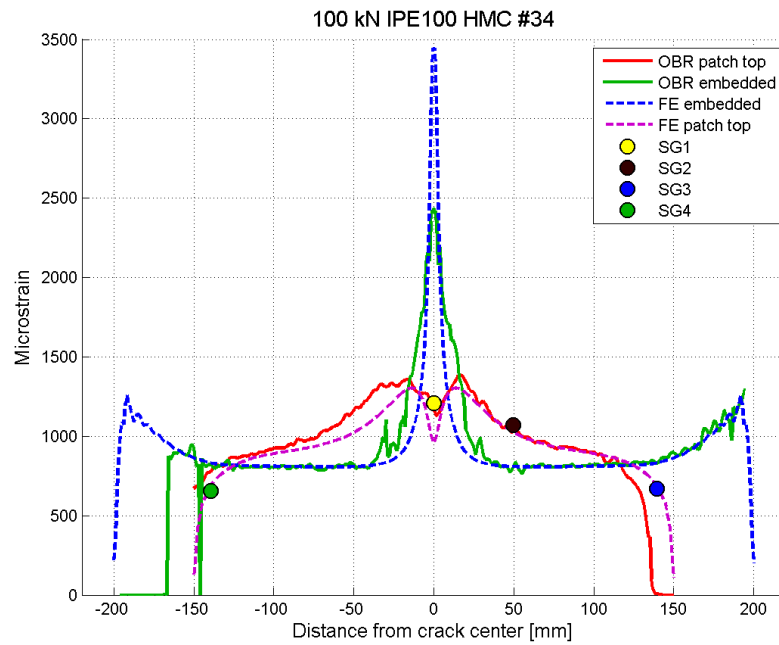
Figure 93: Comparison of OBR, FEA and strain gauges at 100kN load. Beam 34.
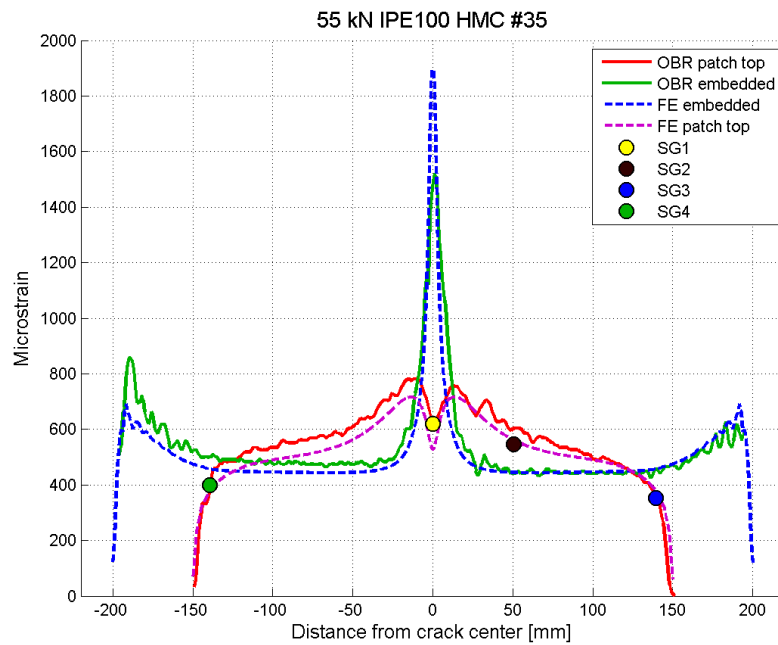
Figure 94: Comparison of OBR, FEA and strain gauges at 55 kN load. Beam 35.
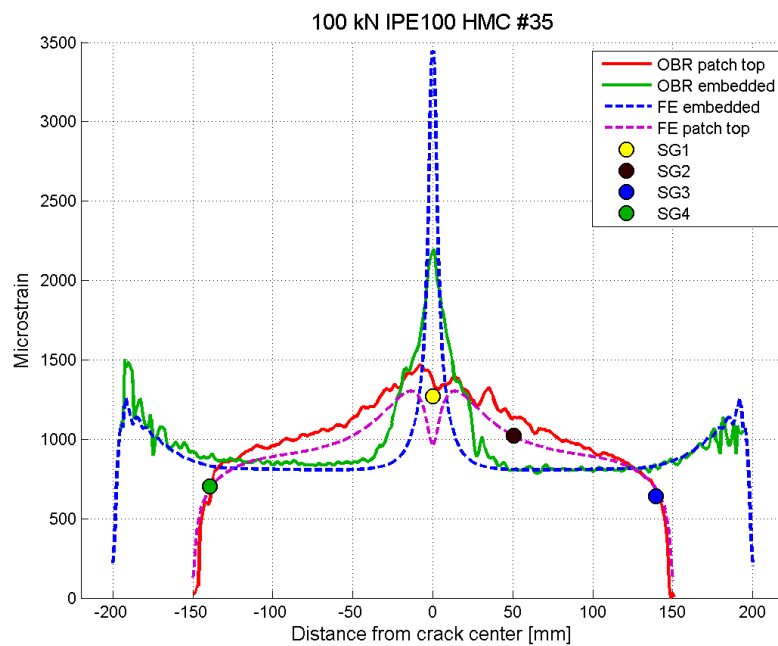
Figure 95: Comparison of OBR, FEA and strain gauges at 100kN load. Beam 35.
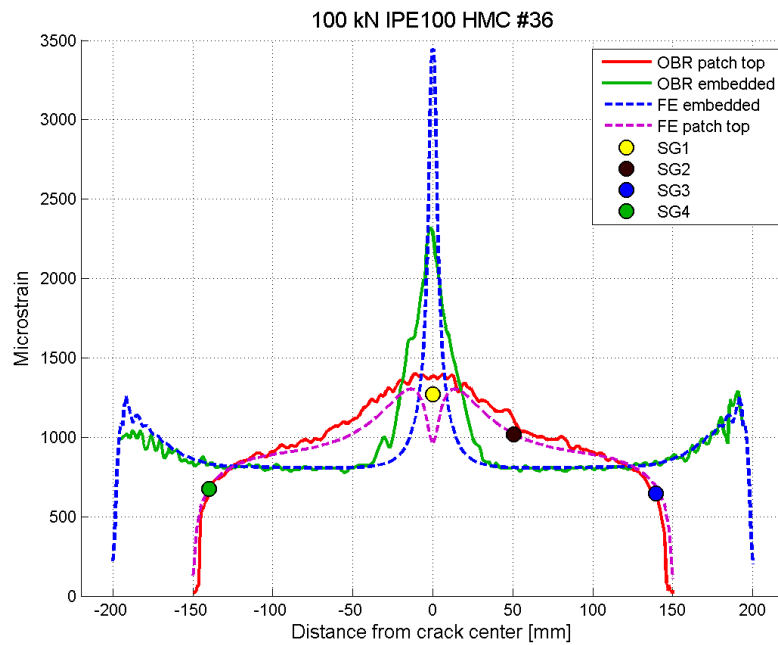
Figure 96: Comparison of OBR, FEA and strain gauges at 100kN load. Beam 36.
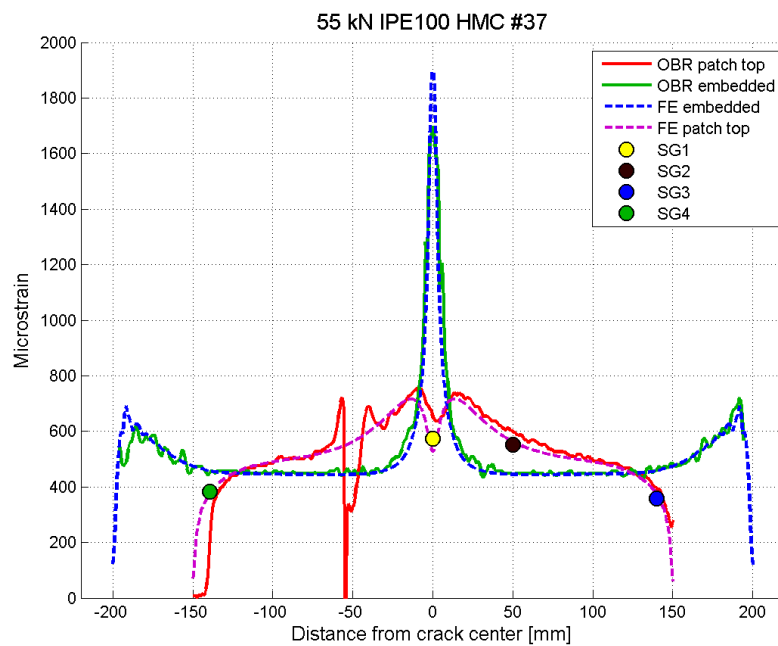
Figure 97: Comparison of OBR, FEA and strain gauges at 55 kN load. Beam 37.
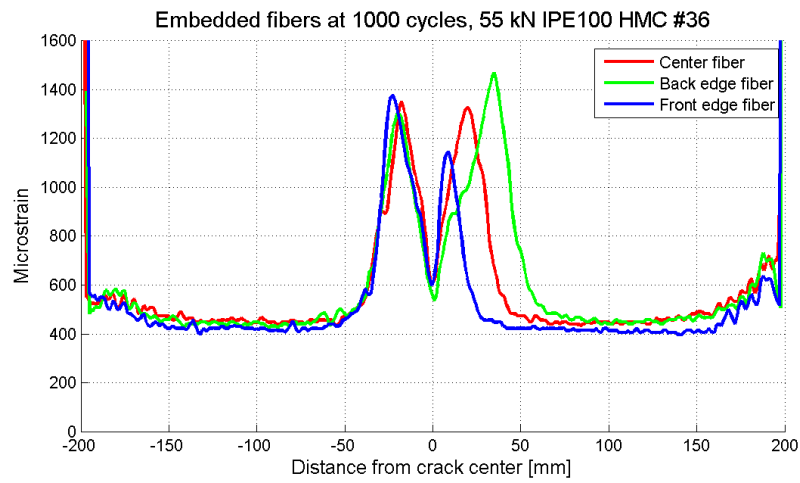
Figure 98: Three embedded fibers, 1000 cycles. Beam 36.
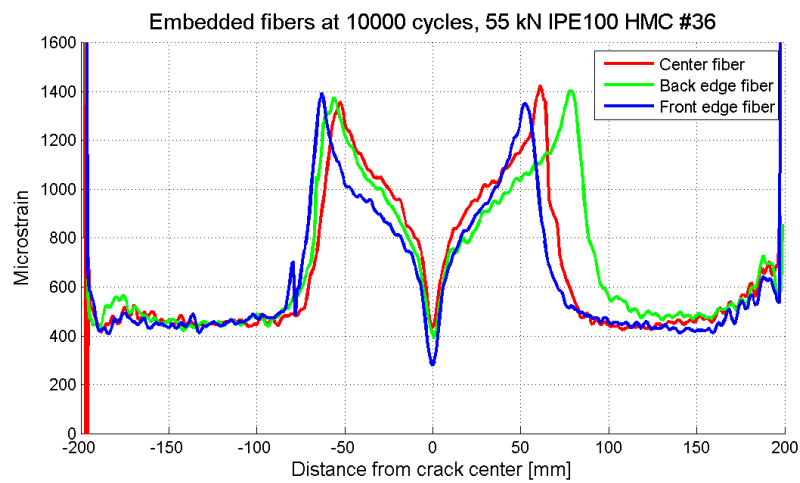
Figure 99: Three embedded fibers, 10 000 cycles. Beam 36.
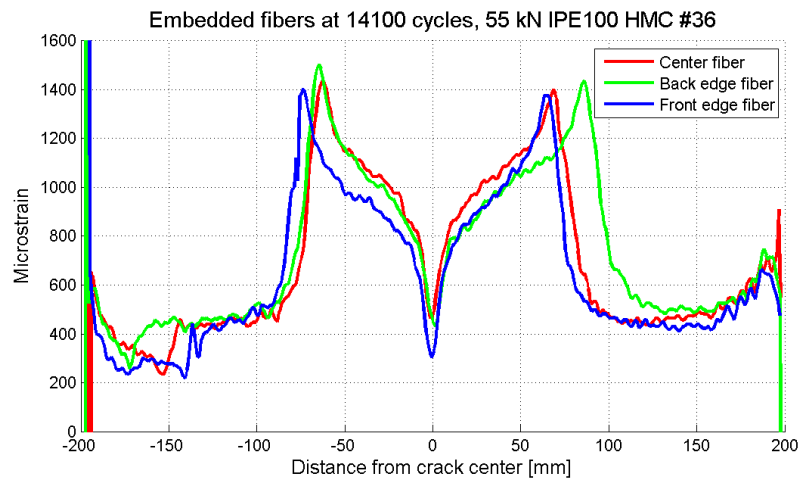
Figure 100: Three embedded fibers, 14 100 cycles. Beam 36.
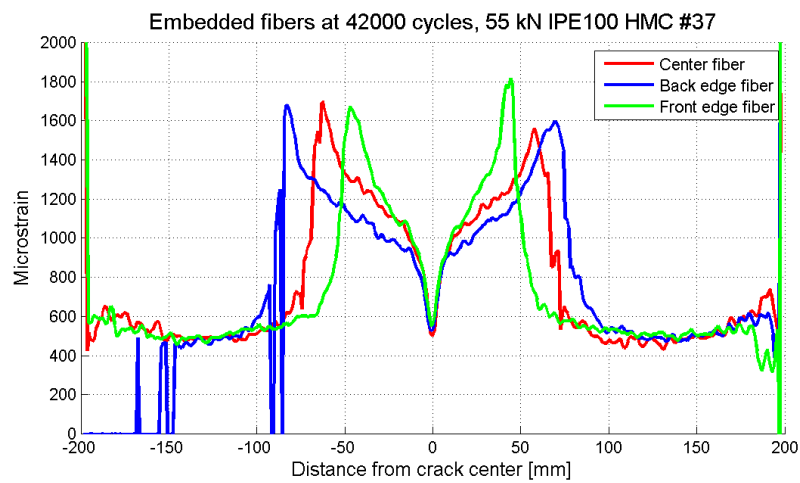
Figure 101: Three embedded fibers, 42 000 cycles. Beam 37.
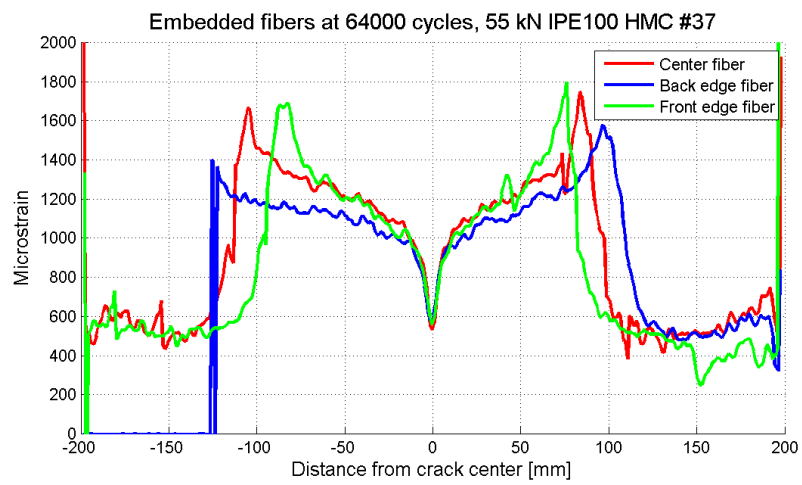
Figure 102: Three embedded fibers, 64 000 cycles. Beam 37.

B   Steel characterization report

FP7-SST-2008-RTD-1 Sustainable Surface Transport

Co-Patch

Composite Patch Repair for Marine and Civil Engineering Infrastructure Applications

Project No: SCP8-GA-2009-233969

Title: **Steel Characterization Test**

(Deliverable D3.3.4)

DOCUMENT HISTORY:

Version	Date	Revised Pages	Description of Changes
0	10/04/13	-	First issue

Table of Contents

1. INTRODUCTION

These laboratory experiments were performed by NTNU in December 2012 in order to characterize the yield strength, tensile strength and the modulus of elasticity of the steel for the Small-Scale Short-Term beam tests [1]. The tested beams were delivered by Smith Stål, a local supplier in Trondheim. A certificate for the IPE100 beams is attached in the Appendix. On the basis of ASTM standard E8/E8M-11[2] and ISO standard 6892-1:2009 [3], the geometric configurations of specimens, test procedure and experimental instrumentations were planed with adaptation.

This report includes the description of the steel specimens, the experimental instrumentation and test procedure, and the experimental results including the strength and modulus of elasticity.

2. EXPERIMENTAL INVESTIGATIONS

2.1. Specimen configurations

Six steel coupons were cut from an IPE100 beam of steel quality S355J2+AR [4] provided by Smith Stål. Four specimens were cut from the flange, and two from the web. The specimen dimensions are shown in Fig.1. L = 250 mm, W = 25 mm and the thickness, t, is different for the flange and the web.

Steel specimens to be tested:

• Four steel coupons cut from the flange of an IPE100 beam.

• Two steel coupons cut from the web of an IPE100 beam.

The length between the wedge grips was 50 mm on each side. For every specimen, its relevant dimensions were measured at three cross-sections in the central region of the specimen, following the instruction in ASTM E8/E8M [2]. All measurements are presented in Appendix A. According to these measurements, the average width, thickness and cross-sectional area are calculated.
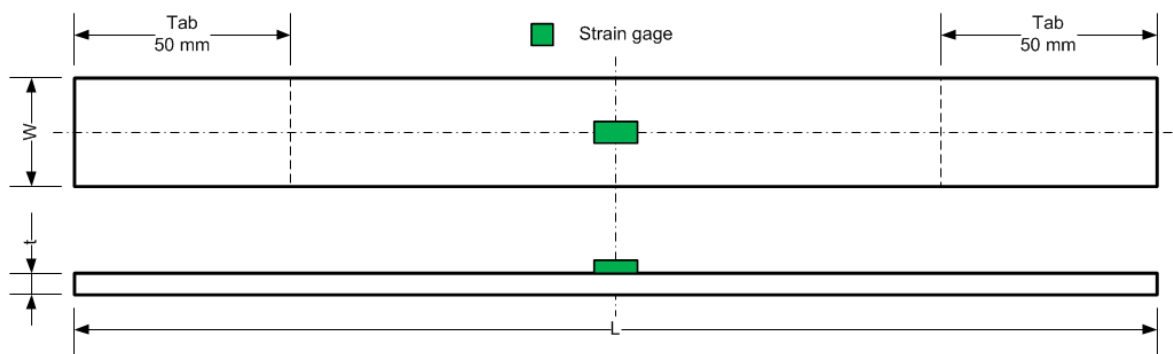
Figure 2-1: Dimensions and instrumentations of steel coupons for tensile testing.

2.2. Experimental set-up and instrumentations

The tests were performed in the fatigue lab at IPM NTNU with the use of an Instron Model 1342 100 kN machine. The specimens were loaded in tension and displacement control was used. In order to obtain the modulus of elasticity (E), each specimen had three cycles of loading to 25 kN and unloading at the displacement rate of 0.3 mm/min. Then they were loaded to failure with a displacement rate of 1.0 mm/min. Each specimen was instrumented with one 0/90° strain gage rosette, 6 mm gage length, 119,9±0,5(?) and a gage factor of 2,10.

The following data were collected from the tests:

• Electrical signal from the strain gages, giving precise values for the strain development.

• Electrical signal from the test machine load cell, giving precise values for the load applied to the specimen.

• Electrical signal from the displacement of the test machine, giving a precise value for the total displacement between the heads of the test machine.

The electrical signals of the load, displacement from the machine and the strain from the strain gages were recorded at a frequency of 10 Hz during the test. The recording device used was National Instruments cDAQ-9172.
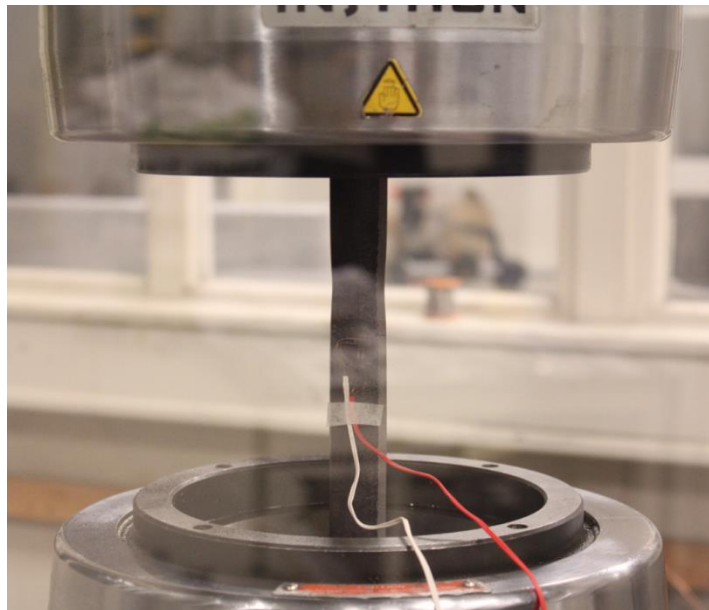
Figure 2-2: The test setup.

3. EXPERIMENTAL RESULTS

Four out of six specimens were tested.

3.1. Failure modes

The failure modes of the specimens are shown in Figure 3-1. The necking region was close to the grips for specimen 4.1 and 4.4. For specimen 4.2 and 4.3 the necking region was located closer to the center of the specimen. Only specimen 4.2 and 4.3 had a complete rupture, this can be seen closer in Figure 3-2.

Figure 3-1: Typical failure modes of the specimens.

Figure 3-2: Rupture of specimen 4.2(top) and 4.3(bottom).
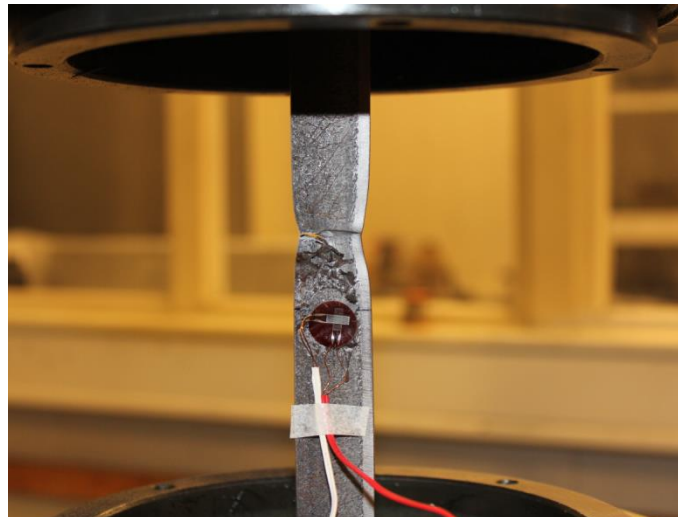
Figure 3-3: Specimen 4.3.
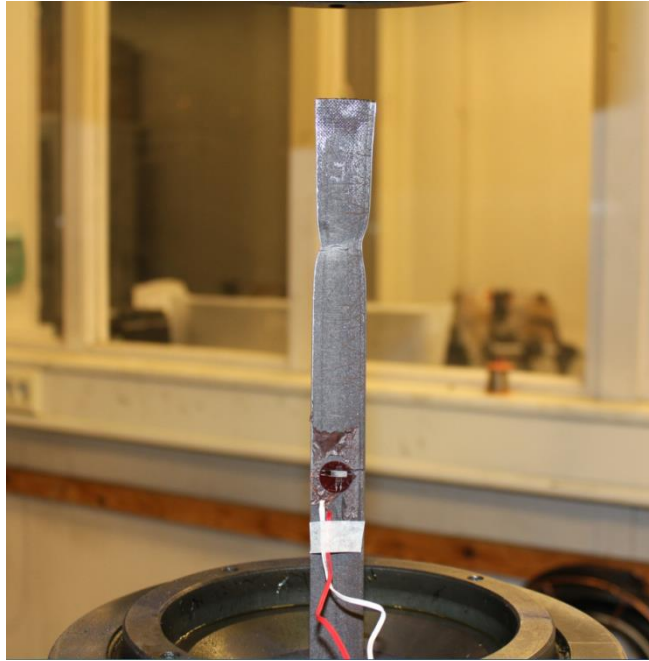
Figure 3-4: Specimen 4.4

3.2. Yield strength, tensile strength and modulus of elasticity

The load-displacement and stress-strain curves for specimens 4.2 and 4.3 are shown in Figure 3-5 and Figure 3-6. The yield and tensile strength were determined for four specimens and are presented in Table 3-1. The average yield and tensile strength were 450,3 MPa and 525,2 MPa respectively with standard deviation of 21,8 and 20,6. The yield strength was found by use of the extension-under-load method described in [1].

The modulus of elasticity (E_1) was calculated from the slope of the linear part of the stress-strain curve. The average value is 203,1 GPa with 5,6 as the standard deviation. The Poisson's ratio was found to be 0,29 with a standard deviation of 0,02. These values are also presented in Table 3-1.
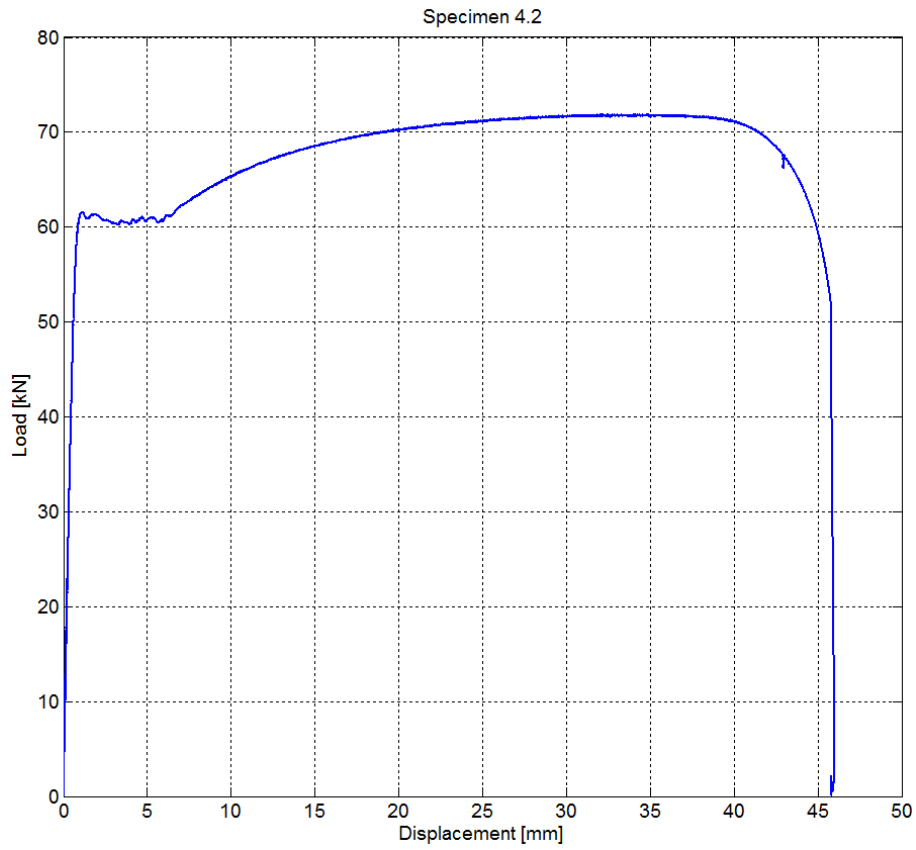
Figure 3-5: Load-displacement curve of specimen 4.2.
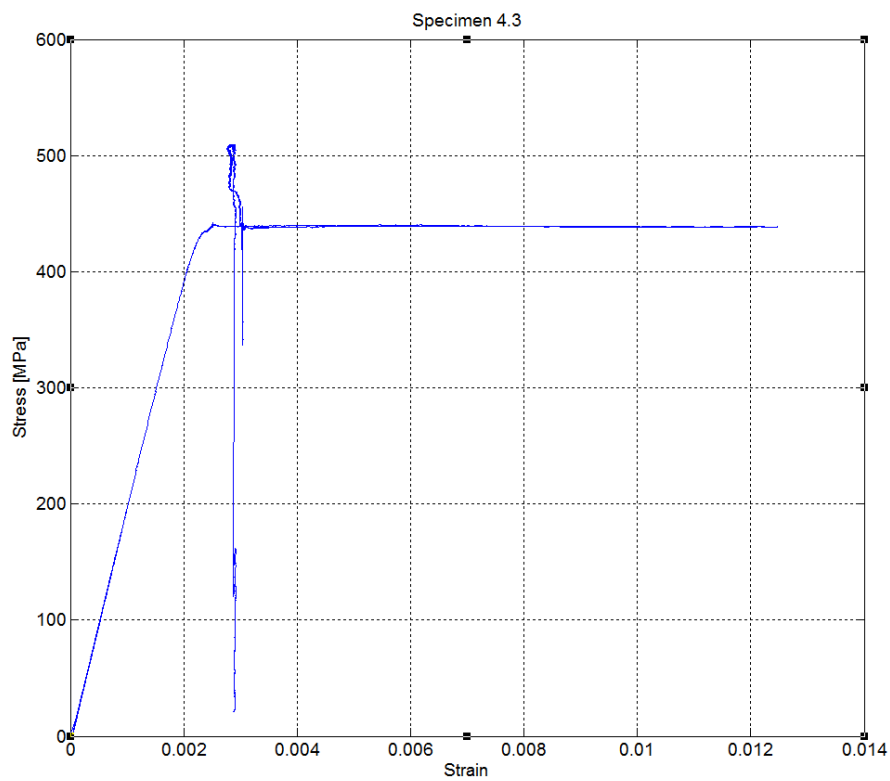
Figure 3-6: Stress-strain curve of specimen 4.3.

Table 3-1: Specimen dimensions, yield and tensile strength, and ultimate strain.

Specimen	Width [mm]	Thickness [mm]	Cross-sectional area [mm^2]	E [GPa]	Yield Strength [Mpa]	Tensile Strength [Mpa]	Ultimate strain* [%]	Poisson's ratio
Steel 4.1	24,99	4,43	110,62	209,0	481,0	554,0	27,5	0,27
Steel 4.2	24,78	5,68	140,69	199,5	431,1	511,2	30,7	0,28
Steel 4.3	24,98	5,74	143,47	197,4	439,7	509,7	30,0	0,31
Steel 4.4	24,98	5,88	146,99	206,7	449,5	526,0	31,4	0,29
Average	-	-	-	203,1	450,3	525,2	29,9	0,29
Standard Deviation	-	-	-	5,6	21,8	20,6	1,7	0,02
Coefficient of Variance (%)	-	-	-	2,7	4,8	3,9	5,8	5,6

4. CONCLUSIONS

From the tensile testing of the specimens the mean yield and tensile strength were determined to be 450,3 MPa (449 MPa) and 525,2 MPa (540 MPa). The mean modulus of elasticity was found to be 203,1 GPa and the Possion's ratio 0,29.The values in brackets are values from the certificate (see appendix) and agrees with the test.

References

[1]   Grave, J.H. and A.T. Echtermeyer, *Manufacturing and short-term test results of beam specimens*, 2013: Co-Patch.
[2]   Internation, A., *ASTM E8/E8M – 11 Standard Test Methods for Tension Testing of Metallic Materials*, 2011.
[3]   Standard, N., *NS-EN ISO 6892-1:2009 Metallic materials - Tensile testing - Part 1: Method of test at room temperature*, 2009.
[4]   Standard, N., *Hot rolled products of structural steels* in *Part 2: Technical delivery conditions for non-alloy structural steels,* 2005.

APPENDIX A

Table 0-1: Measured width and thickness of specimens (through three cross-sections).

Specimen	Thickness [mm]				Width [mm]			
	t_1	t_2	t_3	t	W_1	W_2	W_3	W
4.1	4,43	4,42	4,43	4,4	25,01	24,99	24,98	25,0
4.2	5,69	5,67	5,67	5,7	24,78	24,78	24,79	24,8
4.3	5,75	5,73	5,75	5,7	24,97	24,98	24,99	25,0
4.4	5,90	5,93	5,82	5,9	25,03	24,96	24,96	25,0
4.5	5,95	5,99	6,00	6,0	24,90	24,92	24,94	24,9
4.6	4,46	4,47	4,47	4,5	25,00	25,00	25,02	25,0

C   Safety evaluations for experimental work

Sikkerhets- og kvalitetsgjennomgang av laboratorietester og verkstedsarbeid
Safety and Quality Evaluation of Activities in the Laboratory and Workshop

◘ NTNU

Perleporten

1 Identifikasjon - *Identification*	Dokumentnr. – *Document no.*:	
Kundenavn – *Customer name* C'OPATCH	Prosjektnavn – *Project name* FATIGUE OT SMART COMPOSITE METAL JOIN T3	Projektnr. – *Project no.*
Beskrivelse av arbeid – *Description of job* UTMATTINGSTEST AV IPE100 BJELKE. 4 pkt. Loye. TENSILETEST AV SLS.		Dato – *Date* 1/3/2013

2 Projekt - *Team*

Prosjektleder og organisasjon – *Project manager and organisation*	ANDREAS ECHTERMEYER	Ansvarlig for instrumentering – *Responsible for instrumentation.*	EVEN V. LUNDER
Leiestedsansvarlig – *Laboratory responsible*	"	Operatør – *Operator*	EVEN V. LUNDER
Auditør for sikkerhets og kvalitetsgjennomgang – *Auditer for safety check*	"	Ansvarlig for styring av forsøk – *Responsible for running the experiment.*	EVEN V. LUNDER
Ansvarlig for eksperimentelt faglig innhold – *Responsible for experimental and scientific content*	"	Ansvarlig for logging av forsøksdata – *Responsible for logging and storing experimental data*	EVEN V. LUNDER
Ansvarlig for dimensjonering av last og trykkpåkjente komponenter – *Reponsible for dimensioning load bearing and pressurized components*	JON HARALD GRAVE	Ansvarlig for montering av testrigg – *Responsible for building the rig*	JON HARALD GRAVE

3 Viktig!! – *Important!!*   J: Ja – *Yes* / N: Nei - *No*

Er arbeidsordren signert? – *Is the work order signed?*	
Har operatøren nødvendig kurs/trening i bruk av utstyret? - *Has the operator the required courses/training on the equipment?*	J
Har operatøren sikkerhetskurs? (påbudt) – *Has the operator followed the safety courses? (mandatory)*	J

4.1 Sikkerhet – *Safety* (Testen medfører – *The test contains*)   J: Ja – *Yes* / N: Nei - *No*

Stor last – *Bib loads*	J	Brannfare – *Danger of fire*	N
Tunge løft – *Heavy lifting*	N	Arbeid i høyden – *Working at heights*	N
Hengende last – *Hanging load*	N	Hydraulisk trykk – *Hydraulic pressure*	J
Gasstrykk – *Gas pressure*	N	Vanntrykk – *Water pressure*	N
Høy temperatur – *High temperature*	N	Lav temperatur – *Low temperature*	N
Deler i høy hastighet – *Parts at high velocity*	N	Farlige kjemikalier – *Dangerous chemicals*	N
Sprutakselerasjon ved brudd – *Sudden acceleration at fracture/failure*	J	Forspente komponenter – *Pre-tensioned components*	N
Farlig støv – *Dangerous dust*	N	Kraftig støy – *Severe noise*	N
Klemfare – *Danger of pinching*	J	Roterende deler – *Rotating parts*	N

4.2 Påkrevet verneustyr – *Required safety equipment*   J: Ja – *Yes* / N: Nei - *No*

Briller (påbudt) – *Glasses (mandatory)*	J	Vernesko – *Safet shoes*	N
Hjelm – *Helmet*	N	Hansker – *Gloves*	J
Skjerm – *Screen*	J	Visir – *Visir*	N
Hørselsvern – *earprotection*	J	Løfteredskap – *Lifting equipment*	N
Yrkessele, fallsele, etc. –*harness ropes, other measures to prevent falling down.*	N		

Rev. 06 – Jan 2011

Sikkerhets- og kvalitetsgjennomgang av laboratorietester og verkstedsarbeid

◻ NTNU
Perleporten

5.1 Beskrivelse av aktivitet – *Description of the activity* (*see Appendix*)

Vurdering skal være basert på en skriftlig prosedyre for bruk av maskinen. I enkelte tilfeller kan prosedyre bli beskrevet direkte i tabellen nedenfor.

The evaluation shall be based on a written operating procedure for the machine. For simple cases the procedure can be directly described in the tables below.

Nr.	Beskrivelse av aktivitet – *Description of activity*	Fare - *Danger*	Prosedyre nr. – *Procedure no.*	Sannsynlighet – *Probability*	Konsekvens – *Consequence*	Risiko – *Risk*
1	TENSILE TEST AV SINGLE LAP JOINT	S PLINTER FRA LAMINATET	1	3	1	3
2	4 PUNKT BØYEPRØVE AV 1 FEIDO BJELKE	SPLINTER FRA LAMINATET	2	3	3	3
3		KLEMFARE	3	1	3	3

5.2 Korrigerende Tiltak – *Corrective Actions*

Nr.	Korrigerende tiltak – *Corrective action*	Sannsynlighet – *Probability*	Konsekvens – *Consequence*	Risiko – *Risk*	Utført dato – *Date of action*
1	AVSKJERMING	1	1	1	2/3/2013
2	– '' –	1	1	1	''
3	– '' – DON'T TOUCH WHEN LOADED	1	1	1	''

Sikkerhets og kvalitetsgjennomgang av laboratorietester og verkstedsarbeid

⊡ **NTNU**
Perleporten

5.3 Feilkilder – *Reasons for mistakes/errors*
Sjekkliste: Er følgende feilkilder vurdert? – Check list: Is the following considered?   J: Ja – *Yes* / N: Nei - *No*

Tap av strøm – *Loss of electricity*		Overspenning – *Voltage surge*	
Elektromagnetisk støy – *Electromagnetic noise*		Manglende aggregatkapasitet av hydraulikk – *Insufficient power of the machine*	
Jordfeil – *Electrical earth failure*		Vannsprut – *Water jet*	
Ustabilt trykk av hydraulikk/kraft – *Unstable pressure or hydraulic force*		Tilfeldig avbrudd av hydraulikk/kraft – *Unintended interruption of power supply*	J
Last-/ forskyvnings grenser etablert ? – *Are load and displacement limits established?*	J	Lekkasjer (slanger/koblinger, etc.) – *Leakage of pipes, hoses, joints, etc.*	
Mulige påvirkninger fra andre aktiviteter – *Possible interference from other activities*		Mulige påvirkninger på andre aktiviteter – *Possible interference towards other activities*	N
Problemer med datalogging og lagring – *troubles in loading and storage*		Brann i laboratoriet – *Fire in the laboratory*	

6 Kalibreringsstatus for utstyr – *Calibration of equipment*
(ex: load cell, extensometer, pressure transducer, etc)

I.D.	Utstyr - *Equipment*	Gyldig til (dato) – *Valid until (date)*

7 Sporbarhet – *Tracebility*

Eksisterer – Is there	J: Ja – *Yes* / N: Nei - *No*
Er alle prøvematerialene kjente og identifiserbare? – *Are all experimental materials known and traceable?*	J
Eksisterer det en plan for markering av alle prøvene? – *Is there a plan for marking all specimens?*	J
Er dataloggingsutstyret identifisert? – *Is the data aquisition equipment identified?*	J
Er originaldata lagret uten modifikasjon? – *Are the original data stored safely without modification?*	J
Eksisterer det en backup-prosedyre? – *Is there a back-up procedure for the data (hard disk crash)?*	J
Eksisterer det en plan for lagring av prøvestykker etter testing? – *Is there a plan for storing samples after testing?*	J
Eksisterer en plan for avhending av gamle prøvestykker? – *Is there a plan for disposing of old samples?*	J

8 Kommentarer – *Comments*

9 Signaturer – *Signatures*
Godkjent (dato/sign) – Approved (date/signature)

Sikkerhets og kvalitetsgjennomgang av laboratorietester og verkstedsarbeid

■ NTNU
Perleporten

APPENDIX Bakgrunn - Background

Sannsynlighetskategorier:		Probability Categories:	
1:	Lite sannsynlig, 1x pr. 50 år el.sjeldnere	1:	Very unlikely, 1 time per 50 years or less
2:	Mindre sannsynlig, 1x pr. 10 år el.sjeldnere	2:	Unlikely, 1 time per ten years or less
3:	Sannsynlig, 1x pr. år el.sjeldnere	3:	Probable, 1 time per year or leaa
4:	Meget sannsynlig, 1x pr. måned el. oftere	4:	Very Probable, 1 time per week or more
5:	Svært sannsynlig, 1x pr. år el.sjeldnere	5:	Nearly certain, 1 time per week

Konsekvenskategorier: Consequence Categories:

	Gruppe / Group	Konsekvens / Consequence
1 Lite alvorlig *Not serious*	Sikkerhet, mennesket Safety	Ingen fysisk ubehag. Ingen helsemessig konsekvens. Enkelttilfeller med misnøye. No physical discomfort. No health consequences. In some cases feeling a bit badly.
	Omdømme Reputation	Liten påvirkning på troverdighet og respekt. Little influence on trustworthiness and respect.
	Ytre miljø Environment	Ubetydelig skade og kort restitusjonstid Negligible damage and short recovery time.
	Øk/matr. Economic/ material	Drifts eller aktivitetsstans <1 dag, økonomisk tap inntil NOK 50.000 Shutdown of operation or activities < 1 day. Economic loss less than NOK 50 000.
2 Mindre alvorlig *Slightly serious*	Sikkerhet, mennesket Safety	Skade som ikke trenger legehjelp. Belastende forhold for gruppe mennesker uten målbare konsekvenser Injury that does not need medical treatment. Unpleasant circumstances for a group of people are without measurable consequences.
	Omdømme Reputation	Negativ påvirkning på troverdighet og respekt. Negative influence on trustworthiness and respect.
	Ytre miljø Environment	Mindre skade og kort restitusjonstid. Little damage and short recovery time.
	Øk/matr. Economic/ material	Drifts eller aktivitetsstans <1 uke. Økonomisk tap inntil NOK 250.000 Shutdown of operation or activities < 1 week. Economic loss less than NOK 250 000.
3 Alvorlig *Serious*	Sikkerhet, mennesket Safety	Skade som trenger legehjelp. Misnøye som fører til fravær. Injury that needs medical treatment. Unpleasant circumstances may lead to sick leave.
	Omdømme	Troverdighet og respekt svekket.

	Reputation	Trustworthiness and respect are reduced.
	Ytre miljø Environment	Mindre skade og lang restitusjonstid. Little damage and long recovery time.
	Øk/matr. Economic/ material	Drifts eller aktivitetsstans <1 mnd. Økonomisk tap inntil NOK 5 mill Shutdown of operation or activities < 1 month. Economic loss less than NOK 5 million.
4 Meget Alvorlig *Very serious*	Sikkerhet, mennesket Safety	Skade som må behandles av lege og som medfører fravær. Stor grad av mistrivsel. Injury that needs medical treatment and will cause sick leave. Severe consequences for well being.
	Omdømme Reputation	Troverdighet og respekt betydelig svekket. Trustworthiness and respect are severely reduced.
	Ytre miljø Environment	Langvarig skade og lang restitusjonstid Long term damage and long recovery time.
	Øk/matr. Economic/ material	Driftsstans < 0,5 år. Aktivitetsstans i inntil 1 år. Økonomisk tap inntil NOK 5 mill. Shutdown of operation or activities < 0.5 years. Economic loss less than NOK 5 million.
5 Svært Alvorlig *Ex- tremely serious*	Sikkerhet, mennesket Safety	Død eller alvorlig skade på en eller flere personer. Gjennomgående fravær med stor grad av mistrivsel. Death or serious injury to one or more people. Will cause long term sick leave and leads to severe consequences for well being.
	Omdømme Reputation	Troverdighet og respekt betydelig og varig svekket. Trustworthiness and respect are severely reduced for a long time.
	Ytre miljø Environment	Svært langvarig og ikke reversibel skade. Very long term damage and non reversible damage.
	Øk/matr. Economic/ material	Drifts- eller aktivitetsstans> 1 år. Økonomisk tap > NOK 5 mill. Shutdown of operation or activities > 1 year. Economic loss more than NOK 5 million.

Risikomatrise – Risk matrix:	
Risiko = Sannsynlighet * Konsekvens	Risk = Probability * Consequence

(Grønt – green)	Eventuelle risikoreduserende tiltak planlegges Eventually risk reducing actions have to be planed.	Verdisetting, prioritering og oppfølging
(Gult - yellow)	Risikoreduserende tiltak skal planlegges. Risk reducing actions have to be planed.	
(Rødt - red)	Stopp. Risikoreduserende tiltak skal gjennomføres. Stop. Risk reducing actions have to be planed.	

Risikoverdi = Sannsynlighet x Konsekvenser
Beregn risikoverdi for menneske. Enheten vurderer selv om de i tillegg beregner risikoverdi for ytre miljø, Øk/ matr og omdømme. I så fall beregnes disse hver for seg.

Risk = Probability x Consequence
Calculate risk level for humans. The section shall evaluate itself if it shall calculate in addition risk for the environment, economic/material and reputation. If so, they shall be calculated separately.

Til Kolonnen "Korrigerende Tiltak":
Tiltak kan påvirke både sannsynlighet og konsekvens. Prioriter tiltak som kan forhindre at hendelsen inntreffer, dvs sannsynlighetsreduserende tiltak foran skjerpende beredskap, dvs konsekvensreduserende tiltak.

For Column "Corrective Actions"
Corrections can influence both probability and consequence. Prioritize actions that can prevent an event from happening.

Oppfølging:
Tiltak fra risikovurderingen skal følges opp gjennom en handlingsplan med ansvarlige personer og tidsfrister.

Follow Up
Actions from the risk evaluation shall be followed through by an action plan with responsible persons and time limits.

Verdisetting, prioritering og oppfølging

K O N S E K V E N S		Lite sannsynlig 1	Mindre sannsynlig 2	Sannsynlig 3	Meget sannsynlig 4	Svært sannsynlig 5
	Svært alvorlig 5					
	Meget alvorlig 4					
	Alvorlig 3					
	Mindre alvorlig 2					
	Lite alvorlig 1					
		SANNSYNLIGHET				